Development of a Novel High-Voltage Arbitrary-Waveform Generator

by

Eckhard Detlef Schwardt

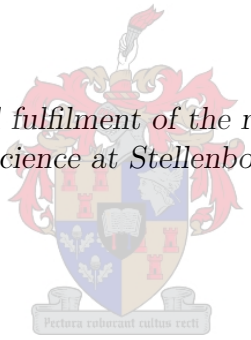

Thesis presented in partial fulfilment of the requirements for the degree of Master of Science at Stellenbosch University

Supervisor: Dr E.G. Rohwer

March 2007

Declaration

I, the undersigned, hereby declare that the work contained in this thesis is my own original work and that I have not previously in its entirety or in part submitted it at any university for a degree.

Signature: .....
E.D. Schwardt

Date: .....

Abstract

The dielectric-barrier discharge (DBD) is a source of non-equilibrium plasma that has seen widespread industrial application in recent years. A high-voltage arbitrary-waveform generator has been designed, built and characterised for the purpose of investigating the influence that the applied voltage waveform has on the operation of a DBD.

The developed arbitrary-waveform generator is based on the principle of Fourier synthesis. Up to twenty Fourier components are generated by means of a digital circuit board, and then separately amplified by Class-AB amplifiers. Twenty step-up transformers are subsequently used to transform the Fourier components to higher voltages; the summation of the Fourier components are realised by the series connection of the transformer secondary sides.

It was found that the digital generation of the Fourier components is very accurate and provides for the easy configuration of arbitrary waveforms. Furthermore, the amplification of the Fourier components by the Class-AB amplifiers introduces very little distortion. The principle of adding the Fourier components via the step-up transformers has been demonstrated; however, the large distributed capacitances of the transformers adversely affect the operation of the Class-AB amplifiers, leading to the introduction of distortion into the generated waveform. Furthermore, it was found that care had to be taken to limit the introduction of EMI through the system's large ground plane.

Opsomming

Die diëlektriese versperringsontlading (DVO) is 'n bron van nie-ekwilibrium plasma wat in die afgelope jare wye toepassing in die nywerheid gevind het. 'n Arbitrêre-golfvorm hoogspanningskragbron is ontwerp, gebou en gekarakteriseer, met die doel om die invloed wat die aangewende spanningsgolfvorm het op die werking van die DVO, te ondersoek.

Die ontwikkelde arbitrêre golfvormgenerator is gebaseer op die beginsels van Fourier samestelling. Tot twintig Fourier komponente word digitaal gegenereer, en dan afsonderlik versterk deur Klas-AB versterkers. Twintig transformators word dan gebruik om die Fourier komponente na hoër spannings te transformeer. Die sommasie van die Fourier komponente geskied deur die serieskakeling van die transformators se sekondêre windings.

Daar is bevind dat die digitale generasie van die Fourier komponente baie akkuraat is, en dat die arbitrêre golfvorms maklik verstel kan word. Verder versterk die Klas-AB versterkers die Fourier komponente sonder enige noemenswaardige vervorming. Die gebruik van die transformators om die Fourier komponente saam te voeg, is gedemonstreer. Die groot verspreide kapasitansies van die transformators beïnvloed egter die funksioneering van die Klas-AB versterkers, wat lei tot 'n vervorming van die uittree. Daar is ook bevind dat die toetrede van EM versteurings deur die grondvlak van die sisteem problematies kan wees.

Acknowledgements

I would like to express my sincere gratitude to the following people and organisations who have contributed to making this work possible:

- Defencetek, for providing the funding for this project.
- The NRF (National Research Foundation), for bursaries provided.
- Dr E.G. Rohwer, for supervising this project and always being supportive.
- Timo Stehmann, for providing valuable assistance as project leader, and ever being encouraging.
- My parents, for their love and support.

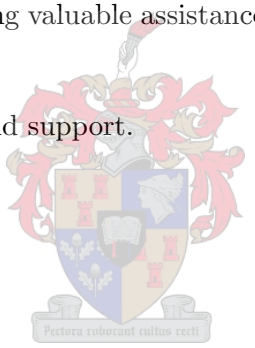

Contents

List of Figures

List of Tables

List of Symbols

Symbols

a	turns ratio
B	bandwidth, Hz
C	capacitance, F
D	duty cycle, s
f	frequency, Hz
i	time-dependent current, A
I	constant current, A
L	inductance, H
Q	Q-factor
R	resistance, Ω
t	time, s
T	constant time, s
v	time-dependent voltage, V
V	constant voltage, V
Z	impedance, Ω
$\jmath$	imaginary unit
θ	phase angle, rad
ω	angular frequency, rad·s^{-1}
τ	pulse width, s

Subscripts

0	constant, fundamental, initial, starting
a	case a
A	amplitude
b	case b
c	cell, Fourier component
Cu	copper

d	dielectric, digital, distributed
D	drain
DQ	drain quiescent
dc	dc
e	error, effective
eq	equivalent
g	gas
i	internal
I	input
leak	leakage
load	load
LP	low-pass
mag	magnetisation
max	maximum
min	minimum
n	n-channel enhancement-mode MOSFET
N	Nyquist
O	output
p	plasma, p-channel enhancement-mode MOSFET
peak	peak
pi	power input stage
po	power output stage
pri	primary side
PWM	pulse-width modulation
r	relative
res	resonant
s	sampling, source
sec	secondary side
sg	sinusoid generators
sg+amp	sinusoid generators connected to the Class-AB amplifiers
supply	supply
t	truncated
test	test
vg	variable-gain stage
w	waveform, winding
ZOH	Zero-order hold

Π	rectangular function

Acronyms

APGD	Atmospheric-pressure glow discharge
DAC	Digital-to-analogue converter
DBD	Dielectric-barrier discharge
DFT	Discrete Fourier transform
EMI	Electromagnetic interference
FFT	Fast Fourier transform
FPGA	Field-programmable gate array
GTO	Gate-turn-off thyristor
IGBT	Insulated-gate bipolar transistor
I/O	Input/output
LTI	Linear, time-invariant
MOSFET	Metal-oxide-semiconductor field-effect transistor
PCB	Printed circuit board
PLR	Parallel-loaded resonant
PQFP	Plastic quad flat package
PWM	Pulse-width modulation
RAM	Random access memory
RMS	Root mean square
SD	Silent discharge
THD	Total harmonic distortion
UV	Ultraviolet
VUV	Vacuum-ultraviolet

Chapter 1

Introduction

The dielectric-barrier discharge (DBD)[1], recently reviewed by Kogelschatz [1], is an attractive source of non-equilibrium or non-thermal plasma at atmospheric pressure. Non-equilibrium plasmas are characterised by energetic electrons that have much higher temperatures than the heavier particles (such as ions and neutral species) in the plasma. Compared to other sources of non-equilibrium plasma [2, 3, 4], the DBD has many advantages: operation at atmospheric pressure is possible, making the use of expensive vacuum systems unnecessary; discharge configurations are simple to implement, and can easily be scaled up for industrial applications; and, a variety of feed gases can be used, with the gas temperature staying close to ambient temperature during discharges.

The DBD is a gas discharge between two metal electrodes that have one or more dielectrics inserted between them. The electrodes are usually set up in parallel planar or coaxial cylindrical configurations, resulting in a volume discharge[2] in the feed gas. Typical feed gases are air, nitrogen and noble gases such as helium, neon and argon. Preferred dielectrics include glass, quartz, ceramics, and thin enamel or polymer layers. Since the dielectrics are insulating, the DBD can only be operated with an alternating voltage, thereby generating an alternating electric field between the electrodes. The discharge is initiated when the applied electric field is large enough to cause electrical breakdown in the gas, with the dielectric barrier preventing the discharge from transitioning into an arc discharge.

[1] Sometimes also referred to as a silent discharge.
[2] There are also electrode arrangements that allow for surface discharges [5].

The technology of the DBD has been around for more than a century; yet, developments over the last two decades have led to a renewed interest in this form of gas discharge. The first DBD was realised by W. Siemens [6] in 1857, which he used to generate ozone from atmospheric-pressure oxygen and air. Further development of this ozoniser technology led to its implementation in large-scale, industrial water-purification installations across Europe by the turn of the century. Research on DBDs in the first half of the 20th century focused on improving ozone generators; an important contribution was T.C. Manley's [7] derivation of the power formula for DBDs in 1943, which helped in the design of subsequent DBD power supplies. Modern diagnostic and modelling tools began to be employed in DBD research from the 1970s onwards, and consequently a range of new industrial applications opened up for the DBD. Today, DBDs are not only utilised in ozone generation [8, 9], but also the surface treatment of various materials [10, 11, 12, 13, 14], plasma-enhanced chemical vapour deposition [15, 16, 17, 18, 19], air pollution control [20, 21, 22, 23], the excitation of silent-discharge (SD) CO_2 lasers [24, 25], ultraviolet (UV) and vacuum-ultraviolet (VUV) excimer lamps [26, 27], and plasma display panels used in large-area television screens [28, 29]. Plasma display panels alone are presently driving a multi-billion US$ industry. Potential future applications of the DBD include the destruction of hazardous organic compounds [30, 31, 32, 33], aerodynamic flow control [34, 35, 36, 37], plasma-assisted combustion [38], frost control in refrigeration systems [39], and possibly even pest control [40].

1.1 Problem Statement

The operation of the DBD at atmospheric pressure is usually characterised by a filamentary mode [41], which consists of many micro discharges that have a stochastic spatiotemporal distribution over the surface area of the electrodes. Currently, most DBD applications make use of this kind of discharge. On the other hand, it has been shown [15, 42, 43] that it is also possible to operate the atmospheric-pressure DBD in a homogeneous mode, which is characterised by a discharge that is spread uniformly over the surface area of the electrodes[3]. The homogeneous mode has several advantages over the filamentary mode, such as reproducibility and homogeneity. Consequently, the homogeneous mode has not only pioneered new applications for the DBD, but also stands to improve the performance of existing DBD applications that are based upon the filamentary mode [44, 45, 46, 47].

[3]The homogeneous mode has actually been observed to exhibit two distinct types of discharges, namely a Townsend-like discharge and a glow-like discharge, of which the latter is often referred to as the atmospheric-pressure glow discharge (APGD).

The generation of the DBD's homogeneous mode is, however, not trivial; this is due to the fact that the homogeneous mode is very unstable at atmospheric pressure and tends to undergo rapid filamentation. At present, the fundamental physical processes responsible for the atmospheric-pressure homogeneous mode are not fully understood yet. Various mechanisms of pre-ionisation, such as ion-trapping [48], metastable-metastable or metastable-surface collisions [43], and thermal desorption of surface electrons [49], have been put forward as reasons for the generation of the homogeneous mode at atmospheric pressure; however, experimental evidence does not unambiguously corroborate these proposed mechanisms [50]. Further research into the conditions needed for the homogeneous mode to be stable, are therefore necessary.

Many different operating conditions have been investigated in an attempt to improve the stability of the DBD's homogeneous mode. In terms of feed gases, helium [51] and mixtures of argon and acetone [52] have been found to be conducive to stable discharges, whereas even small admixtures of oxygen can lead to filamentation [53]. With the help of special electrode configurations (e.g. brush electrodes [15] or wire-mesh electrodes [42]), dielectric barriers (e.g. electrets [54]) and other operating conditions, homogeneous modes have also been obtained in nitrogen [43], air [54] and neon [55]. Other parameters that influence the discharge stability, include the gas pressure, discharge gap distance and state of overvoltage.

One operating parameter that has not seen extensive investigation so far, is the waveform of the applied voltage. The standard waveforms used for the excitation of both the filamentary and homogeneous modes of the DBD, are sinusoidal and square-wave voltages, although the use of sub-microsecond, unipolar voltage pulses have also been demonstrated [56, 57]. Certain recent studies have indicated, however, that the voltage waveform could play an important role in the control of the homogeneous mode. Somekawa *et al.* [58] reported on a novel high-voltage power supply that utilised a unique pulsed voltage waveform to generate a stable homogeneous mode in air. They found that the presence of a second voltage pulse, with opposite polarity, after the first voltage pulse, played an important role in stabilising the homogeneous mode. In another study, Deng *et al.* [59] used an one-dimensional hydrodynamic model to simulate the effects of several non-standard waveforms on the homogeneous mode in helium. They found that, compared to the sinusoidal waveform, an appropriately chosen non-standard waveform could reduce by more than 50 % the electric power required to sustain the homogeneous mode, or alternatively increase the electron density in the discharge by 68 %. Further-

more, according to Shin *et al.* [60], certain characteristics of the applied voltage waveform, such as the rate of voltage change and the duration of continuous voltage increase per half cycle, controlled the pulse phenomena of the homogeneous mode in helium. They consequently proposed a "ramp-plus-plateau" voltage waveform as means of controlling these pulse phenomena.

It is therefore clear that an experimental study of the effects that the applied voltage waveform has on the DBD, is called for; however, in order to perform such experiments, a power supply that is capable of producing arbitrary voltage waveforms, is required.

1.2 Aim

The aim of this project is to design, build and characterise a prototype power supply capable of generating arbitrary voltage waveforms. This waveform generator must be able to provide the high voltages that are necessary for the excitation of a DBD; furthermore, the waveform generator must be capable of driving capacitive loads, as DBDs are modelled as being capacitive. An important goal is that the parameters of the power supply's output voltage, i.e. the amplitude, repetition rate, and waveform, must be configurable with great accuracy. Finally, the waveform generator must be flexible in its operation, so that different arbitrary waveforms can be investigated with ease.

1.3 Outline

Chapter 2 gives an overview of possible approaches that can be taken to generate arbitrary voltage waveforms. First, a few design guidelines are set out for the project in Section 2.1. This is followed by an investigation into the applicability of power amplifiers and multilevel inverters as arbitrary waveform generators, which are found in respectively Sections 2.2 and 2.3. Two approaches based on Fourier synthesis are discussed in Section 2.4; one of the Fourier-based topologies, namely that of the cascaded multichannel amplifier, was chosen for this project.

In Chapter 3, the theoretical background is presented for the utilisation of Fourier analysis to characterise electronic signals and systems. Section 3.1 introduces the frequency-domain description of periodic signals, while Section 3.2 looks at the characteristics of linear, time-invariant electronic systems. Finally, Section 3.3 considers the influence that some practical aspects of the chosen topology's implementation have on the generated

voltage waveforms.

Chapter 4 outlines the design and implementation of the cascaded multichannel amplifier. The main components of the chosen waveform-generator topology consist of respectively the sinusoid generators, the Class-AB amplifiers, and the step-up transformers; the design goals for each of these components can be found in Sections 4.1-4.3.

The results from testing the cascaded multichannel amplifier are presented in Chapter 5. The performance of the various components are tested by means of three test waveforms, which are specified in Section 5.1. In Section 5.2, the sinusoid generators' ability to generate Fourier components accurately, are investigated. The transfer function of the Class-AB amplifiers are measured in Section 5.3, while important transformer parameters are measured in Section 5.4. Finally, the overall operation of the cascaded multichannel amplifier's connected components is tested in Section 5.5.

In Chapter 6, the operation of the cascaded multichannel amplifier is evaluated. Section 6.1 studies the accuracy of the sinusoid generators, whereas Section 6.2 evaluates the Class-AB amplifiers' ability to amplify voltage signals without introducing distortion. The characteristics of the step-up transformers, along with their influence on the operation of the cascaded multichannel amplifier, are discussed in Section 6.3. Finally, some system-wide effects are commented on in Section 6.4.

Chapter 7 summarises the conclusions that can be made about the performance of the cascaded multichannel amplifier. Additionally, some recommendations are made regarding possible improvements to the system; potential future work are also touched upon.

Chapter 2

Selection of an arbitrary-waveform power-supply topology

This chapter evaluates several power-supply topologies for the generation of arbitrary voltage waveforms. A selection of guidelines for the power supply are stated first, setting the desired parameter space for the power supply to operate in. This is followed by an investigation of three potential approaches to generating arbitrary voltage waveforms: the first approach is based on the use of a power amplifier and step-up transformer; the second approach relies on the multilevel-inverter topology; and the third approach proposes the concept of Fourier synthesis as a solution. The chapter ends with a summary and the selection of the arbitrary-waveform power-supply topology.

2.1 Power-supply design guidelines

The set of requirements for the arbitrary-waveform power supply is as follows:

- **Large bandwidth (200 kHz):** In order for the output voltage to have an arbitrary waveform, the bandwidth of the power supply needs to be large.
- **High voltage (10 kV to 20 kV):** The peak output voltage needs to be high in order to establish a DBD in a variety of gasses at atmospheric pressure.
- **High repetition rate (4,5 kHz to 10 kHz):** This is a frequency range that is commonly employed for DBDs described in the literature.

- **Medium power (∼100 W):** Due to the prototype nature of the power supply, high power requirements are not essential.
- **Capacity to drive a capacitive load:** The DBD can be modelled as a capacitive load; Figure 2.1 shows equivalent circuits of the DBD for respectively when no discharge takes place, and the homogeneous mode[1].

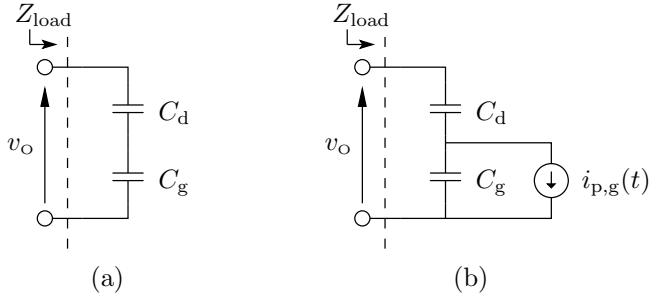

Figure 2.1: (a) The load Z_{load} that is presented by the DBD-arrangement, can be modelled as the equivalent capacitance of the dielectrics C_{d} in series with the capacitance of the feed gas C_{g} when no discharge takes place. (b) The DBD's homogeneous mode can be modelled as a voltage-controlled current source $i_{\text{p,g}}(t)$ in parallel with the gas capacitance C_{g} for arbitrary voltage waveforms [61].

Three different approaches to realise the above-mentioned goals for an arbitrary--waveform power supply, are discussed in the following three sections.

2.2 Power amplifiers

The most simple approach to implement an arbitrary-waveform power supply, is to utilise a power amplifier to amplify a low-power arbitrary-waveform signal to the necessary degree. This type of arrangement is typically found in audio systems, where signals that have bandwidths of up to 20 kHz, are amplified to have output powers of up to the kilowatt range. In order for this approach to meet the high-voltage requirements, a step-up transformer has to be inserted between the amplifier and the load. Furthermore, the low-power signal can easily be generated by a microprocessor. Figure 2.2 shows a schematic of the required arrangement.

[1]The filamentary mode cannot be modelled in terms of lumped circuit elements due to its stochastic nature.

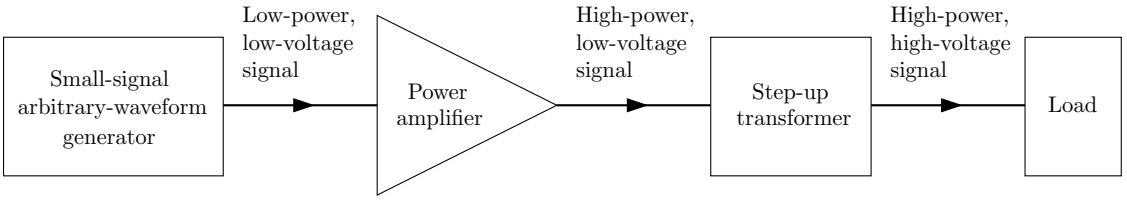

Figure 2.2: A block diagram of a high-voltage arbitrary-waveform power supply that is based on the use of a power amplifier.

Various power-amplifier topologies have been developed for audio applications, and the most significant ones are discussed in the following section.

2.2.1 Power-amplifier topologies

Two types of power amplifiers that have been widely employed in audio applications, are considered here:

- the Class-AB amplifier [62], and
- the Class-D amplifier [63].

The selection of an amplifier topology is usually governed by a decision between optimum linearity and optimum efficiency: Class-D amplifiers are exemplified by their high efficiencies, but do not have the best linearity, while Class-AB amplifiers provide a good compromise between linearity and efficiency.

The *Class-AB amplifier* consists of two power transistors that are connected as a complementary push-pull output stage, along with a particular biasing network. In Figure 2.3(a), transistor Q_n amplifies the input signal v_I linearly when v_I is positive, but is effectively switched off when v_I is negative; the converse is true for Q_p. The resulting conduction of the two transistors are shown in Figure 2.3(c) for $v_I = V_A \sin(\omega t)$ (see Figure 2.3(b)). The biasing network is arranged in such a way that each transistor never truly switches off, but rather conducts a small quiescent current I_{DQ}: this ensures that the output signal v_O, which is a combination of the two transistors' outputs, has no distortion when amplification of the input is switched from one transistor to the other. The Class-AB amplifier therefore has excellent linearity across the full range of its input; unfortunately, the maximum efficiency is only between 50 % and 78,5 %.

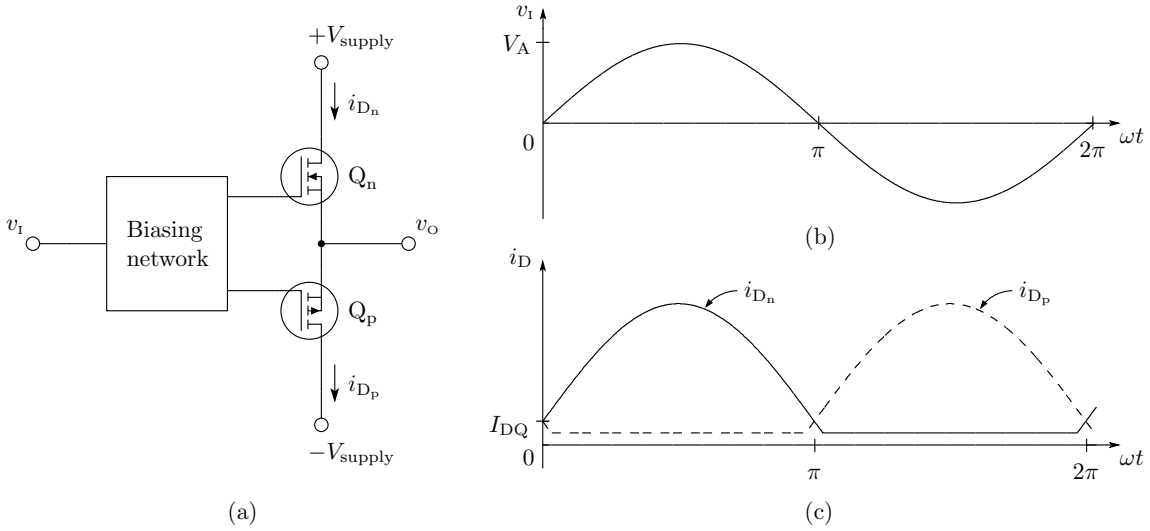

Figure 2.3: (a) A schematic diagram of the Class-AB amplifier, where the power transistors Q_p and Q_n are shown as MOSFETs; i_{D_n} is the drain current of Q_n, while i_{D_p} is the drain current of Q_p. (b) A sinusoidal voltage input v_I. (c) The drain currents of Q_n and Q_p over one cycle of v_I.

The *Class-D amplifier* is based on the utilisation of power transistors as switches, which are generally controlled by a pulse-width modulation (PWM) scheme; Figure 2.4 shows a schematic diagram of how the Class-D amplifier operates. The input signal v_I is compared to a triangular carrier signal that has a frequency which is much greater than the bandwidth of v_I; the output of the comparator is set high when v_I is larger than the carrier signal, and vice versa. Thus, the comparator approximates the amplitude and frequency of v_I by a series of pulses, and these pulses are used to drive the power transistors as switches. Due to the switch-mode operation of the transistors, the output is very distorted; a low-pass filter is therefore added to remove the distortion caused by switching. Class-D amplifiers generally have efficiencies greater than 90 %, but their linearity depends on their ability to filter out the switching frequency f_s.

2.2.2 Feasibility

The main design concerns for this approach are the power amplifier and the step-up transformer.

In terms of the amplification stage, the Class-AB amplifier is the most suitable: with the proper selection of components, notably metal-oxide-semiconductor field-effect tran-

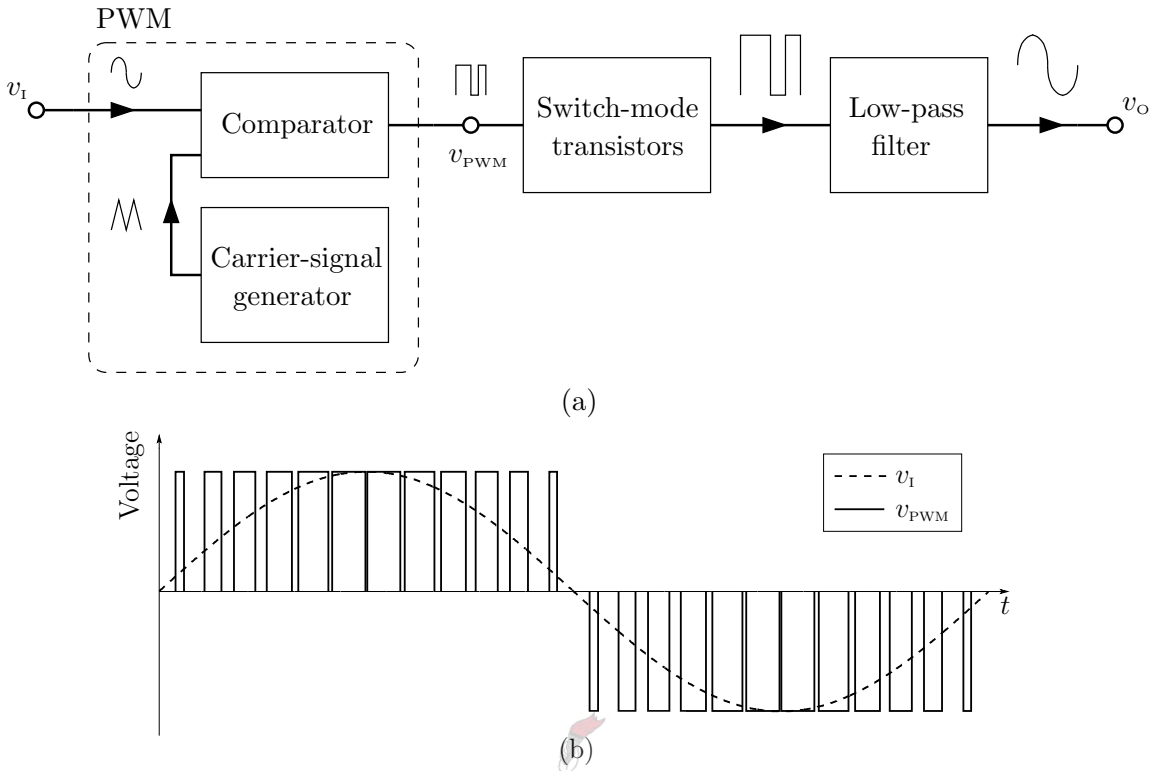

Figure 2.4: (a) A block diagram of Class-D amplifier. The input v_I is converted through the PWM into a series of pulses, which are then amplified by the power transistors. The output is passed through a low-pass filter to retain the waveform of v_I. (b) The pulse-width-modulated signal v_PWM is shown for a sinusoidal v_I.

sistors (MOSFETs) as the power transistors, the Class-AB amplifier is capable of amplifying 200 kHz-bandwidth signals with minimal distortion. The Class-D topology, on the other hand, poses problems when working with such large bandwidths. The required switching frequency f_s must be at least ten times greater than the signal bandwidth for proper operation, i.e. $f_\mathrm{s} \geq 2\,\mathrm{MHz}$; such a high f_s is at the limit of what is possible with semiconductor switching devices. Furthermore, the cut-off frequency f_c of the low-pass filter also needs to be at least ten times greater than the signal bandwidth to prevent the filter from introducing distortion into the output; since $f_\mathrm{c} \approx f_\mathrm{s}$, the switching harmonics will not be attenuated effectively, leaving the output waveform with substantial distortion.

The step-up transformer introduces significant difficulties for arbitrary-waveform generation. Any transformer connected to a capacitive load forms a series resonant circuit

that has a resonant frequency at

$$f_{\mathrm{r}} = \frac{1}{2\pi\sqrt{L_{\mathrm{leak}}C_{\mathrm{load}}}}, \tag{2.2.1}$$

where L_{leak} is the leakage inductance of the transformer and C_{load} is the capacitance of the load. The impedance of the resonant circuit is a minimum at f_{r}, resulting in an increase in the current drawn by the load at that frequency; this is undesirable, since it introduces distortion in the output and could even lead to the failure of components. The step-up transformer therefore needs to be designed for a minimised leakage inductance; however, several of the stated system goals counter this requirement. Firstly, in order to prevent the transformer core from saturating, the transformer has to be designed for the signals with the lowest frequency; since this frequency is quite low (4,5 kHz), the transformer dimensions will be large. Secondly, the high voltage requirement necessitates a large amount of insulation between the primary and secondary windings of the transformer to ensure electrical isolation. These two requirements significantly increase the leakage inductance of the step-up transformer, thereby lowering its resonant frequency to within the bandwidth of the power supply.

The problems due to working with a large step-up transformer can only be remedied by limiting the bandwidth of the power supply, and, therefore, its ability to generate arbitrary voltage waveforms. The approach described in this section is therefore not suitable.

2.3 Multilevel inverters

The second option in terms of arbitrary-waveform generation is multilevel inverters [64], which have become a popular alternative in the field of high-power energy control. Their advantages include very high efficiency and low electromagnetic interference (EMI). Multilevel inverters have seen extensive utilisation in large, electric motor drives [65] (e.g. in laminators, compressors, pumps and conveyor belts), and utility applications such as power-line conditioning for electricity distribution networks [66]. The typical voltage ratings for these applications are medium voltages (2,3 kV to 6,9 kV) in the case of motor drives, and high voltages (11 kV to 16 kV) in the case of utility applications; the applied voltage waveforms are sinusoidal, with frequencies below 400 Hz.

The principle of operation of the multilevel inverter is to synthesise a desired ac voltage by adding several levels of dc voltages, resulting in a stepped voltage waveform. The voltage levels are provided by dc voltage sources that can deliver high voltages[2], thereby making the need for a step-up transformer unnecessary. The accuracy with which a multilevel inverter can synthesise a desired voltage waveform, is determined by the number of output voltage levels of the inverter — the greater the number of levels, the greater the accuracy.

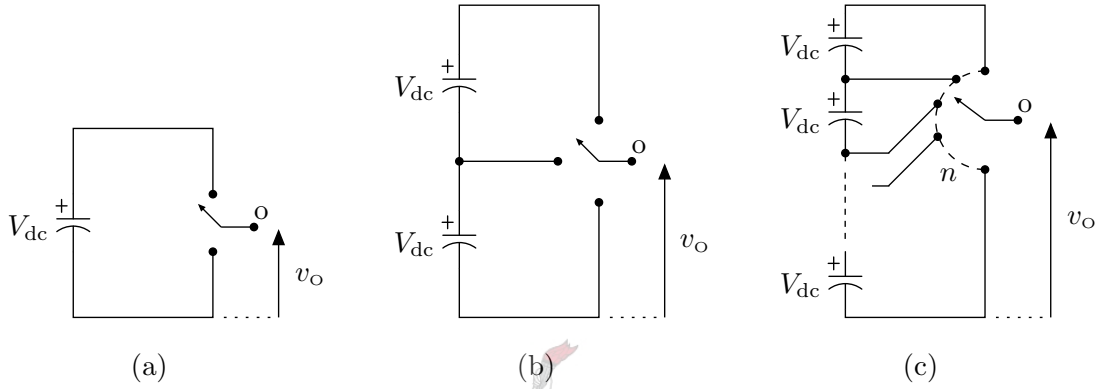

Figure 2.5: The output voltage v_O of a multilevel inverter, which is referenced to the negative terminal on the dc side, can take on a discrete number of voltage levels. A (a) two-level, (b) three-level and (c) n-level inverter are shown here schematically, with the semiconductor switches represented by ideal switches that have several positions.

The addition of the dc voltage levels in a multilevel inverter is controlled by the commutation of power semiconductor switches, as is illustrated schematically in Figure 2.5. Power semiconductor switches are characterised by their switching speeds and the rated voltages that they can withstand. A trade-off generally exists between these two properties; Table 2.1 summarises the characteristics of three common power semiconductor devices, namely the gate-turn-off thyristor (GTO), the insulated-gate bipolar transistor (IGBT) and the MOSFET. Since a single semiconductor device cannot be connected directly to a high-voltage load, several devices in series are required. Various high-voltage arrangements that allow individual semiconductor devices to withstand only reduced voltages, have been developed. These multilevel topologies, along with the control strategies needed to switch the semiconductor devices, are discussed in the following section.

[2]Generally distribution-network line voltages that have been rectified and filtered.

Device	Voltage-blocking capability	Switching speed
GTO	High (∼5 kV)	Slow (<1 kHz)
IGBT	Medium (∼3 kV)	Medium (∼100 kHz)
MOSFET	Low (≤1 kV)	Fast (∼1 MHz)

Table 2.1: A comparison of the characteristics of three common types of power semiconductor devices.

2.3.1 Multilevel topologies and their control techniques

There are three main multilevel topologies:

- diode-clamped inverters [67],
- capacitor-clamped inverters [68], and
- cascaded multicell inverters [69].

Various hybrid derivatives [70, 71] of the cascaded multicell topology have also been developed. The different topologies can be categorised according to the number of dc voltage sources that they require: diode-clamped and capacitor-clamped inverters utilise dc-link capacitors to provide multiple voltage levels from a single dc voltage source, whereas the cascaded multicell topology and its hybrid derivatives employ multiple dc voltage sources to accomplish the same effect.

The diode-clamped and capacitor-clamped inverters exhibit some problems that limit their applicability. The *diode-clamped inverter* uses diodes to manage the voltages that the semiconductor switches have to block. Unfortunately, the number of required diodes increases quadratically with the number of output voltage levels, thus making the system impractical at a sufficiently high number of voltage levels. The reverse recovery of the diodes also becomes problematic as the switching speeds of the semiconductor devices are increased. The *capacitor-clamped inverter*, on the other hand, relies on additional capacitors to control the voltages over its switches. The uneven charging and discharging of these capacitors can lead to voltage imbalances on the dc-link capacitors, thereby jeopardising the operation of the inverter. Additionally, the capacitor-clamped inverter suffers from the same scaling problem as the diode-clamped inverter when the number of output voltage levels is increased. Due to these reasons, the first two topologies are not considered here.

The *cascaded multicell inverter* is composed of full-bridge inverters [72] (referred to as cells) connected in series. Each cell is connected to a separate dc voltage source that has the same voltage; this arrangement is called a unary cell configuration. A diagram of the full-bridge inverter is shown in Figure 2.6; it is connected to a dc voltage source V_{dc} and has four semiconductor switches (S_1, S_2, S_3, S_4). The output voltage v_{o} can take on three different values, depending on the states of the switches[3]: V_{dc} (S_1 on, S_4 on), 0 (S_1 on, S_3 on; or S_2 on, S_4 on), or $-V_{\mathrm{dc}}$ (S_2 on, S_3 on). Although the output has a $2V_{\mathrm{dc}}$ voltage swing, the voltage that every switch has to block in its off state, is limited to only V_{dc}.

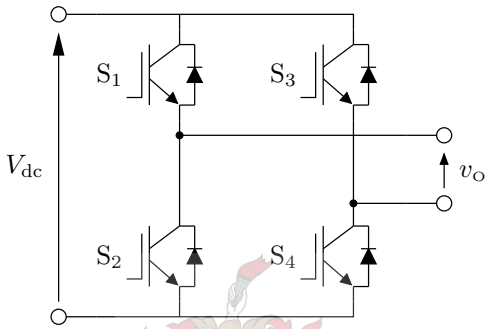

Figure 2.6: The full-bridge inverter, with dc voltage source V_{dc} and output voltage v_{o} shown. The four switches (S_1, S_2, S_3, S_4) are represented as IGBTs along with their antiparallel diodes.

Proper control of the semiconductor switches in a cascaded multicell inverter is required to produce the desired output; however, only a few control options are available for single-phase arbitrary-waveform generation[4]. The most basic control method is called fundamental-frequency switching, in which every cell's semiconductor switches are turned on once per period of the output voltage. Figure 2.7 shows the resulting output voltage from each cell in a cascaded multicell 7-level inverter that utilises fundamental-frequency switching, as well as the inverter's resulting output voltage. The fundamental-frequency switching method provides a stepped approximation of the desired voltage waveform,

[3]Switches (S_1, S_2) and (S_3, S_4) form complementary pairs, thereby ensuring that the dc voltage source is never shorted out.

[4]Most applications of multilevel inverters require three-phase voltages, where each phase is provided by a separate multilevel inverter; because of this, the control strategies developed so far for multilevel inverters cater almost exclusively for three-phase loads.

with the error of the approximation decreasing as the number of voltage levels increases.

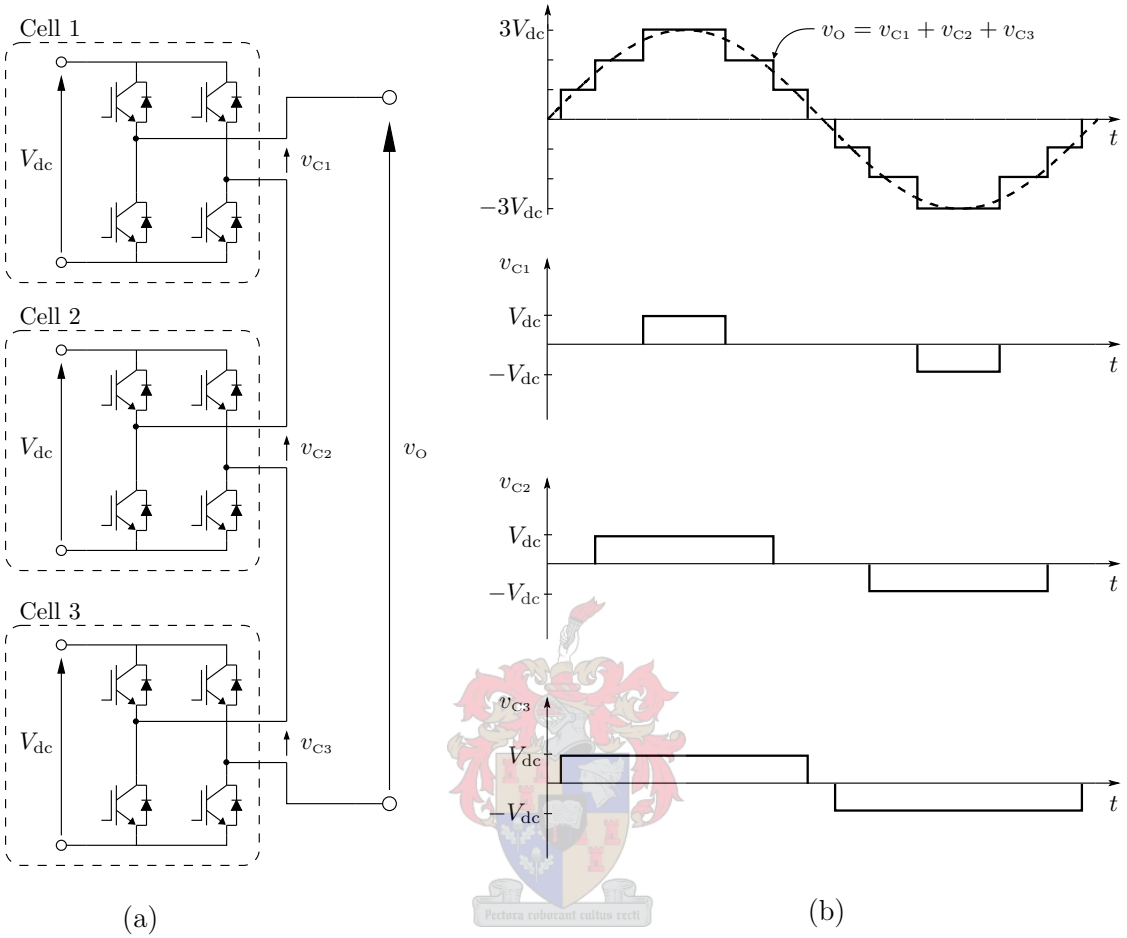

Figure 2.7: (a) A cascaded multicell 7-level inverter, consisting of three cells connected in series. (b) The output voltage v_O is synthesised from the output voltages of the three cells (v_{C1}, v_{C2} and v_{C3}). The dashed-line in the top graph indicates the sinusoidal voltage waveform that is intended to be synthesised.

The fundamental-frequency switching method has its limitations: the range of possible output-voltage amplitudes that the inverter can produce, is restricted by the available number of voltage levels, while distortion due to switching is introduced into the output voltage waveform that cannot be filtered out effectively. Control of the inverter's output can be improved by incorporating PWM (see Section 2.2.1); the concept of PWM has been extended to multilevel inverters by the introduction of multiple carrier signals [73].

The carrier signals are arranged contiguously into bands, so that each carrier signal is associated with a voltage level that can be switched. The carrier signals are compared simultaneously to a single reference signal, resulting in a fast-stepping output voltage, such as is shown in Figure 2.8. The time average of a multi-carrier PWM output waveform is therefore superior to that of the fundamental-frequency switching technique.

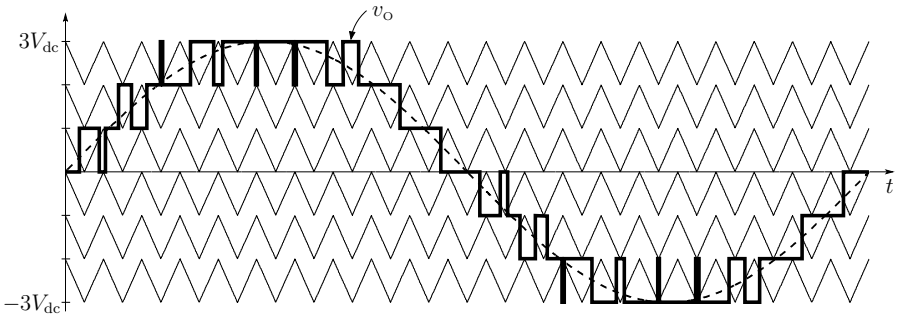

Figure 2.8: The output voltage v_o generated by a 7-level inverter using multi-carrier sinusoidal PWM. The reference voltage is indicated as a dashed line, while the six triangular carrier signals have switching frequencies that are 21 times greater than the repetition rate of the reference signal.

One drawback of the cascaded multicell topology is the number of separate dc voltage sources that are required: given n dc voltage sources, the number of output voltage levels m that can be generated, is

$$m = 2n + 1 \quad \text{(unary cell configuration)}. \tag{2.3.1}$$

Several hybrid topologies, based on the cascaded multicell inverter, have been developed in order to increase the amount of output voltage levels that can be generated from the available dc voltage sources. There are two arrangements of the hybrid multilevel topology: the mixed-level hybrid multilevel inverter, and the asymmetric hybrid multilevel inverter. In the mixed-level hybrid inverter, the cells connected in series are not full-bridge inverters, but rather multilevel inverters themselves; either the diode-clamped or capacitor-clamped multilevel inverter can be used as a cell, and different cells do not have to employ the same type of topology. In view of the problems stated earlier for the diode-clamped and capacitor-clamped inverters, this topology is not considered. On the other hand, the asymmetric hybrid inverter employs full-bridge inverters as cells, but

the dc voltage sources connected to the cells do not all have the same voltages. The voltages of the dc voltage sources are usually related to each other by natural ratios, such as binary (2:1) or ternary (3:1) ratios. The number of output voltage levels m obtained with the binary and ternary cell configurations, is given as [71]

$$m = 2^{n+1} - 1 \quad \text{(binary cell configuration)}, \tag{2.3.2}$$

$$m = 3^n \quad \text{(ternary cell configuration)}. \tag{2.3.3}$$

Compared to the cascaded multicell topology, the asymmetric hybrid multilevel inverter can therefore greatly reduce the number of separate dc voltage sources that are required for a given number of voltage levels.

2.3.2 Feasibility

There are only two multilevel topologies that can be considered for arbitrary-waveform generation, and that is the cascaded multicell and the asymmetric hybrid multilevel inverters. Additionally, the inverters must utilise either MOSFETs or IGBTs as switches, since they are the most suitable types of semiconductor devices to provide the fast switching speeds required by the system specifications.

Considering the switching speeds that MOSFETs and IGBTs are capable of, they can easily be controlled with the fundamental-frequency switching method to provide the necessary system bandwidth; however, the output voltage waveform is a stepped approximation of the intended waveform. Multi-carrier PWM is only possible with MOSFETs, but faces the same implementation difficulties as normal PWM (see Section 2.2.2). Although the time-averaged output of the multi-carrier PWM is better than that of the fundamental-frequency switching technique, it also contains more switching artifacts, which could affect DBD formation in an unpredictable manner.

Many voltage levels are needed to minimise the error that the multilevel inverter makes by its stepped approximation of the output voltage waveform. Due to the relatively low voltage-blocking capabilities of MOSFETs and IGBTs in terms of the high-voltage requirements, a large number of voltage levels entails many high-voltage dc voltage sources in the case of the cascaded multicell inverter, which is costly. The asymmetric hybrid inverter can reduce the number of dc voltage sources needed; however, its higher-voltage cells require several switches stacked in series to block the applied voltages. Due to the size of the overall system, the driving circuits of the switches become complex and man-

agement of the voltages over the individual switches are difficult.

The implementation of a multilevel inverter for arbitrary-waveform generation is costly and complex. Furthermore, the stepped nature of the multilevel inverter's output entails that one does not have control over the actual slope of the voltage waveform, which could play an important role in DBD formation. Due to these concerns, the multilevel-inverter approach is not pursued.

2.4 A novel approach: Fourier synthesis

The standard high-voltage power-supply topologies are not conducive to arbitrary-waveform generation; a new approach is therefore called for. The proposed approach is the utilisation of Fourier synthesis to generate arbitrary voltage waveforms.

Any periodic voltage waveform can be decomposed into its Fourier components, which are sinusoidal voltages that have specific amplitudes, frequencies and phases. The Fourier-synthesis approach proposes to generate these Fourier components separately, and then to add them at the load, thereby synthesising the intended arbitrary voltage waveform; Figure 2.9 shows a schematic diagram of the proposed approach. The advantage of this approach is that sinusoidal voltages are much easier to generate at high voltages than an arbitrary-waveform voltage; the addition of the Fourier components, however, can be complicated. Furthermore, since it is possible for an arbitrary waveform to be composed of an impracticable number of Fourier components, the selection of Fourier components to be generated can influence the accuracy with which the intended waveform is synthesised.

The following section discusses possible topologies for implementing the Fourier-synthesis approach.

2.4.1 Topologies for Fourier synthesis

The following topologies are proposed for the realisation of the Fourier-synthesis approach:

- a cascaded multi-resonant inverter, and
- a cascaded multichannel amplifier.

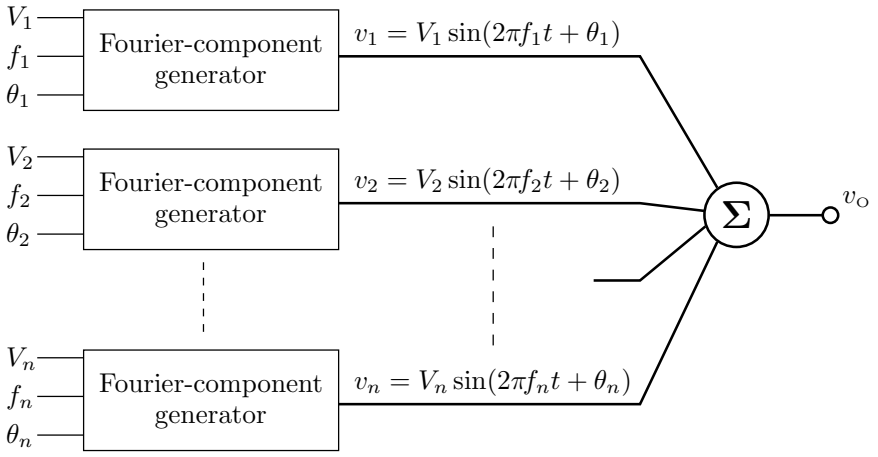

Figure 2.9: A block diagram of the proposed Fourier-synthesis approach. The n^{th} Fourier component is specified by its amplitude V_n, frequency f_n and phase θ_n; each Fourier component is generated separately and then added to provide the output voltage v_O.

The *cascaded multi-resonant inverter* makes use of multiple resonant inverters to implement the Fourier-synthesis approach. Various resonant-inverter topologies have been successfully employed as DBD power supplies [74, 75, 76, 77]; the most suitable topology for Fourier synthesis, however, is the parallel-loaded resonant (PLR) inverter. The basis for the PLR inverter is the resonant circuit shown in Figure 2.10(a); the transfer function of the circuit can be written as

$$\frac{v_\mathrm{O}(\jmath\omega)}{v_\mathrm{I}(\jmath\omega)} = \frac{1}{\left(1 - \frac{\omega^2}{\omega_0^2}\right) + \jmath\left(\frac{1}{Q}\frac{\omega}{\omega_0}\right)}, \tag{2.4.1}$$

where $\jmath$ is the imaginary unit, ω is angular frequency, $\omega_0 = \frac{1}{\sqrt{LC}}$ is the resonant frequency, and $Q = \frac{1}{R}\sqrt{\frac{L}{C}}$ is called the Q-factor. As can be seen from the magnitude and phase spectra shown in Figures 2.10(b) and (c), the circuit presents a voltage gain at the resonant frequency that is sharply dependent on the value of Q: the larger Q is, the greater the gain and the narrower the bandwidth of the resonant circuit. This resonant circuit therefore acts as a frequency-selective gain stage, which forms the core of the PLR inverter's function.

The layout of the cascaded multi-resonant inverter is composed of n PLR inverters connected in series, where each PLR inverter is responsible for a Fourier component; Figure 2.11(a) shows a diagram of this arrangement. The resonant frequency of a PLR

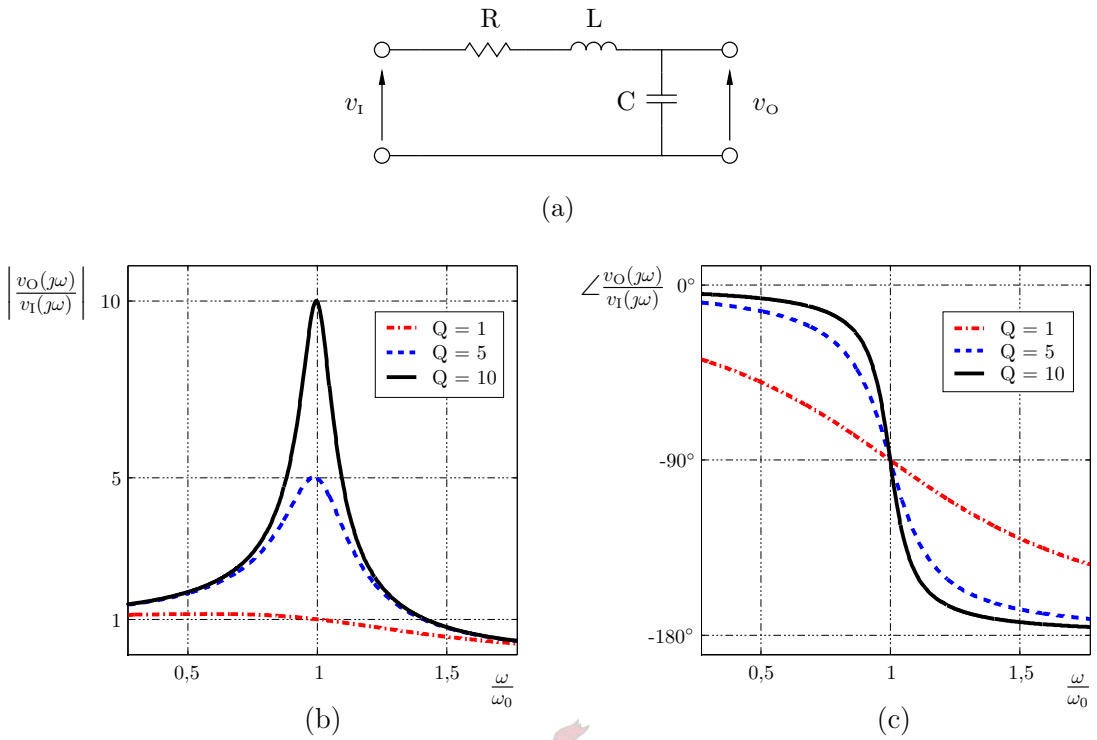

Figure 2.10: (a) The resonant circuit of a PLR inverter, with v_I the input voltage and v_O the output voltage. (b) The magnitude spectrum and (c) the phase spectrum of the PLR inverter for respectively $Q = 1$, $Q = 5$ and $Q = 10$.

inverter is set to the frequency of the Fourier component that it is to generate; by driving the PLR inverter with a square-wave source (usually a full-bridge inverter), which has a repetition rate that matches the resonant frequency, the resonant circuit lets through only the fundamental frequency of the square wave, resulting in a sinusoidal output voltage that is the generated Fourier component. The Fourier component's amplitude is determined by the Q-factor of the resonant circuit, and a large enough Q makes the use of a step-up transformer unnecessary. Since a PLR inverter acts as an ideal voltage source [72], all the series-connected inverters' outputs are added together, thereby managing the addition of the Fourier components.

Loading effects on the PLR inverters can be investigated by applying the principle of superposition[5]; Figure 2.11(b) shows the load seen by the second PLR inverter in

[5]The principle of superposition states that the response of a linear system driven by multiple independent sources, is the sum of the system's responses to the individual sources driving the system one at a time [78].

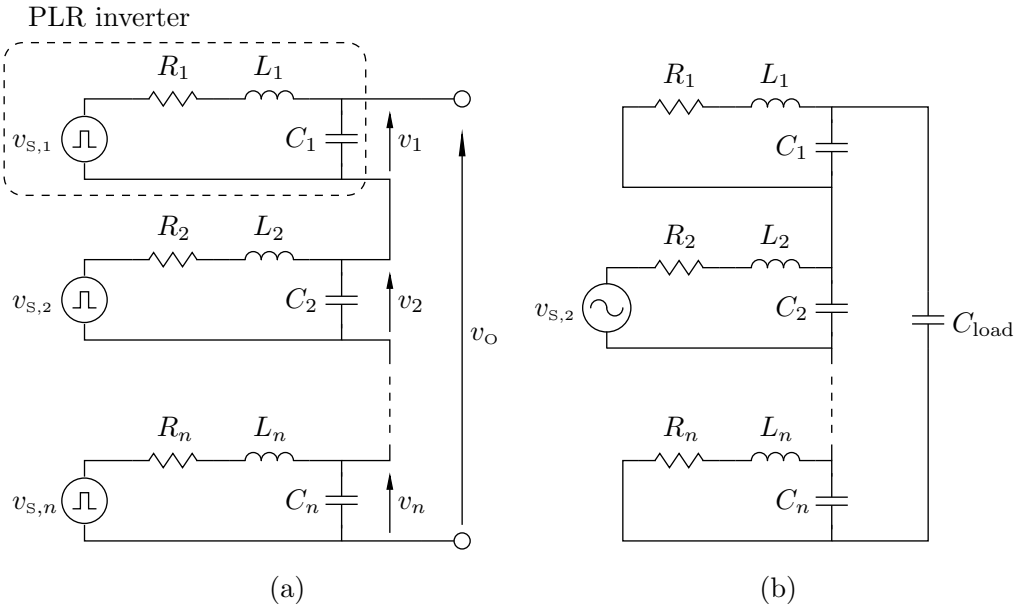

Figure 2.11: (a) A schematic diagram of the cascaded multi-resonant inverter that is composed of n PLR inverters. The outputs of the PLR inverters (v_1,v_2,...,v_n) are the Fourier components. (b) The equivalent circuit diagram of the load seen by the second PLR inverter.

Figure 2.11(a) as an example. The square-wave input voltage is approximated by its fundamental-frequency sinusoid [79], while the other PLR inverters appear as parallel-resonant circuits in series with the capacitive load. Ideally the PLR inverter should be loaded by only the capacitive load; however, if the different PLR inverters' resonant frequencies are too close to each other, the inverters will appear as loads to each other as well[6]. This can be avoided by increasing the Q-factors of the PLR inverters, thereby limiting their loading effects to a small frequency range around their resonant frequencies.

The *cascaded multichannel amplifier* incorporates the ideas discussed in Section 2.2 and adapts them to the requirements of Fourier synthesis. The basic component of the cascaded multichannel amplifier is the amplifier unit: an amplifier unit consists of a Class-AB power amplifier that is connected to a step-up transformer, and driven by a sinusoid generator. Each amplifier unit is designed to generate Fourier components that lie within a specific subrange, or channel, of the system's bandwidth. The addition of the generated Fourier components is managed by connecting the secondary windings of each

[6]The impedance of a parallel-resonant circuit is a maximum at the resonant frequency of the circuit.

amplifier unit's step-up transformer in series. Figure 2.12(a) shows a schematic diagram of such an arrangement, where each step-up transformer is represented by its equivalent circuit model [72]. Finally, the cascaded output voltages of all the amplifier units are connected across the load.

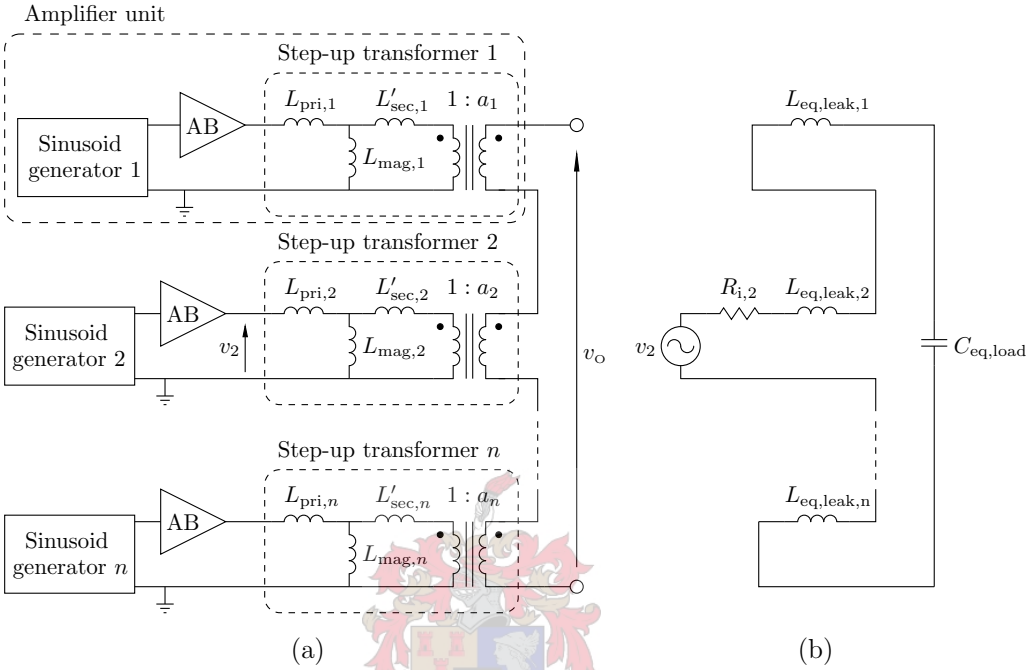

Figure 2.12: (a) A block diagram of the cascaded multichannel amplifier which has n amplifier units and output voltage v_{O}. The amplifier units are connected in series on the secondary sides of their step-up transformers. (b) A circuit diagram of the equivalent load seen by the output of the Class-AB amplifier in the second amplifier unit.

The connection of the transformers is the key to adding the generated Fourier components in the cascaded multichannel amplifier; however, undesirable loading effects can arise from such an arrangement. Using the principle of superposition, Figure 2.12(b) shows the load that is seen by the output of the Class-AB amplifier in the second amplifier unit of Figure 2.12(a) as an example. The Class-AB amplifier acts as an ideal sinusoidal voltage source v_2, with a small internal resistance $R_{\text{i},2}$. The leakage inductances of the transformers (indicated in terms of their equivalent values on the primary

side of step-up transformer 2) are connected in series with the capacitive load[7]. Ideally the Class-AB amplifier should only see the capacitive load; however, for large enough leakage inductances (see Section 2.2.2), the voltage drop across them, which varies for every Fourier component, can introduce distortion in the voltage applied to the load. It is therefore important to minimise the leakage inductances of the transformers.

2.4.2 Feasibility

There are two issues that need to be addressed in order for the Fourier-synthesis approach to be feasible: firstly, the Fourier components have to be generated in such a way that their amplitudes, frequencies and phases can be controlled accurately; and secondly, the Fourier components have to be added in a consistent manner.

The cascaded multi-resonant inverter controls the parameters of each Fourier component through different parts of the relevant PLR inverter. Frequency is determined by the resonant frequency of the PLR inverter; however, a change in the required frequency necessitates a replacement of the inductors and capacitors, which makes the system cumbersome. Amplitude and phase are governed by the square-wave source; since the proper addition of the Fourier components require that the PLR inverters have high Q-factors, these parameters are, however, very dependent on frequency, with any slight deviation in the frequency from the resonant frequency introducing large distortion.

The cascaded multichannel amplifier controls each Fourier component's parameters entirely through the sinusoid generators of the relevant amplifier units. The sinusoid generators can be implemented with digital electronics, thereby providing easy and comprehensive control over the Fourier components. The correct addition of the Fourier components require that the step-up transformers have low leakage inductances. Since each amplifier unit is designed for a specific channel of the bandwidth, the step-up transformers need only be designed for the lowest frequency in their assigned channels, as opposed to the lowest frequency requirement of the whole system; furthermore, individual Fourier components require lower voltages than the resultant arbitrary waveform to be applied to the load. Taking these two considerations into account, the necessary size of the transformers are greatly reduced, thereby decreasing their leakage inductances.

[7]The magnetisation inductances of the transformers are normally sufficiently large, and the output impedances of the other Class-AB amplifiers sufficiently small, to be safely ignored in this investigation.

The cascaded multi-resonant inverter requires exact frequency control in all of its PLR inverters in order to operate properly; the implementation of this topology is therefore difficult. On the other hand, the proposed cascaded multichannel amplifier promises easy control and accurate generation of the Fourier components, and is therefore the most suitable topology for arbitrary-waveform generation.

2.5 Summary

A set of design guidelines for an arbitrary-waveform power supply are presented. The combination of high voltages and large bandwidth makes the selection of a suitable power-supply topology especially difficult.

It is found that the approach based on the use of a power amplifier that is connected to a step-up transformer, does not meet the requirements for an arbitrary-waveform power supply. The main problem lies with the high leakage inductance of the step-up transformer, which, combined with the capacitive load, limits the bandwidth of the system.

An approach based on multilevel inverters is a viable option for the generation of high-voltage arbitrary waveforms. The overall size of the required system, however, makes the driving circuits difficult to implement, and the system as a whole costly. The stepped nature of multilevel inverters' voltage waveforms is also undesirable.

Fourier synthesis is suggested as a means for arbitrary-waveform generation. The first of the Fourier-synthesis topologies proposed, the cascaded multi-resonant inverter, proves too difficult to control. The cascaded multichannel amplifier, on the other hand, potentially offers easy control and accurate generation of arbitrary voltage waveforms, and is therefore selected for this project.

Chapter 3

Fourier analysis of electronic systems and signals

The proposed topology for the arbitrary-waveform power supply is the cascaded multichannel amplifier. This power supply consists of several amplifier units, with each unit having a sinusoid generator, Class-AB amplifier and step-up transformer. The cascaded multichannel amplifier is based on the concept of Fourier synthesis, and this forms the focus of the present chapter. First, the Fourier theory of the periodic signals that are to be generated, is discussed. This is followed by a look at how electronic systems can be characterised in the frequency domain. Next, the effects that the cascaded multichannel amplifier has on the signals it generates, are considered. The chapter ends with a summary.

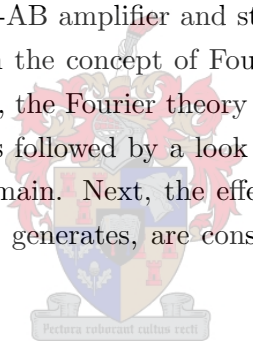

3.1 Fourier theory of periodic functions

It is well established that periodic functions can be represented by their Fourier-series expansions. Let $x(t)$ be a complex, time-dependent function that is piecewise continuous, periodic with period T_0, and square-integrable[1] over any time interval of length T_0; $x(t)$

[1] A function $x(t)$ is square-integrable over a time interval T, if

$$\int_{t_0}^{t_0+T} \left|x(t)\right|^2 \mathrm{d}t < +\infty,$$

where t_0 is an arbitrary point in time.

can then be expanded into a complex exponential Fourier series, i.e.

$$x(t) = \sum_{n=-\infty}^{\infty} X_n \, \mathrm{e}^{\jmath 2\pi n f_0 t}, \tag{3.1.1}$$

where $f_0 = \frac{1}{T_0}$ is the repetition rate and

$$X_n = \frac{1}{T_0} \int_{t_0}^{t_0+T_0} x(t) \, \mathrm{e}^{-\jmath 2\pi n f_0 t} \, \mathrm{d}t \tag{3.1.2}$$

are the complex Fourier coefficients of $x(t)$. The Fourier-series expansion in Equation 3.1.1 is an exact representation of $x(t)$ for all t, except at points of jump discontinuity, where the series converges to the arithmetic mean of the left- and right-hand limits. Furthermore, the functions $\left\{\mathrm{e}^{\jmath 2\pi n f_0 t}\right\}$ form a complete, orthonormal basis set of $x(t)$, making the Fourier-series expansion of $x(t)$ unique — once the Fourier expansion of a periodic function is found, there exist no other Fourier expansions for that function. If $x(t)$ is real, and one writes Equation 3.1.2 in terms of its magnitude and argument, i.e.

$$X_n = |X_n| \, \mathrm{e}^{\jmath \angle X_n}, \tag{3.1.3}$$

then Equation 3.1.1 can be written in an equivalent trigonometric form:

$$x(t) = X_0 + 2 \sum_{n=1}^{\infty} |X_n| \cos\left(2\pi n f_0 t + \angle X_n\right). \tag{3.1.4}$$

X_0 represents the time-average component of $x(t)$, while the $n = 1$ term is called the fundamental component, the $n = 2$ term is called the second harmonic component, and so forth. A real, periodic function can therefore be expressed as a superposition of Fourier components, with each component's amplitude and phase shift determined by a single Fourier coefficient, and its frequency equal to an integer multiple of the repetition rate.

A periodic function can be completely synthesised from its Fourier-series expansion, granted that the Fourier coefficients and repetition rate of the function are known. The Fourier series, however, proves cumbersome when used to analyse periodic functions, due to its discrete representation of periodic functions in the frequency domain. The continuous Fourier transform, on the other hand, maps functions to continuous spectra of their frequency components, thereby providing an elegant means of investigating the characteristics of those functions. It is thus desirable to compose and analyse periodic

functions via Fourier transforms. The continuous Fourier transform [80, 81] of a function $x(t)$ is defined as

$$X(f) = \mathscr{F}\{x(t)\} = \int_{-\infty}^{\infty} x(t)\,\mathrm{e}^{-\jmath 2\pi f t}\,\mathrm{d}t, \tag{3.1.5}$$

where $\mathscr{F}\{\cdot\}$ is the Fourier transform operator and f is frequency. The Fourier transform $X(f)$ can be seen as a complete, complex, frequency-domain representation of the time-dependent function $x(t)$. The inverse Fourier transform, which is symbolised by the operator $\mathscr{F}^{-1}\{\cdot\}$ and defined as

$$\mathscr{F}^{-1}\{X(f)\} = \int_{-\infty}^{\infty} X(f)\,\mathrm{e}^{\jmath 2\pi f t}\,\mathrm{d}f = x(t), \tag{3.1.6}$$

converts the Fourier transform $X(f)$ back to the time domain. Sufficient conditions for a function to have a Fourier transform are given by Dirichlet's conditions [80].

Periodic functions do not have Fourier transforms in the strict mathematical sense, but their Fourier coefficients can be expressed in terms of the Fourier transform through the Poisson summation formula [80]:

$$x(t) = \sum_{m=-\infty}^{\infty} p(t - mT_0) = f_0 \sum_{n=-\infty}^{\infty} P(nf_0)\,\mathrm{e}^{\jmath 2\pi n f_0 t}. \tag{3.1.7}$$

In Equation 3.1.7, $x(t)$ is periodic with period T_0 and qualifies to have a Fourier-series expansion, while $p(t)$ is a pulse-like function that has the Fourier transform $P(f) = \mathscr{F}\{p(t)\}$. The Poisson summation formula states that the sample values $P(nf_0)$ of $P(f)$, multiplied by the repetition rate f_0, are the Fourier coefficients of $x(t)$, i.e. $X_n = f_0 P(nf_0)$. Substitution of this result into Equation 3.1.4 shows that a periodic function's Fourier components can therefore be determined by the Fourier transform of a pulse-like function. The pulse-like function $p(t)$ in Equation 3.1.7 is chosen to coincide with the waveform of the periodic function, since the waveform is normally used, in combination with the repetition rate, to specify a periodic function. The waveform $p_{\mathrm{w}}(t)$ of a periodic function $x(t)$ can be defined as

$$p_{\mathrm{w}}(t) = \begin{cases} 0 & t \leq 0, \\ x_1(t) & 0 < t \leq 1, \\ 0 & t > 1, \end{cases} \tag{3.1.8}$$

where $x_1(t)$ is $x(t)$ with a normalised repetition rate; Figure 3.1 illustrates a triangu-

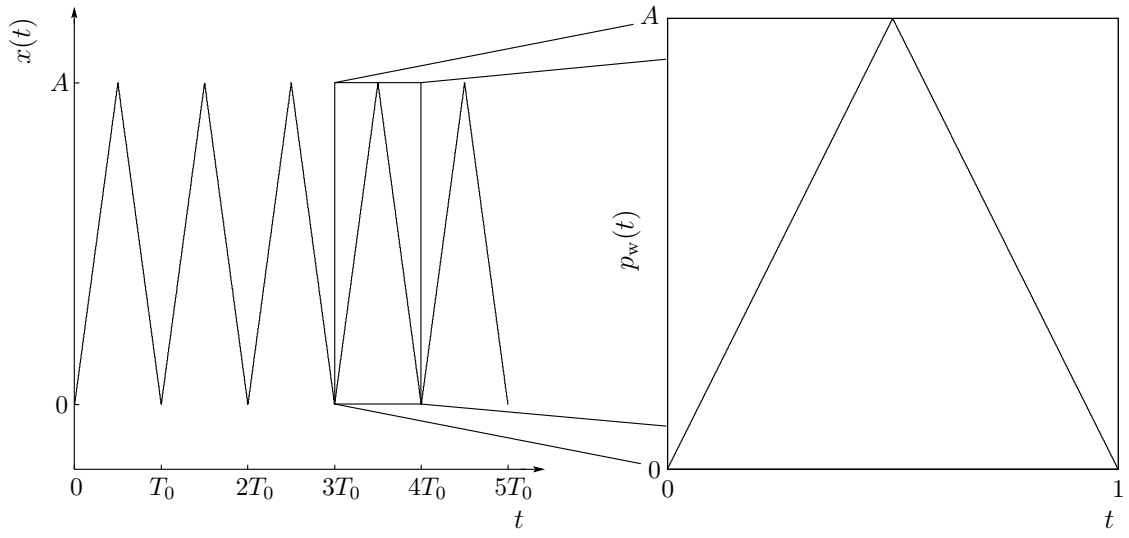

Figure 3.1: The wave shape of a periodic function $x(t)$ can be represented by the waveform function $p_{\mathrm{w}}(t)$, which in this case is the triangular waveform.

lar waveform as an example. Using Equation 3.1.8 and the scale-change theorem [80], Equation 3.1.7 can be written as

$$x(t) = \sum_{m=-\infty}^{\infty} p_{\mathrm{w}}\left(\frac{t - mT_0}{T_0}\right) = \sum_{n=-\infty}^{\infty} P_{\mathrm{w}}(n)\, \mathrm{e}^{\jmath 2\pi n f_0 t}, \tag{3.1.9}$$

where $P_{\mathrm{w}}(f) = \mathscr{F}\{p_{\mathrm{w}}(t)\}$. The left-hand side of Equation 3.1.9 expresses $x(t)$ as a superposition of all the individual periods that constitute it, while the right-hand side is the Fourier-series expansion of $x(t)$, with $X_n = P_{\mathrm{w}}(n)$. Equation 3.1.4 can thus be rewritten as

$$x(t) = |P_{\mathrm{w}}(0)| + 2\sum_{n=1}^{\infty} |P_{\mathrm{w}}(n)| \cos\big(2\pi n f_0 t + \angle P_{\mathrm{w}}(n)\big). \tag{3.1.10}$$

It is clear from Equation 3.1.10 that a periodic function's Fourier components can be completely specified in terms of the repetition rate and the Fourier transform of the waveform. Periodic functions can thus be synthesised by utilising the Fourier transform.

The full utility of the Fourier transform lies in the analysis of functions in the frequency domain. Periodic functions can be synthesised in terms of the Fourier transforms of their waveforms, according to Equation 3.1.10, but the discrete nature of the equation still limits the analysis of such periodic functions. In order to analyse periodic functions in

the frequency domain, they need to be expressed in terms of the Dirac comb function. The Dirac comb function is defined as

$$\Delta_T(t) = \sum_{m=-\infty}^{\infty} \delta(t - mT), \tag{3.1.11}$$

where T is the period of the Dirac comb function, and $\delta(t)$ is the Dirac delta function [80, 81] that defines an unit impulse. The Dirac comb function is therefore an infinite series of unit impulses separated by intervals of T. Using Equations 3.1.9 and 3.1.11, together with the sifting property [80, 81] of $\delta(t)$, the periodic function $x(t)$ can be expressed as

$$\begin{aligned} x(t) = \sum_{m=-\infty}^{\infty} p_{\mathrm{w}}\left(\frac{t - mT_0}{T_0}\right) &= \sum_{m=-\infty}^{\infty} \int_{-\infty}^{\infty} p_{\mathrm{w}}\left(\frac{\lambda}{T_0}\right) \delta(t - mT_0 - \lambda)\,\mathrm{d}\lambda \\ &= \int_{-\infty}^{\infty} p_{\mathrm{w}}\left(\frac{\lambda}{T_0}\right) \sum_{m=-\infty}^{\infty} \delta(t - \lambda - mT_0)\,\mathrm{d}\lambda \\ &= \int_{-\infty}^{\infty} p_{\mathrm{w}}\left(\frac{\lambda}{T_0}\right) \Delta_{T_0}(t - \lambda)\,\mathrm{d}\lambda \\ &= p_{\mathrm{w}}\left(\frac{t}{T_0}\right) * \Delta_{T_0}(t), \end{aligned} \tag{3.1.12}$$

where $*$ is the convolution operator. The convolution [80, 81] of two functions $f(t)$ and $g(t)$ is defined as

$$f(t) * g(t) = \int_{-\infty}^{\infty} f(\lambda)\, g(t - \lambda)\,\mathrm{d}\lambda. \tag{3.1.13}$$

According to Equation 3.1.12, a periodic function can be synthesised by convolving its waveform with a Dirac comb function. The Dirac comb function acts as a replicator, repeating the waveform $p_{\mathrm{w}}\left(\frac{t}{T_0}\right)$ with a period of T_0; Figure 3.2 illustrates this replicating effect for the case where $x(t)$ is a triangular wave. The Dirac comb function is furthermore pivotal in the frequency-domain analysis of periodic functions: periodic functions can only be considered to have Fourier transforms, if their Fourier transforms are expressed in terms of the Dirac comb function. It can be shown [80, 81] that the Dirac comb

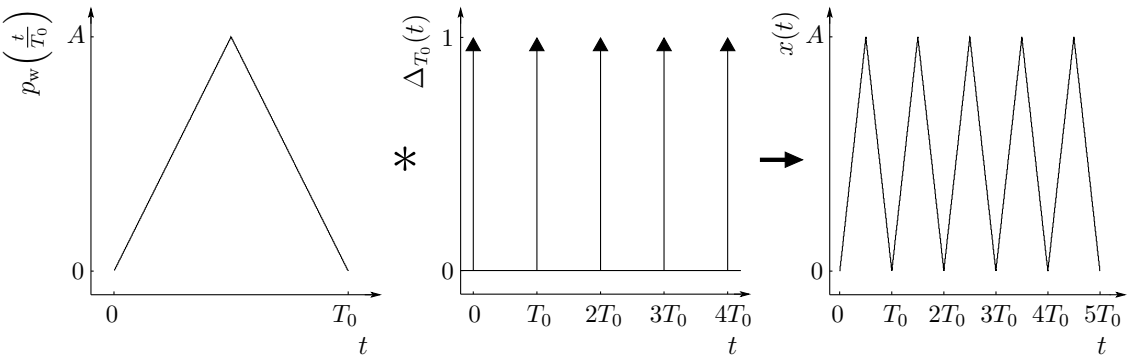

Figure 3.2: The triangular wave $x(t)$, which has period T_0 and amplitude A, can be obtained by convolving its waveform function $p_{\mathrm{w}}\left(\frac{t}{T_0}\right)$ with the Dirac comb function $\Delta_{T_0}(t)$.

function, although periodic itself, can be considered to have a Fourier transform, i.e.

$$\begin{aligned}\mathscr{F}\{\Delta_{T_0}(t)\} &= \mathscr{F}\left\{\sum_{m=-\infty}^{\infty}\delta(t-mT_0)\right\}\\ &= f_0\sum_{n=-\infty}^{\infty}\delta(f-nf_0)\\ &= f_0\,\Delta_{f_0}(f).\end{aligned} \tag{3.1.14}$$

Thus, the Fourier transform of the Dirac comb function is itself another Dirac comb function. Using Equations 3.1.12 and 3.1.14, the convolution theorem[2] and the scale-change theorem, the Fourier transform of a periodic function $x(t)$ can be expressed as follows:

$$\begin{aligned}X(f) &= \mathscr{F}\left\{p_{\mathrm{w}}\left(\frac{t}{T_0}\right) * \Delta_{T_0}(t)\right\}\\ &= P_{\mathrm{w}}\left(\frac{f}{f_0}\right)\Delta_{f_0}(f).\end{aligned} \tag{3.1.15}$$

The Dirac comb function acts as a sampler in Equation 3.1.15, causing the spectrum of the periodic function to be impulsive. Figures 3.3(a) and (b) are respectively the double-sided magnitude and phase spectra of the triangular wave from Figure 3.2, and illustrate the sampling effect of the Dirac comb function. Equation 3.1.15 can hence be

[2]The convolution theorem [80, 81] states that convolution in the time domain translates to multiplication in the frequency domain over the Fourier transform.

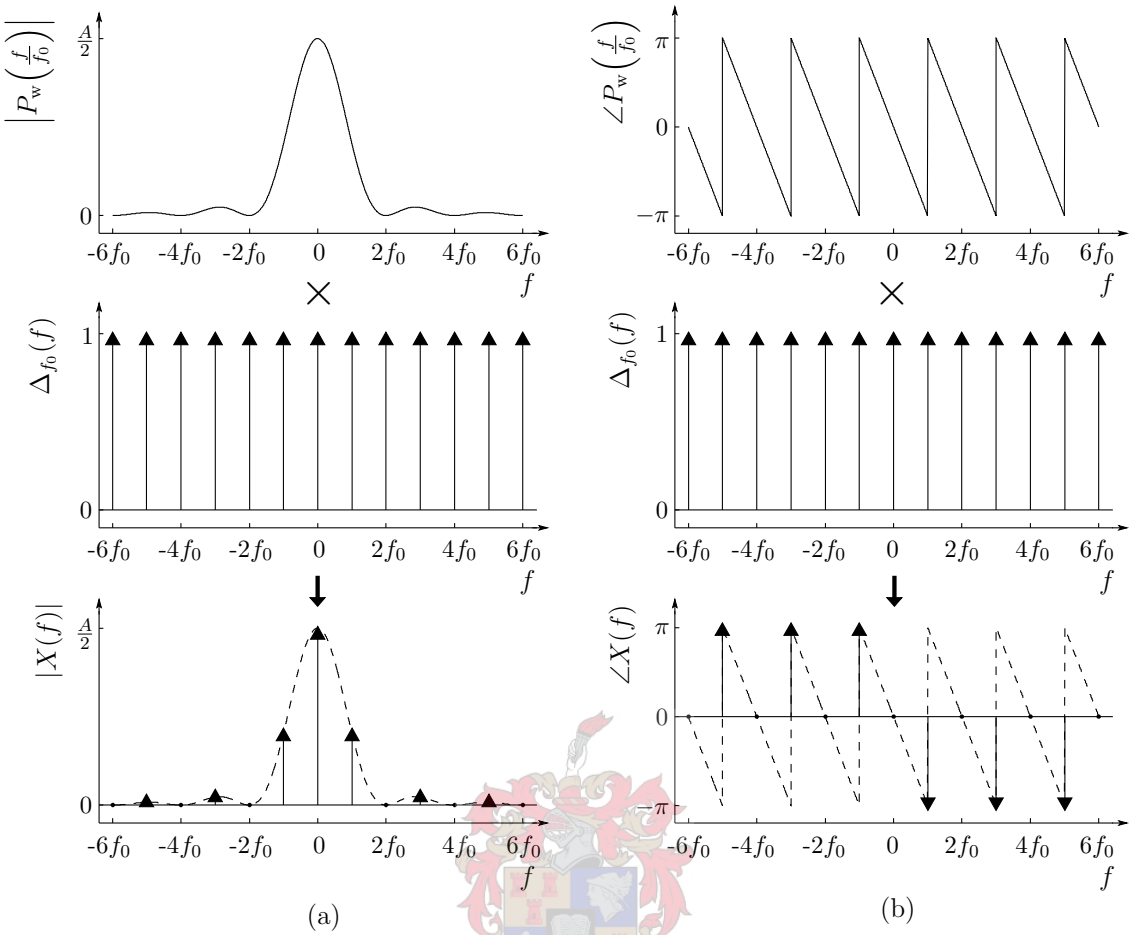

Figure 3.3: (a) The double-sided magnitude spectrum $|X(f)|$ and (b) the double-sided phase spectrum $\angle X(f)$ of the triangular wave $x(t)$ can be obtained by respectively multiplying the waveform's magnitude spectrum, $\left|P_{\mathrm{w}}\left(\frac{f}{f_0}\right)\right|$, and phase spectrum, $\angle P_{\mathrm{w}}\left(\frac{f}{f_0}\right)$, by the Dirac comb function $\Delta_{f_0}(f)$.

used to determine the parameters of each Fourier component in Equation 3.1.10 from the frequency domain: the n^{th} Fourier component has an amplitude that is the sum of the magnitudes at nf and $-nf$ in the magnitude spectrum, and a phase that is equal to the phase at nf in the phase spectrum. The frequency-domain analysis of periodic functions is therefore made possible through the introduction of the Dirac comb function.

It has been shown in this section that periodic functions can be fully analysed in the frequency domain. The benefits of doing so can now be elucidated by referring to Equation 3.1.15: the waveform and repetition rate of a periodic function can be deter-

mined independently by respectively investigating the functions $P_{\mathrm{w}}\left(\frac{f}{f_0}\right)$ and $\Delta_{f_0}(f)$. In the impulsive spectrum of a periodic function, $P_{\mathrm{w}}\left(\frac{f}{f_0}\right)$ determines the amplitudes of the impulses[3], whereas $\Delta_{f_0}(f)$ determines the spacing between the impulses, as is shown in Figure 3.4. Thus, by inspecting a periodic function's Fourier transform, the separate examination of the periodic function's waveform and repetition rate is made possible, in addition to obtaining full knowledge of the periodic function's Fourier components.

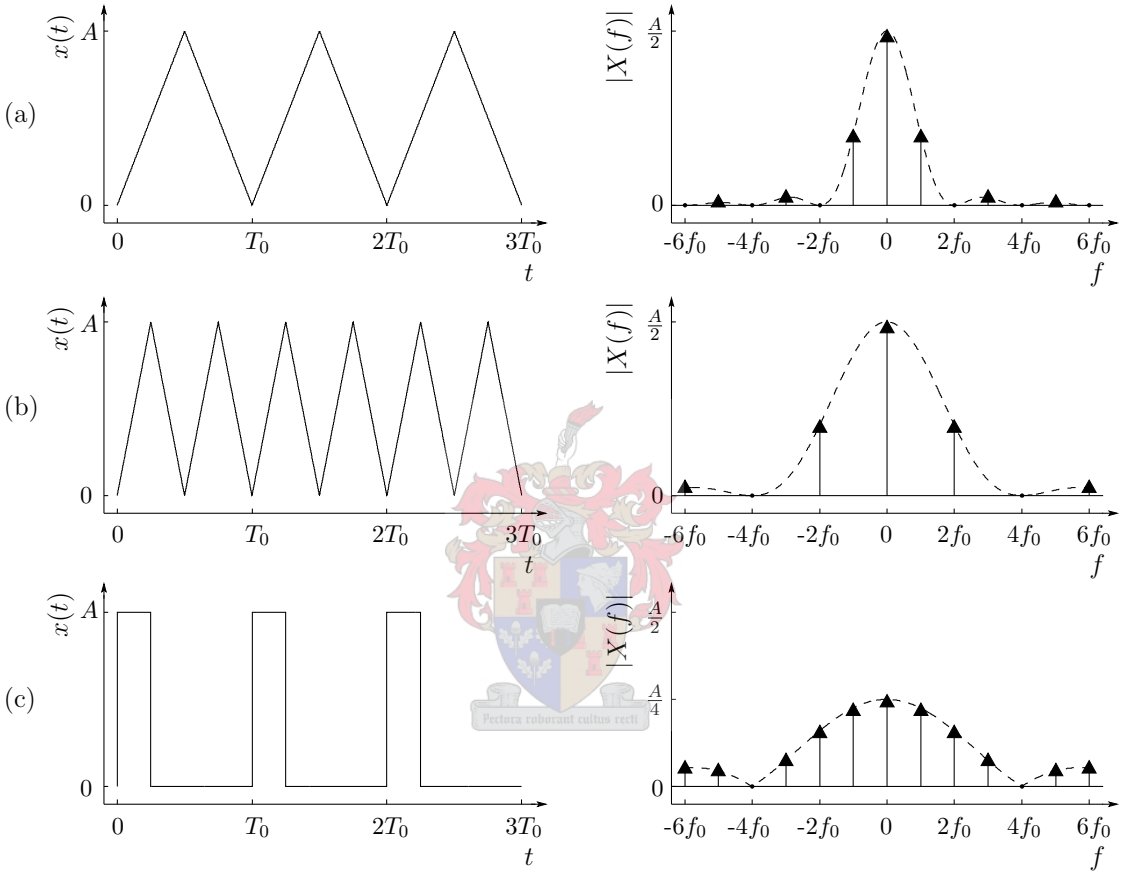

Figure 3.4: (a) A periodic function $x(t)$ that has repetition rate f_0 and a triangular waveform, along with its magnitude spectrum $|X(f)|$. (b) Doubling the repetition rate of $x(t)$ while keeping the waveform constant, leads to a doubling of the spacing between the impulses in the spectrum, with the amplitudes of the impulses staying unchanged. (c) Changing the waveform of $x(t)$ while keeping the repetition rate constant, leads to a change of the amplitudes of the impulses in the spectrum, with the spacing between the impulses staying unchanged.

[3]The amplitude of an impulse refers here to the area under the Dirac delta function.

3.2 Linear, time-invariant systems

Any system that can be described by a linear, homogeneous differential equation with constant coefficients, is a linear[4], time-invariant[5] (LTI) system [80, 81]. In electronics, electrical circuits with components that behave as resistors, inductors and capacitors, are modelled as LTI systems. Other nonlinear components, such as transistors and operational amplifiers, can be approximated as being linear within certain sets of conditions, and are therefore included in LTI system descriptions. Electronic components that cannot be linearised, are characterised through simulation.

In general, a single-input, single-output, electronic system is symbolically written as

$$y(t) = \mathscr{H}[x(t)]\,, \tag{3.2.1}$$

where the input $x(t)$ and output $y(t)$ are real, time-dependent voltage and/or current signals, and the operator $\mathscr{H}$ represents the operation of the electronic system. Using this notation, a LTI system can be entirely characterised in the time domain by the output of the system to a unit impulse applied at $t = 0\,\mathrm{s}$, i.e.

$$h(t) = \mathscr{H}[\delta(t)]\,, \tag{3.2.2}$$

where $\delta(t)$ is the Dirac delta function. $h(t)$ is known as the impulse response of the system. The relation between the output $y(t)$ and an arbitrary input $x(t)$ of a LTI system can be shown [80, 81] to be the convolution of the system's impulse response with the input, i.e.

$$y(t) = h(t) * x(t) = \int_{-\infty}^{\infty} h(t-\lambda)x(\lambda)\,\mathrm{d}\lambda. \tag{3.2.3}$$

Conversely, a LTI system can be fully characterised in the frequency domain by its transfer function $H(f) = \mathscr{F}\{h(t)\}$. By taking the Fourier transform of Equation 3.2.3 and using

[4] In a linear system, given that the inputs $x_1(t)$ and $x_2(t)$ respectively result in the outputs $y_1(t)$ and $y_2(t)$, and that α_1 and α_2 are arbitrary constants, the input $\alpha_1 x_1(t) + \alpha_2 x_2(t)$ produces the output

$$\begin{aligned} y(t) = \mathscr{H}[\alpha_1 x_1(t) + \alpha_2 x_2(t)] &= \alpha_1 \mathscr{H}[x_1(t)] + \alpha_2 \mathscr{H}[x_2(t)] \\ &= \alpha_1 y_1(t) + \alpha_2 y_2(t), \end{aligned}$$

irrespective of the choice of $x_1(t)$ and $x_2(t)$.

[5] In a time-invariant system, a delayed input $x_1(t - t_0)$ results in the delayed output

$$y_1(t - t_0) = \mathscr{H}[x_1(t - t_0)]$$

for all t_0 and $x_1(t)$.

the convolution theorem, the output of the system in the frequency domain is given by

$$Y(f) = \mathscr{F}\{h(t) * x(t)\} = H(f)\,X(f), \tag{3.2.4}$$

where $Y(f) = \mathscr{F}\{y(t)\}$ and $X(f) = \mathscr{F}\{x(t)\}$[6]. The transfer function can thus be written as

$$H(f) = \frac{Y(f)}{X(f)}. \tag{3.2.5}$$

Since $Y(f)$, $X(f)$ and $H(f)$ are all complex functions, they are customarily analysed in terms of their magnitude and phase spectra; the magnitude spectrum of $H(f)$ is called the gain of the system, and is defined as

$$|H(f)| = \frac{|Y(f)|}{|X(f)|}, \tag{3.2.6}$$

while the phase spectrum of $H(f)$ is called the phase shift of the system, and is defined as

$$\angle H(f) = \angle Y(f) - \angle X(f). \tag{3.2.7}$$

In practice, LTI systems are specified in terms of their gains and phase shifts.

The response of a LTI system to a real, periodic signal can be investigated easier in the frequency domain than in the time domain. This is due to the fact that the operation of multiple LTI systems on a signal can be calculated by simply multiplying the input signal's Fourier transform by the respective systems' transfer functions, as opposed to calculating multiple convolutions in the time domain. Using Equations 3.1.15 and 3.2.4, the Fourier transform of a LTI system's output to a periodic input is given by

$$\begin{aligned} Y(f) &= H(f)\,P_{\mathrm{w}}\left(\frac{f}{f_0}\right)\Delta_{f_0}(f) \\ &= Y_{\mathrm{w}}(f)\,\Delta_{f_0}(f), \end{aligned} \tag{3.2.8}$$

where $Y_{\mathrm{w}}(f)$ is the Fourier transform of the output's waveform. The output spectrum $Y(f)$ is as impulsive as the input spectrum in Equation 3.1.15, due to the multiplication by the same $\Delta_{f_0}(f)$, but the amplitudes of the impulses are adjusted by the transfer function $H(f)$. The transfer function therefore only affects the waveform $P_{\mathrm{w}}\left(\frac{f}{f_0}\right)$ of the input, and not the repetition rate. The operation of a LTI system on a real, periodic input can be summarised as follows:

[6] All physically-realisable, electronic signals have Fourier transforms [81].

- The magnitude spectrum of the input is attenuated (or amplified) by the gain of the system, resulting in

$$|Y_{\mathrm{w}}(f)| = |H(f)| \cdot \left| P_{\mathrm{w}}\left(\frac{f}{f_0}\right) \right|. \tag{3.2.9}$$

- The phase spectrum of the input is shifted by the phase shift of the system, resulting in

$$\angle Y_{\mathrm{w}}(f) = \angle H(f) + \angle P_{\mathrm{w}}\left(\frac{f}{f_0}\right). \tag{3.2.10}$$

- The repetition rate f_0 of the input is unaffected by the system.

3.3 Practical considerations

The cascaded multichannel amplifier can affect the periodic signals it generates in a number of ways. Section 3.3.1 looks at how limiting the number of generated Fourier components influences the waveform of the intended periodic signal. Section 3.3.2 examines the consequences of using digital electronics to implement the sinusoid generators of the amplifier units, as well as the transfer function that an amplifier unit needs in order to transmit a Fourier component to the load without introducing distortion.

3.3.1 Signal-related effects

The different factors that can impact a periodic signal, can be illustrated more effectively by means of an example. For this purpose, the periodic function $x_{\Pi}(t)$, which is shown in Figure 3.5(a), is introduced. $x_{\Pi}(t)$ is defined as

$$x_{\Pi}(t) = 2 \sum_{\substack{n>0 \\ n \text{ odd}}}^{\infty} |P_{\mathrm{w}}(n)| \cos\big(2\pi n f_0 t + \angle P_{\mathrm{w}}(n)\big); \tag{3.3.1}$$

in Equation 3.3.1, $P_{\mathrm{w}}(\frac{f}{f_0})$ is the Fourier transform of the rectangular waveform, which can be written in terms of the sinc function[7], i.e.

$$P_{\mathrm{w}}\left(\frac{f}{f_0}\right) = AD \operatorname{sinc}\left(\frac{Df}{f_0}\right) \mathrm{e}^{-\jmath\pi D \frac{f}{f_0}}, \tag{3.3.2}$$

[7]The sinc function is defined as

$$\operatorname{sinc}(z) = \frac{\sin(\pi z)}{\pi z}.$$

where A is the amplitude and D the duty cycle[8]. As can be seen in the single-sided[9] magnitude spectrum of $x_{\Pi}(f)$, which is shown in Figure 3.5(b), the example function has half-wave symmetry[10] to ensure that the cores of the step-up transformers are not saturated by dc voltages; this is the reason why $|X_{\Pi}(f)|$ only has odd harmonics.

The cascaded multichannel amplifier consists of a finite number of amplifier units; it is, however, possible for an arbitrary waveform to consist of a very large, even infinite, number of Fourier components. The proposed power supply therefore limits the total number of Fourier components that can be generated, which affects the synthesised waveform. Using the example function $x_{\Pi}(t)$ from Equation 3.3.1, this limitation can be expressed mathematically as the truncation of the summation of Fourier components at the N^{th} component, i.e.

$$x_{\Pi,\text{t}}(t) = 2 \sum_{\substack{n>0 \\ n \text{ odd}}}^{N} |P_{\text{w}}(n)| \cos\big(2\pi n f_0 t + \angle P_{\text{w}}(n)\big), \tag{3.3.3}$$

where N indicates the number of amplifier units in the power supply. The effect of this truncation is to introduce oscillations around points of discontinuity in the periodic signal, and is known as the Gibbs phenomenon [81]. These oscillations cause the generated periodic signal to overshoot on both sides of any discontinuity, but never by more than 9 % of the amount of the discontinuity. Figures 3.6(a) and (b) show the effects of truncation on $x_{\Pi,\text{t}}(t)$ in respectively the time and frequency domains.

3.3.2 System-related effects

The sinusoid generators of the amplifier units are to be implemented with digital electronics; to study the effect that digital generation of the Fourier components has on the

[8]The duty cycle D of a periodic rectangular function is defined as the ratio between the pulse duration τ and the period T, i.e.

$$D = \frac{\tau}{T}.$$

[9]A function's single-sided magnitude spectrum can be obtained by taking the positive half of the double-sided magnitude spectrum and doubling all the magnitudes for $f > 0$, while keeping the magnitude at $f = 0$ constant.

[10]Half-wave symmetry in a periodic signal $x(t)$ is defined as

$$x\left(t \pm \frac{1}{2}T\right) = -x(t) \qquad \text{for all } t,$$

where T is the period of $x(t)$.

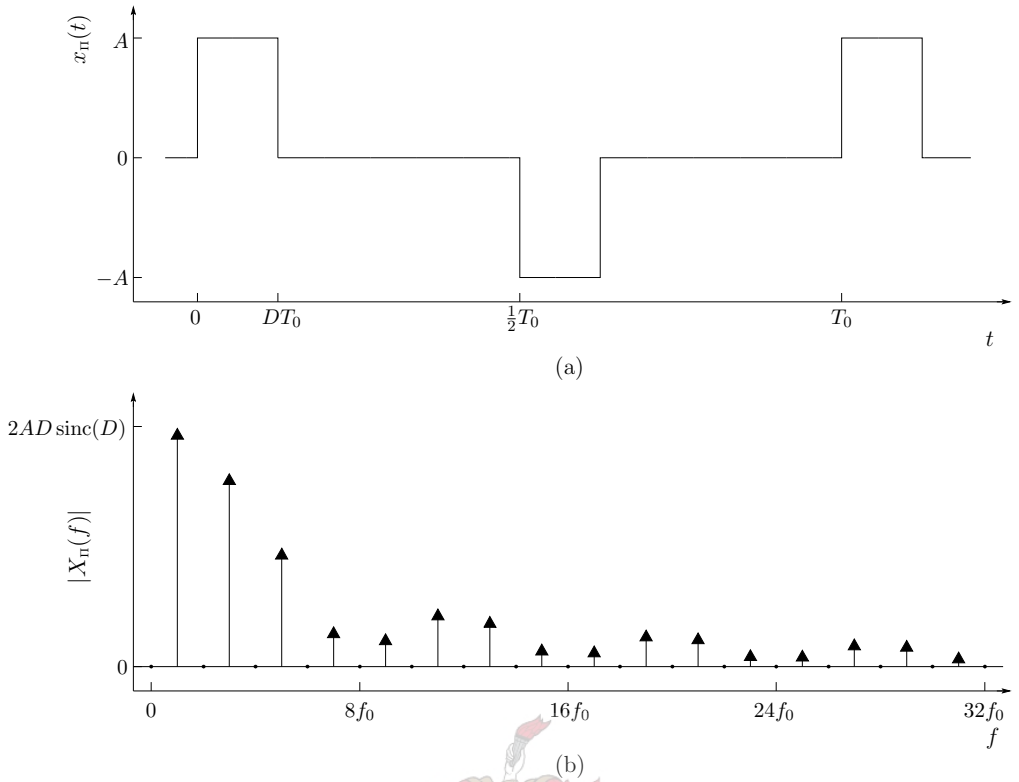

Figure 3.5: (a) An example periodic function $x_\Pi(t)$ that has alternating rectangular pulses as waveform. (b) The single-sided magnitude spectrum of $x_\Pi(t)$, with the first 32 harmonics shown. The half-wave symmetry of $x_\Pi(t)$ means that only odd harmonics have non-zero magnitudes.

output waveform, $x_{\Pi,t}(t)$ from Equation 3.3.3 is used as an example again.

A Fourier component can be represented in digital electronics as a sequence of samples that are separated by the sampling interval T_s; the sampling frequency of a Fourier component with frequency f_c is then given by

$$f_\mathrm{s} = \frac{1}{T_\mathrm{s}} = N f_\mathrm{c}, \tag{3.3.4}$$

where N is the number of samples in a single period of the Fourier component. The digital representation of the n^{th} Fourier component of $x_{\Pi,\mathrm{t}}(t)$, $c_n(t)$, can be written as the multiplication of the Fourier component by a Dirac comb function, i.e.

$$c_n(t) = 2|P_\mathrm{w}(n)| \cos\left(2\pi n f_0 t + \angle P_\mathrm{w}(n)\right) \cdot \Delta_{T_\mathrm{s}}(t). \tag{3.3.5}$$

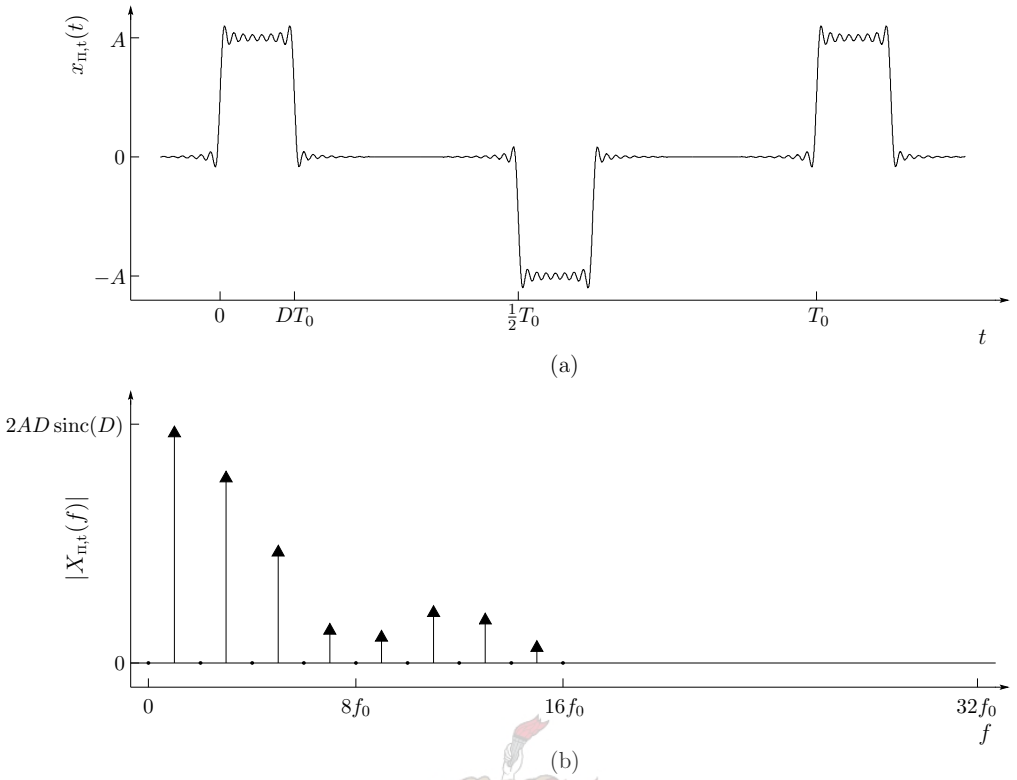

Figure 3.6: (a) The truncation of the number of harmonics leads to oscillations around points of discontinuity in the periodic signal $x_{\Pi,\mathrm{t}}(t)$; $x_{\Pi,\mathrm{t}}(t)$ is synthesised here from its first 64 Fourier components. (b) The single-sided magnitude spectrum of $x_{\Pi,\mathrm{t}}(t)$, which is truncated at the 16^{th} Fourier component.

Figure 3.7(a) displays a digitised Fourier component of $x_{\Pi,\mathrm{t}}(t)$ against time. The sinusoid generator is required to provide an analogue version of $c_n(t)$ to the Class-AB amplifier connected to it. According to the sampling theorem [80, 81], an analogue signal can be accurately reconstructed from its samples, granted that the signal is bandlimited and the sampling frequency f_s is greater than the Nyquist rate[11] f_N. Since $x_{\Pi,\mathrm{t}}(t)$ is already bandlimited, setting $f_\mathrm{s} > f_\mathrm{N}$ ensures that $c_n(t)$ can be accurately reconstructed. Analogue reconstruction is done by a digital-to-analogue converter (DAC); the operation of a DAC can be modelled by a LTI system called the Zero-order hold [80], which has

[11]The Nyquist rate is a property of a bandlimited signal and is equal to twice the largest frequency at which the signal has spectral content. A sampling frequency lower than the Nyquist rate introduces aliasing [80, 81], which makes an accurate reconstruction of the original signal impossible; the Nyquist rate is therefore a lower limit for any acceptable sampling frequency.

the impulse response

$$h_{\mathrm{ZOH}}(t) = \Pi\left(\frac{t - \frac{1}{2}T_\mathrm{s}}{T_\mathrm{s}}\right), \tag{3.3.6}$$

where $\Pi(t)$ is the rectangular function[12]. Using Equations 3.2.3 and 3.3.5, the analogue signal reconstructed from $c_n(t)$ is found to be

$$c_{n,\mathrm{ZOH}}(t) = \Big(2|P_\mathrm{w}(n)|\cos\big(2\pi n f_0 t + \angle P_\mathrm{w}(n)\big)\cdot\Delta_{T_\mathrm{s}}(t)\Big) * h_{\mathrm{ZOH}}(t). \tag{3.3.7}$$

The output of the sinusoid generator (Equation 3.3.7) is therefore an analogue approximation of Equation 3.3.5, and is illustrated in Figure 3.7(b).

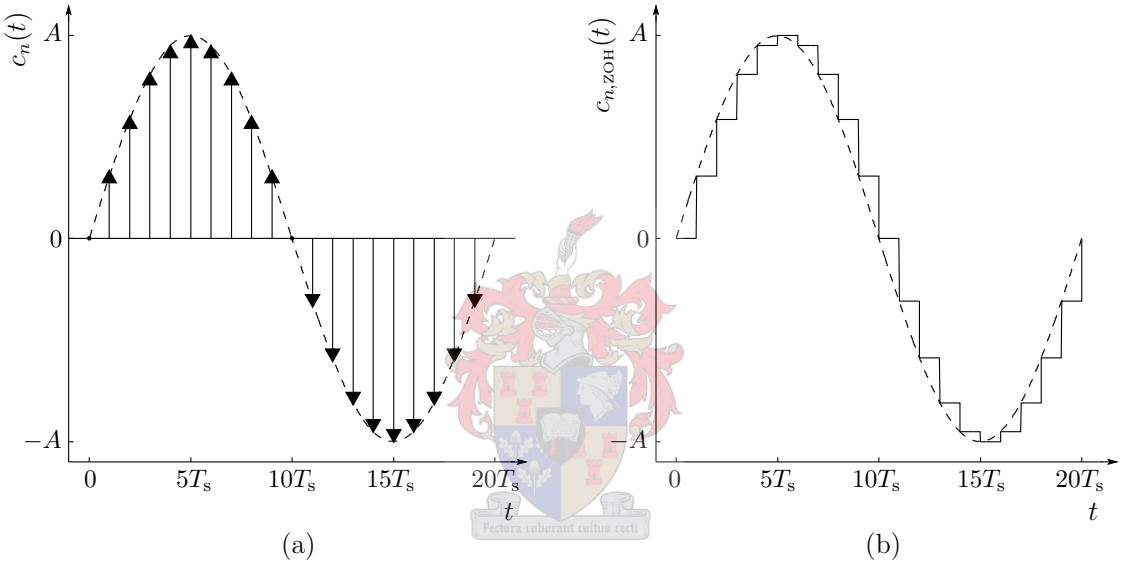

Figure 3.7: (a) A digitised Fourier component $c_n(t)$ that is represented by 20 samples, and has a sampling interval of T_s. (b) The analogue approximation of $c_n(t)$, i.e. $c_{n,\mathrm{ZOH}}(t)$, which is the output of a DAC.

[12]The rectangular function is defined as

$$\Pi(z) = \begin{cases} 0 & |z| > \frac{1}{2}\tau, \\ \frac{A}{2} & |z| = \frac{1}{2}\tau, \\ A & |z| < \frac{1}{2}\tau, \end{cases}$$

where A is the amplitude and τ the width of the rectangle.

The effect that digital generation of a signal's Fourier components has on the signal's waveform, can be elucidated by examining the combined spectra of the separately-generated Fourier components. In order to calculate the combined spectra, the analogue outputs of the different sinusoid generators are first summed; using Equation 3.3.7, the sum of the analogue signals, $x_{\Pi,\mathrm{d}}(t)$, is found to be

$$\begin{aligned} x_{\Pi,\mathrm{d}}(t) &= \sum_{\substack{n>0 \\ n \text{ odd}}}^{N} c_{n,\mathrm{ZOH}}(t) \\ &= \sum_{\substack{n>0 \\ n \text{ odd}}}^{N} \Big(2|P_{\mathrm{w}}(n)| \cos\big(2\pi n f_0 t + \angle P_{\mathrm{w}}(n)\big) \cdot \Delta_{T_{\mathrm{s}}}(t) * h_{\mathrm{ZOH}}(t) \Big) \\ &= \left(2 \sum_{\substack{n>0 \\ n \text{ odd}}}^{N} |P_{\mathrm{w}}(n)| \cos\big(2\pi n f_0 t + \angle P_{\mathrm{w}}(n)\big) \right) \cdot \Delta_{T_{\mathrm{s}}}(t) * h_{\mathrm{ZOH}}(t) \\ &= x_{\Pi,\mathrm{t}}(t) \cdot \Delta_{T_{\mathrm{s}}}(t) * h_{\mathrm{ZOH}}(t). \end{aligned} \tag{3.3.8}$$

The Fourier transform of $x_{\Pi,\mathrm{d}}(t)$ is then

$$X_{\Pi,\mathrm{d}}(f) = X_{\Pi,\mathrm{t}}(f) * \Delta_{f_{\mathrm{s}}}(f) \cdot \mathrm{sinc}\left(\frac{f}{f_{\mathrm{s}}}\right) \mathrm{e}^{-\jmath\pi\frac{f}{f_{\mathrm{s}}}}, \tag{3.3.9}$$

where $X_{\Pi,\mathrm{t}}(f) = \mathscr{F}\{x_{\Pi,\mathrm{t}}(t)\}$; Figure 3.8 illustrates the magnitude spectrum of Equation 3.3.9. A comparison of the spectra in Figure 3.8 and Figure 3.6(b) reveals that the digital generation of the Fourier components has two effects on the periodic signal's magnitude spectrum: firstly, mirror images of $|X_{\Pi,\mathrm{t}}(f)|$ are introduced at multiples of the sampling frequency f_{s}, and secondly, the magnitude spectrum is attenuated by a sinc function that has zero-crossings at multiples of f_{s}[13]. These two effects are unwanted modifications of the intended signal's spectrum, $X_{\Pi,\mathrm{t}}(f)$, and therefore need to be minimised. The effects of digital generation can be reduced in two ways: firstly, by passing $x_{\Pi,\mathrm{d}}(t)$ through a LTI system called a low-pass filter, and secondly, by increasing the sampling frequency. An increase of the sampling frequency shifts the mirror images in Figure 3.8 to higher frequencies, thereby increasing their attenuation by the sinc function in Equation 3.3.9; additionally, the sinc function's distortion of $X_{\Pi,\mathrm{t}}(f)$ is decreased.

Each of the Fourier components that are generated by the sinusoid generators, needs

[13] A comparison of the phase spectra of $X_{\Pi,\mathrm{d}}(f)$ and $X_{\Pi,\mathrm{t}}(f)$ similarly reveals an introduction of mirror images at multiples of f_{s} in the phase spectrum, and a linear phase shift with frequency.

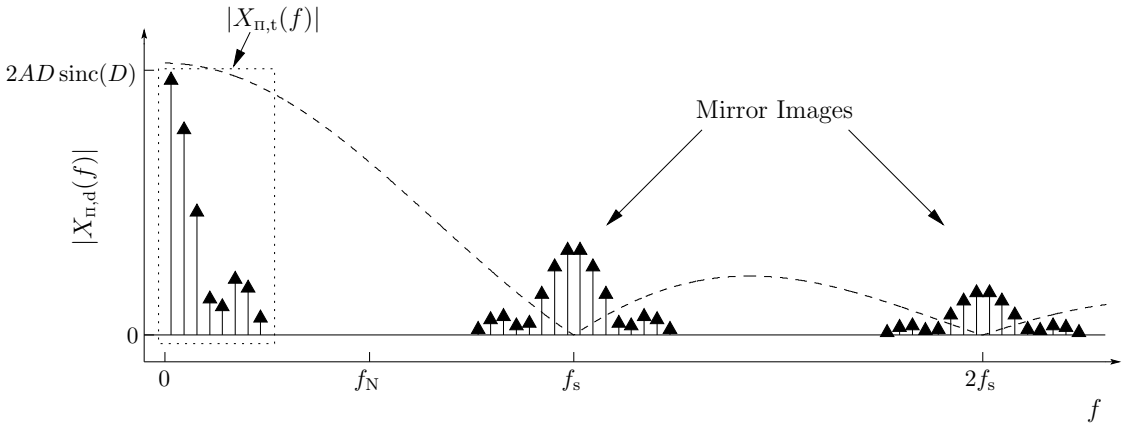

Figure 3.8: The single-sided magnitude spectrum of $x_{\Pi,d}(t)$, showing $|X_{\Pi,t}(f)|$ close to the origin, and mirror images of $|X_{\Pi,t}(f)|$ around multiples of the sampling frequency f_s (the magnitudes of the mirror images are not to scale). The whole spectrum is attenuated by a sinc function, which is indicated by the dashed line. The Nyquist rate f_N is also shown.

to undergo distortionless amplification before being applied to the load; suppression of the mirror images caused by digital generation is also desirable. A LTI system transmits signals without distortion when the system's output $y(t)$ is a scaled, delayed replica of the input $x(t)$, i.e.

$$y(t) = H_0 x\left(t - t_0\right), \tag{3.3.10}$$

where H_0 and t_0 are constants. Using Equation 3.2.5 and the time-delay theorem [80, 81], the transfer function of a distortionless LTI system is found to be

$$H(f) = H_0\, \mathrm{e}^{-\jmath 2\pi f t_0}. \tag{3.3.11}$$

Equation 3.3.11 shows that the characteristics of a distortionless system are constant gain and a linear phase shift with frequency. Ideally the transfer functions of the amplifier units are characterised by Equation 3.3.11 inside the required bandwidth[14] B of the system, with the gain of the Class-AB amplifiers equal to H_0; conversely the amplifier units ideally suppress all signals in the frequency range outside of the system bandwidth. This behaviour is represented by the ideal low-pass filter, which has the transfer function

$$H_{\mathrm{LP}}(f) = H_0\, \Pi\left(\frac{f}{2B}\right) e^{-\jmath 2\pi f t_0}; \tag{3.3.12}$$

[14]The bandwidth of an electronic system is defined as the frequency at which the system's response is at half the maximum power.

Figure 3.9 illustrates $H_{\mathrm{LP}}(f)$. The characteristics of Equation 3.3.12 can, however, only be approximated by electronic circuits[15]; consequently, care must be taken to ensure that the amplifier units operate as closely to the ideal as possible.

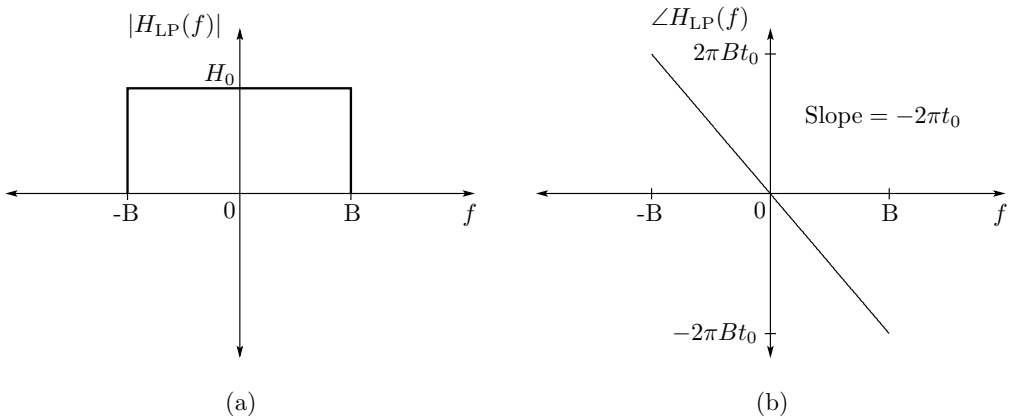

Figure 3.9: (a) The gain and (b) the phase shift of an ideal low-pass filter $H_{\mathrm{LP}}(f)$. The cut-off frequency of $H_{\mathrm{LP}}(f)$ is ideally set to the required bandwidth B of the system.

3.4 Summary

Section 3.1 shows that any periodic signal can be composed by its Fourier components. Furthermore, the utility of the Fourier transform in the analysis of periodic signals is indicated. The decomposition of a periodic signal's frequency-domain description into its waveform and repetition rate proves especially useful for investigating external effects on the signal.

Section 3.2 provides the basis for describing electronic circuits in the frequency domain. The transfer function of a system is defined, and the effects of a system's gain and phase shift on a periodic signal noted.

Section 3.3 discusses the influence that implementation of the cascaded multichannel amplifier has on its generated signals. The finite number of amplifier units leads to the appearance of ringing around discontinuities in the output waveform, whereas the digital

[15]This is mainly due to causality [80] and the presence of stray resistances, capacitances and inductances in components.

generation of the Fourier components introduces mirror images of the signal's spectrum around multiples of the sampling frequency, which requires filtering. Furthermore, the amplifier units can introduce distortion into the generated signal, and must preferably function as ideal low-pass filters.

Chapter 4

Design and implementation of the cascaded multichannel amplifier

Chapter 3 indicated that an arbitrary voltage waveform can be comprised of a large number of Fourier components; furthermore, as described in Chapter 2, the topology of the cascaded multichannel amplifier requires a number of amplifier units to generate the Fourier components. It is therefore necessary to make a compromise between the number of Fourier components that can practicably be generated, and the accuracy with which the arbitrary voltage waveform is to be generated. It was decided that 20 amplifier units would provide sufficient accuracy for arbitrary-waveform generation.

In this chapter, the design and implementation of the cascaded multichannel amplifier is explained. The structure of the chapter generally follows the different stages through which each Fourier component passes in its generation process. The first stage comprises the sinusoid generators, which are responsible for generating small-signal versions of the required Fourier components; the two main aspects concerning the implementation of the sinusoid generators, are their realisation on a digital circuit board and their computer-aided control. The second stage contains the Class-AB amplifiers, which amplify the small-signal Fourier components to the necessary power levels; their implementation consists of twenty variable-gain and power stages. The final stage is composed of the step-up transformers, which ensure the necessary high-voltage amplitudes of the Fourier components and act as their summer.

4.1 The sinusoid generators

The sinusoid generators are the starting point in the generation of the Fourier components. Their function is to produce small-signal Fourier components that already contain the amplitude, frequency and phase information necessary for the intended arbitrary waveform.

It was decided that the sinusoid generators were to be implemented using digital electronics, as such an approach allows the entire system to be controlled from a computer. An overview of the digital design of the sinusoid generators can be given with the help of Figure 4.1. The digital generation of the Fourier components takes place in two logic devices called field-programmable gate arrays (FPGAs); these devices store the digital samples of each Fourier component in a separate internal memory block. A master clock provides the control signal for outputting the digital samples, while digital-to-analogue converters (DACs) are used to convert the outputted digital samples into the small-signal voltages (v_1, v_2, v_3, ...) of the Fourier components. The digital samples are calculated on a computer and loaded into the FPGAs via a microcontroller.

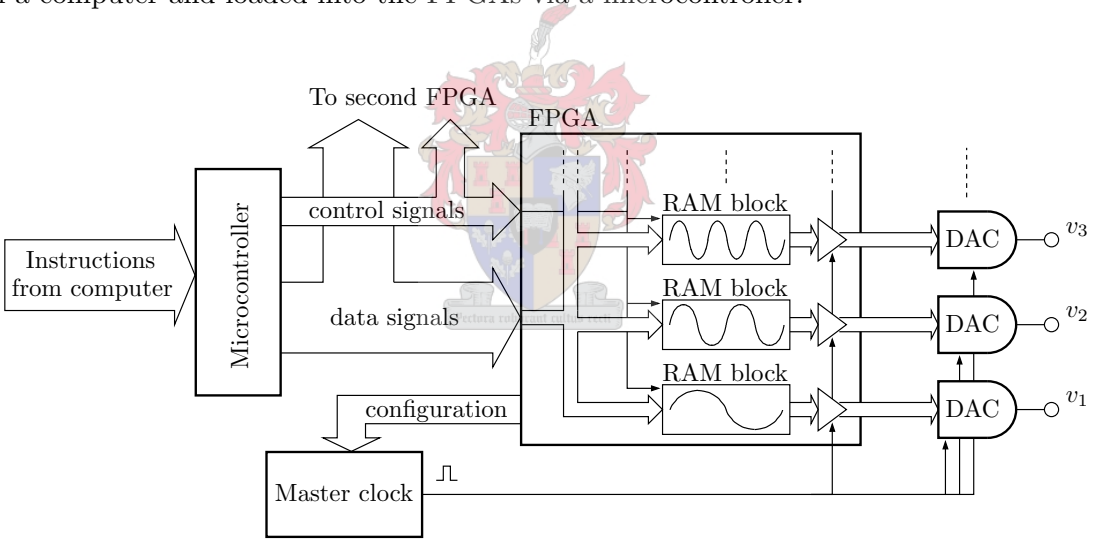

Figure 4.1: A schematic diagram illustrating the interactions between the main elements contributing to the digital generation of the Fourier components.

The details of the digital design are discussed in the following sections. Section 4.1.1 treats the realisation of the sinusoid generators through the digital circuit board, while

Section 4.1.2 discusses how the operation of the sinusoid generators are controlled from a computer.

4.1.1 The digital circuit board

The digital circuit board is the implementation of all the amplifier units' sinusoid generators, and is shown in Figure 4.2. It consists of four main elements: the FPGAs, the master clock, the microcontroller and the DACs. The circuit diagrams that were designed for each of the main elements on the digital board, are found in Appendix A. The operation of the main elements are described in the subsequent subsections.

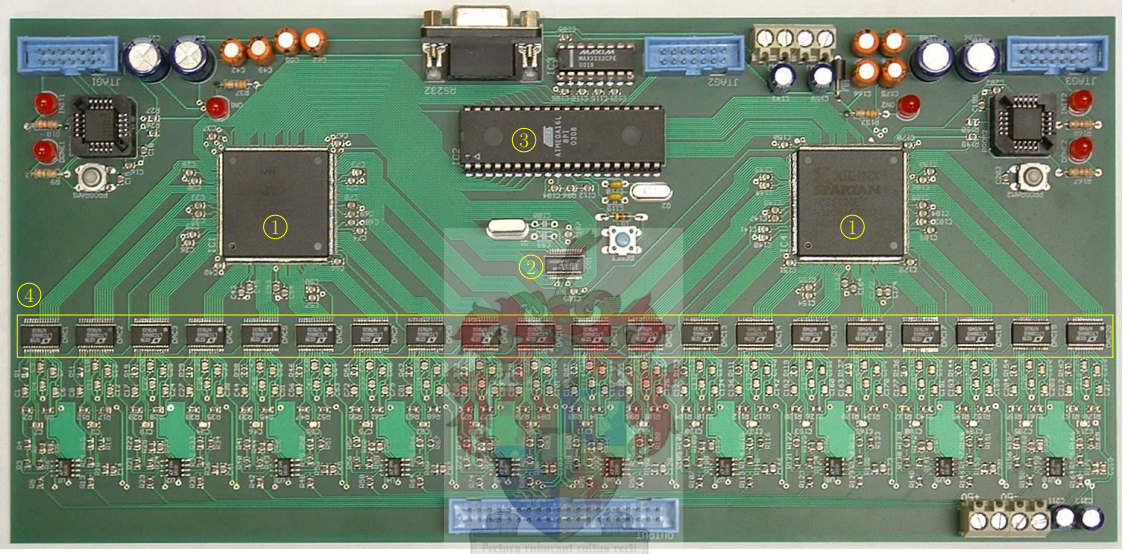

Figure 4.2: The digital circuit board, which has four main elements: (1) the FPGAs, (2) the master clock, (3) the microcontroller, and (4) the DACs.

4.1.1.1 The FPGAs

Two FPGAs were utilised to generate the sinusoids for the 20 amplifier units. The type of FPGA that was selected for use on the digital circuit board, is the Spartan™ IIE XC2S100E-PQ208 from Xilinx[1].

[1]The configuration of each FPGA is managed by a separate programmable read-only memory (PROM), for which the XC18V00 was chosen.

The Spartan IIE has several characteristics that make it suitable for this project. Firstly, each FPGA has 40 Kib of random access memory (RAM) that are divided into ten separately addressable blocks. Each of these RAM blocks can be addressed using different data widths; the data width that was chosen for this project, is 8 bits An 8-bit data width entails that each RAM block can support 512 data points that have 8-bit resolution (i.e. can take on 256 different values). Secondly, the Spartan IIE has 202 input/output (I/O) pins that are user-programmable, which are enough to support all the signals that are required to enter or exit the FPGA. Thirdly, the FPGA is available in a plastic quad flat package (PQFP), which makes mounting and routing of the device on the printed circuit board (PCB) easy.

The operation of the FPGA can be characterised by two modes, depending on the source of its clock signal[2]: a setup mode, in which the microcontroller drives the FPGA's clock signal, and an output mode, in which the master clock drives the clock signal. In the setup mode, the microcontroller loads the set of sampled data points of every Fourier component into a separate RAM block; each of the FPGAs is therefore capable of storing 10 Fourier components. One of the FPGAs also sets the configuration pins of the master clock during the setup mode. In the output mode, on the other hand, the master clock continuously clocks the data points stored in each of the RAM blocks to the DACs; the outputs of the FPGAs are therefore the digital representations of the Fourier components.

4.1.1.2 The master clock

The master clock generates a clock signal that controls the transmission of sinusoid data points from the FPGAs to the DACs. Given that every sinusoid is represented by 512 data points (the size of the RAM block in which it is stored) and that the data points of the different sinusoids are outputted at the same rate (as determined by the master clock), Equation 3.3.4 requires that the frequency information of the Fourier components be maintained by controlling the number of sinusoidal periods that are fitted into each RAM block; for instance, the fundamental component utilises 512 data points to represent a single period, the second harmonic uses 512 data points to represent two periods, and so forth. By setting the master clock to the sampling frequency of the fundamental component, the master clock effectively controls the repetition rate of the arbitrary waveform to be generated.

[2]The FPGA is operated in a synchronous manner, which means that all actions are taken on the rising edge of a global clock signal.

The ICS525-01 OSCaR™ user-configurable clock was chosen to implement the master clock, since it can provide the fast sampling frequencies required (up to 100 MHz), has a high frequency resolution and is easily configured. The frequency of the master clock's output signal is determined by internal dividers on the OSCaR; consequently, the master clock was configured to provide the greatest frequency resolution possible (80 Hz), while supporting repetition rates between 2 kHz and 35 kHz.

4.1.1.3 The microcontroller

The interface between the computer and the digital circuit board is provided by the microcontroller. The functions of the microcontroller are to control the operating states of the FPGAs and the master clock, and to load the sampled data points of the Fourier components into the FPGAs.

The microcontroller operates by receiving instructions from the computer (which is connected through a RS232 serial port), and then performing the necessary actions. The instruction to commence the generation of sinusoids is accompanied by the following data: the repetition rate, and 20 sets of sinusoid data points. The microcontroller uses the repetition rate to calculate the appropriate values for the internal dividers of the master clock, which are then sent to the FPGA that handles the configuration of the master clock; furthermore, each of the 20 data-point sets are loaded by the microcontroller into one of the RAM blocks in the FPGAs. With the FPGAs and the master clock ready for operation, the microcontroller starts the generation of Fourier components by enabling the output of all the RAM blocks. Alternatively, the microcontroller executes the instruction to stop the generation of Fourier components by disabling the output of the FPGAs' RAM blocks.

The microcontroller that was selected for the digital circuit board, is the ATmega16L 8-bit AVR® microcontroller from ATMEL. It was chosen for its large programmable memory (16 KiB), its low operating voltage (2,7 V to 5,5 V) and the number of programmable I/O pins that it has available (32).

4.1.1.4 The DACs

The function of the DACs is to convert the sampled data points outputted by the FPGAs into analogue signals; consequently, the output of each of the 20 RAM blocks located within the FPGAs, is connected to its own DAC. The chosen DAC for this project was the LTC1666IG; it can support the 8-bit digital outputs of the FPGAs, and is fast enough

to accommodate repetition rates of up to 100 kHz (due to its 50 million samples per second update rate).

The operation of the DAC is controlled by the master clock: the same clock signal that outputs a sinusoid data point from the FPGA to the DAC, also enables the DAC to latch the digital value of its input and update its analogue output accordingly. The output of the DAC is a balanced[3] current signal that is fed into a differential amplifier [62]; this arrangement minimises any noise that could be introduced into the output of the DACs. The differential amplifier converts the balanced current signal into an inverted, single-ended[4] voltage signal v_{d}, which it then drives to the next stage, namely the Class-AB amplifier.

4.1.2 Computer-aided control

The sinusoid generators require sampled data points of the Fourier components that they are to generate; thus, a computer program was written to calculate the required data. The advantages of using a computer for this purpose, are that computers have the necessary processing and memory capacities to calculate the Fourier components efficiently, and that existing Fourier transform algorithms, such as the Fast Fourier Transform (FFT) [81], can be utilised. Additionally, the computer program also serves as an user interface for the cascaded multichannel amplifier.

The operation of the computer program contains a number of steps, as is indicated in Figure 4.3. The first step requires the user to input the amplitude, repetition rate and waveform information of the desired output voltage. A FFT algorithm is then used to calculate the single-sided magnitude and phase spectra of the desired waveform, which specify the parameters of the required Fourier components. Next, the number of amplifier units necessary to generate each Fourier component, is determined; each amplifier unit has a limited voltage rating, and Fourier components with large magnitudes therefore require multiple amplifier units to be generated. Starting at the fundamental component, each Fourier component is successively assigned to its allocated number of amplifier units, until all 20 amplifier units have been assigned[5]. Finally, the sinusoid generators on the digital circuit board require sampled data points of the Fourier components; these samples are

[3] A balanced signal is transmitted along two conductors that have the same impedance to ground, with the signals in the two conductors 180° out of phase.

[4] A single-ended signal has a return path that coincides with the ground plane.

[5] The amplifier units are designed for different frequency channels, and Fourier components are therefore assigned to amplifier units that can generate their required frequencies.

calculated by the computer program, using the information from the waveform spectra and the knowledge of how the Fourier components are assigned to the amplifier units. Before commencing, the program displays to the user the waveform to be generated, as reconstructed from the calculated data points; this allows the user to make changes before switching on the power supply. The cascaded multichannel amplifier is then started by sending the necessary control signals, as well as the sampled data points and the requested repetition rate, via a RS232 serial port to the digital circuit board.

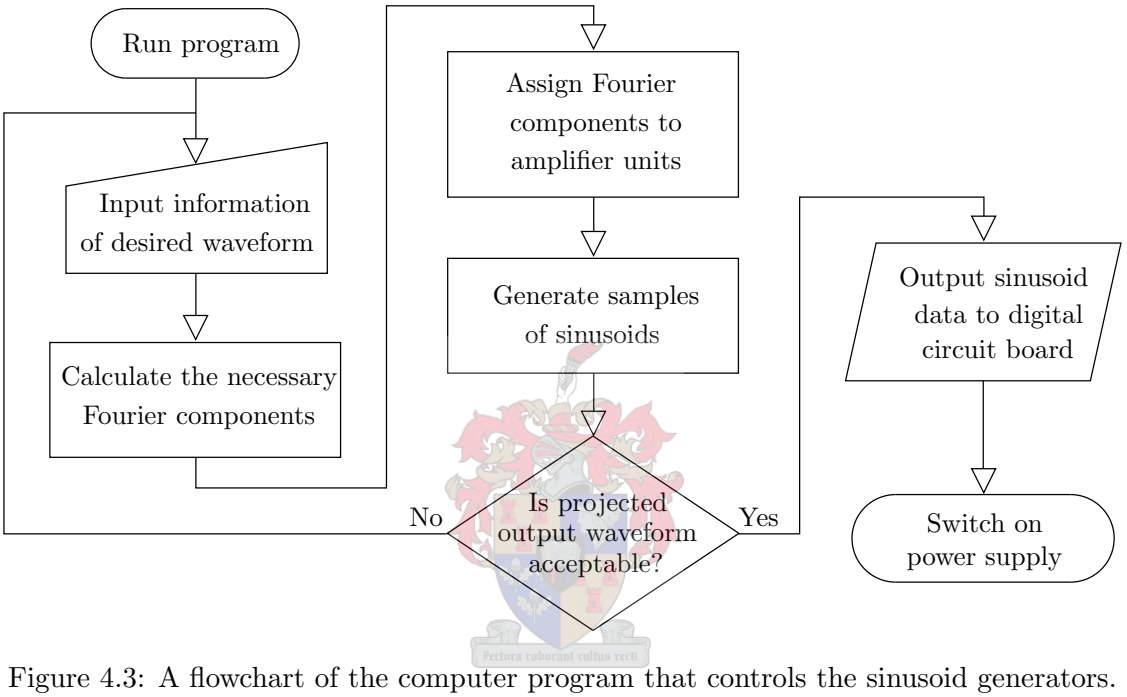

Figure 4.3: A flowchart of the computer program that controls the sinusoid generators.

The computer program was created using the LabVIEW® 7.1 software package.

4.1.3 Summary

The characteristics of the designed sinusoid generators are summarised in Table 4.1.

4.2 The Class-AB amplifiers

As a rule, there exists a trade-off between the gain and bandwidth that are attainable with an electronic amplifier, i.e. amplifiers with large gains have small bandwidths, and vice

Number of sinusoid generators	-	20
Bandwidth	kHz	700
Repetition rate	kHz	2 to 35
Repetition-rate resolution	Hz	80
Number of samples per period	samples	25† to 512‡
Maximum output voltage	mV	230
Amplitude resolution	-	8-bit

†For the 20^{th} harmonic component.

‡For the fundamental component.

Table 4.1: A summary of the characteristics of the designed sinusoid generators.

versa. Taking the design guidelines of Section 2.1 into account, the Class-AB amplifiers of the cascaded multichannel amplifier require large bandwidths in order to amplify the generated sinusoids without introducing distortion. Obtaining such a bandwidth, while still maintaining the necessary overall gain in the system, requires the concatenation of multiple amplification stages. Following the discussion in Section 3.2, it is easy to show that the total gain of the concatenated amplification stages is equal to the product of the gains of the individual stages; the total bandwidth of the multistage system, on the other hand, is determined by the stage with the smallest bandwidth.

Each of the small-signal Fourier components that are generated by the digital circuit board, need to pass through several amplification stages before they can be applied to the step-up transformers, as is indicated in Figure 4.4. Two circuits were designed to implement these amplification stages: the variable-gain stage, which is described in Section 4.2.1, and the power stage, which is described in Section 4.2.2.

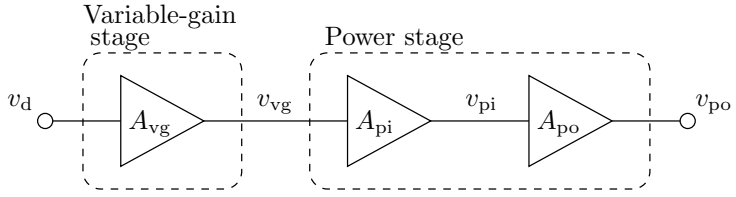

Figure 4.4: The Class-AB amplifier is a concatenation of multiple amplification stages.

4.2.1 The variable-gain stage

The variable-gain stage is the first of the amplification stages that a voltage signal outputted from the digital circuit board, are sent through. The purpose of the variable-gain stage is to facilitate the calibration of the overall gain of the amplification stages from a single point in the circuit.

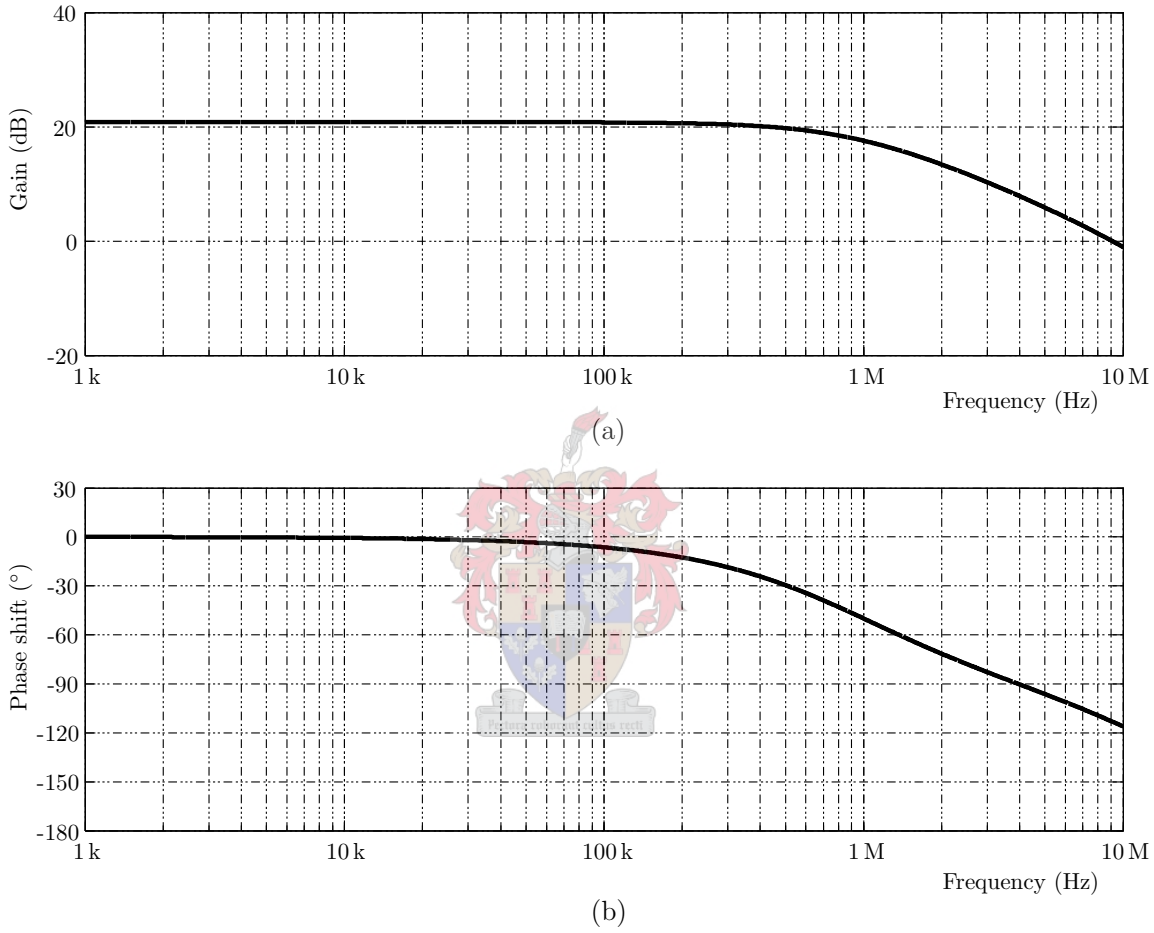

Figure 4.5: The simulation results for the variable-gain stage, in the case of an open load and the gain set to 21 dB: the gain (a) and phase shift (b) of the design are both effectively constant over the bandwidth of the system.

The design of the variable-gain stage can be found in Appendix A. The NE5532AP operational amplifier was chosen to realise the variable-gain stage; the large bandwidth of this operational amplifier (unity-gain bandwidth of 10 MHz), combined with its low

distortion characteristics, makes it a suitable choice. The gain of the variable-gain stage, A_{vg}, was designed to be adjustable from 0 dB to 20,8 dB. A PSpice simulation was run to verify the design, and the results are shown in Figure 4.5 for the case of an open load[6] and maximum gain[7]. The simulation results show that the minimum bandwidth of the design (950 kHz) exceeds the proposed bandwidth of the system (200 kHz), and is therefore acceptable; furthermore, the gain and phase shift of the design are effectively constant over the system bandwidth, which therefore fulfil the requirements of distortionless amplification of the Fourier components. Figure 4.6 shows the circuit board on which the 20 variable-gain stages were implemented.

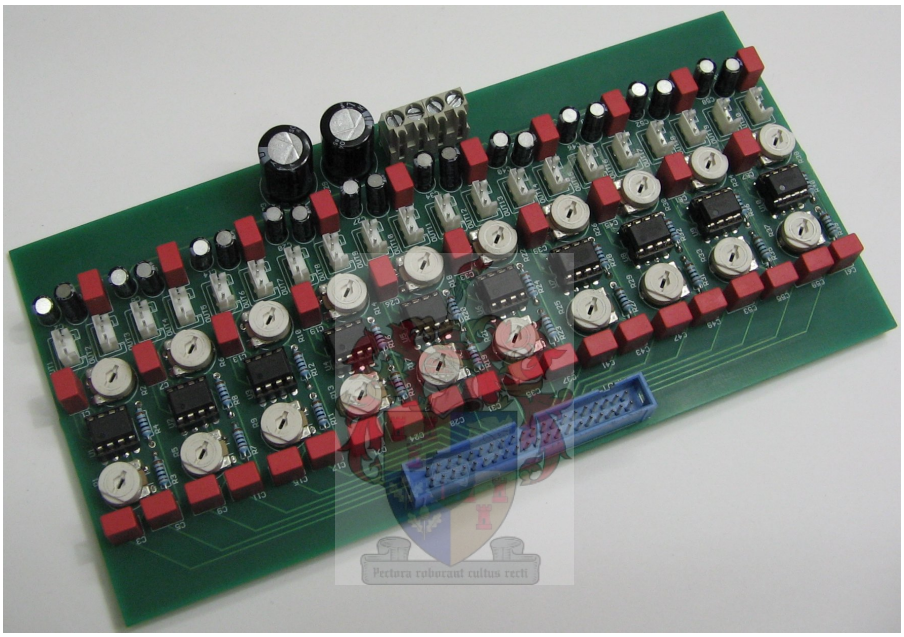

Figure 4.6: The circuit board containing the 20 variable-gain stages; each one of the variable-gain stages is used to calibrate the overall gain of an amplifier unit.

The characteristics of the designed variable-gain stage are summarised in Table 4.2.

[6] An open-load assumption is acceptable, since the input impedance of the power stage is very large.
[7] Maximum gain signifies the worst-case scenario in terms of bandwidth.

Number of variable-gain stages	-	20
Minimum bandwidth	kHz	950
Gain	dB	0 to 20,8
Maximum gain error	dB	0,2
Optimal phase shift	°	0
Maximum phase error	°	−12,6
Maximum input voltage	mV	230
Maximum output voltage	V	1,63

Table 4.2: A summary of the characteristics of the designed variable-gain stages.

4.2.2 The power stage

The power stage is the main amplification stage of a Fourier component, and can be divided into two parts, namely the input stage and the output stage.

The input stage serves as a buffer between the variable-gain stage and the output stage, while also acting as another amplification stage along the path of the Fourier component. The NE5534AP operational amplifier was chosen to implement the input stage; the qualities that make it an appropriate choice, are its large bandwidth (10 MHz unity-gain bandwidth) and high slew rate ($13\,\mathrm{V}\cdot\mu\mathrm{s}^{-1}$ at unity gain). The gain of the input stage, A_{pi}, was designed to have a value of 13,4 dB.

The output stage generates the final voltage signal of the Fourier component that is to be applied to the step-up transformer, and ensures that the necessary current can be sourced to or sinked from the load. The operation of the output stage can be described by means of Figure 4.7, which shows that the circuit forms a closed-loop system that utilises negative feedback [82]; negative feedback is used, since it minimises distortion in the output voltage. The output signal v_{po} is passed through a dynamic-compensation network[8], which is represented by the gain D, and then subtracted from the signal received from the input stage, v_{pi}, which serves as the reference signal for v_{po}. The resulting error signal, v_{e}, is then amplified by the system's open-loop gain K. The gain of the output stage, A_{po}, can be written as

$$A_{\mathrm{po}} = \frac{K}{1 + KD}. \tag{4.2.1}$$

[8]The dynamic compensation network helps the system to suppress high-frequency noise that may appear on the output voltage.

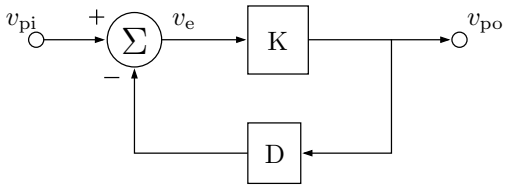

Figure 4.7: A block diagram illustrating the operation of the output stage; the output stage employs negative feedback to minimise distortion in the output voltage of the power stage.

The different elements of Figure 4.7 were implemented in the design of the output stage using various electronic components. A differential amplifier, based on two bipolar junction transistors (BJTs), was used to subtract the output signal from the reference signal. The dynamic compensation network, on the other hand, was formed using passive components. Two power MOSFETs (the IRF530 and IRF9530), connected in a complementary push-pull fashion, were used to drive the output voltage, and were designed to be capable of delivering 10 VA to the output; a biasing network was also set up for the power transistors in order to operate them in a Class-AB mode. The gain A_{po} of the output stage was designed to be 10 dB.

The overall design of the power stage was verified using PSpice simulations, of which the results are shown in Figure 4.8. First of all, the circuit is simulated driving an open load, since this is the ideal case. The results show the design having a good, linear response over the bandwidth of the system, which implies distortionless amplification (the power stage has a 180° phase shift to compensate for the inversion of the voltage signals that takes place at the output of the digital circuit board). The next step in the design process of the power stage is to consider the effects that a load, i.e. the step-up transformers and a DBD cell, has on the operation of the power stage; therefore, further simulations were run. First off, the effect that the capacitive load of the DBD cell has on the output of the power stage, is simulated. A 1 pF DBD load[9], reflected to the primary side of a type 1 transformer (see Section 4.3), is calculated to have a capacitance of 2,7 nF; this scenario represents working with ideal transformers that have zero leakage inductance. As can be seen in Figure 4.8, the capacitive load introduces a pole in the transfer function of the power stage; however, since the pole is far removed from the required bandwidth of the system (i.e. above 3 MHz), the power stage is deemed capable of driving such a capacitive load. Next, the calculated total leakage inductance of the 20

[9]This capacitance is indicative of the size of a typical DBD cell to be investigated.

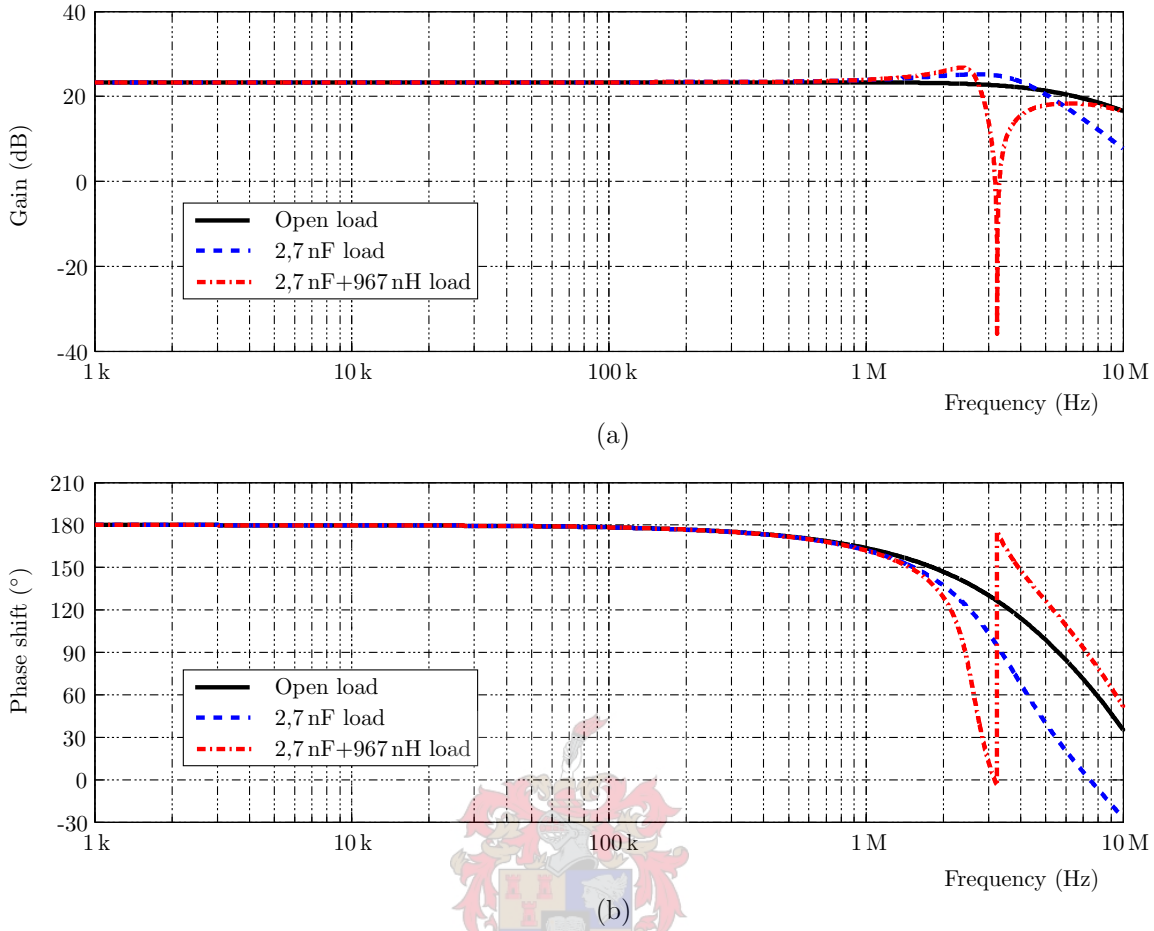

Figure 4.8: The simulation results for the power stage, where (a) is the gain and (b) the phase shift. The capacitive load and the leakage inductance from the transformer design are shown to not affect the bandwidth of the system.

step-up transformers, which has a value of 967 nH when reflected to the primary side of a type 1 transformer (see Section 4.3), is inserted in series with the capacitive load, in order to investigate the influence that the transformers have on a power stage. Figure 4.8 shows that the leakage inductance introduces a zero in the transfer function in the vicinity of the capacitive load's pole; therefore, the ability of the power stages to amplify the Fourier components without introducing distortion, would not be affected by the transformers. Consequently, the design of the power stage was found to be acceptable, and was realised on several circuit boards, of which an example is shown in Figure 4.9. The circuit diagram of a power stage can be found in Appendix A.

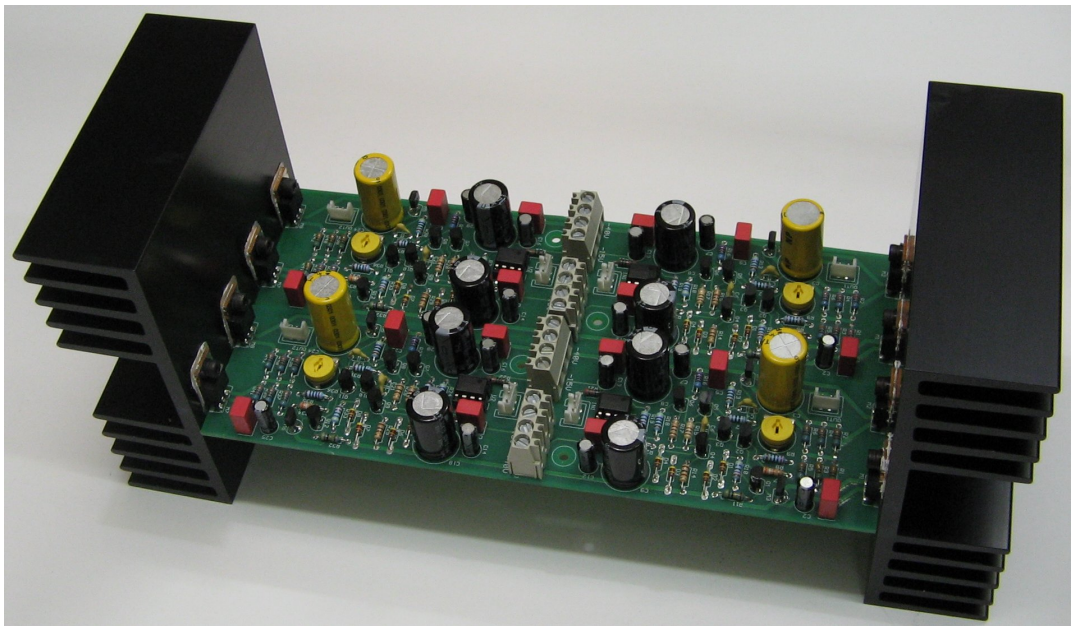

Figure 4.9: Four of the power-stage circuit boards; the power MOSFETs that operate in the Class-AB mode, can be seen where they are connected to the heat sinks.

The characteristics of the designed power stage are summarised in Table 4.3.

Number of power stages	-	20
Minimum bandwidth	MHz	2,8
Gain	dB	23,4
Maximum gain error	dB	0,07
Optimal phase shift	°	180
Maximum phase error	°	−3,2
Maximum input voltage	V	1,63
Maximum output voltage	V	20
Maximum capacitive load	pF	1 (or 2700†)

†Reflected to the primary side of the type 1 transformer.

Table 4.3: A summary of the characteristics of the designed power stages.

4.3 The step-up transformers

The final stage in the generation process of the Fourier components is the step-up transformers. Their role is to facilitate the high voltages that the Fourier components require; at the same time, they are also the means by which the Fourier components are added at the load, which leads to the synthesis of the arbitrary waveform.

The step-up transformers have a profound influence on the characteristics of the amplifier units that they form a part of. Firstly, the transformers determine the voltage ratings of the amplifier units: although the variable-gain stages are able to adjust the overall voltage gains of the different amplifier units, the maximum possible output voltages are set by the transformers. Furthermore, the transformers are responsible for the multichannel design of the power supply: each transformer was designed for a specific frequency range, thereby effectively limiting the selection of Fourier components that can be generated by each of the amplifier units.

Certain compromises had to be made in designing the transformers. These compromises stem from a consideration of the two extreme configurations that the required Fourier components could be arranged in (see Figure 4.10): (a) the case where the arbitrary waveform has a small bandwidth, with a few Fourier components near the fundamental frequency containing most of the signal power (epitomised by the sinusoidal waveform); and (b), the case where the arbitrary waveform has a large bandwidth, with the signal power spread across many Fourier components (epitomised by the impulse waveform). In order to make a compromise between these two situations, the transformers of the first ten amplifier units were designed with case (a) in mind, while the transformers of the last ten amplifier units catered for case (b). Additionally, it was decided that a single Fourier component may not utilise more than four amplifier units in its generation; this decision was another compromise between the voltage and bandwidth requirements of the arbitrary waveforms to be generated.

The design procedure of the step-up transformers[10] was an iterative process, and the transformer parameters were calculated with the aid of a spreadsheet. The following discussions therefore only relates to the most pertinent transformer parameters, which are summarised in Table 4.4; the full list of parameters can be found in Appendix B.

[10] Based on the procedure suggested in [72].

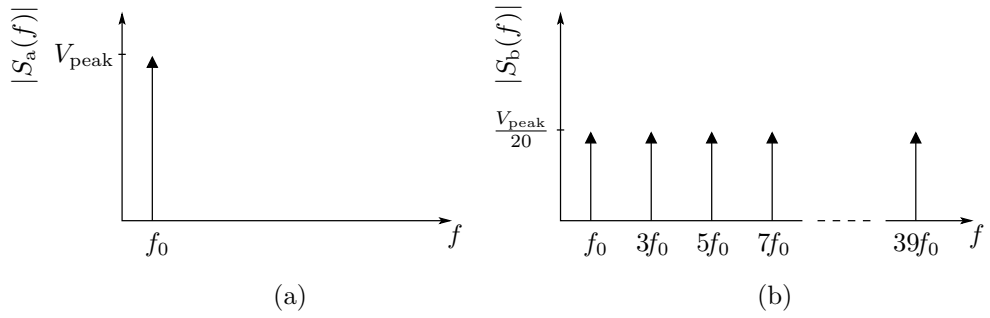

Figure 4.10: Two extreme cases of waveform spectra were considered in the design of the transformers, namely (a) the sinusoidal waveform and (b) the impulse waveform.

			Type 1	**Type 2**	**Type 3**	**Type 4**
$V_{peak,sec}$	Peak secondary voltage	V	1050	1050	600	600
$V_{peak,pri}$	Peak primary voltage	V	20	20	20	20
f_{min}	Minimum frequency	kHz	4,5	9	30	45
f_{max}	Maximum frequency	kHz	45	90	300	450
P	Power	V·A	10	10	2	2
n	Number of transformers	-	5	5	5	5
a	Turns ratio	-	52,5	52,5	30,0	30,0
$L_{leak,total}$	Total leakage inductance †	nH	967	967	2960	2960

†On the primary side of the transformers.

Table 4.4: The main characteristics of the step-up transformers; the shaded cells are design decisions, while the white cells contain calculated parameters.

It was decided that there would be four types of step-up transformers, with five implementations of each type. Taking the previously discussed compromises into account, the first two types of transformers are designed to produce higher secondary voltages (1050 V) and powers (10 VA) than the last two types of transformers (which have respectively 600 V and 2 VA ratings). Such an arrangement allows for a maximum possible output voltage of 16,5 kV, and a total power rating of 120 VA. The primary-side voltages, on the other hand, are chosen to reflect the outputs possible from the Class-AB amplifiers (20 V). The lower frequency limits of the transformers are determined by the harmonics of the lowest repetition rate to be applied, i.e. 4,5 kHz. By taking the limit on the number of amplifier units per Fourier component into account, the type 1 transformers are designed for the lowest fundamental component (4,5 kHz) and the type 2 transformers

for the lowest 2nd harmonic component (9 kHz) applicable. The type 3 and type 4 transformers are designed with respectively the 10th (45 kHz) and 15th (67,5 kHz) harmonic components in mind; however, as a compromise, their frequency limits are reduced in order for them to support lower harmonics as well (to respectively 30 kHz and 45 kHz). Additionally, the upper frequency limits of the transformers are chosen to be ten times their lower frequency limits.

The leakage inductance of the transformers is an important parameter to design for (as was explained in Section 2.2.2) and various measures are taken to minimise this quantity. Firstly, the secondary voltages of the individual transformers are limited to relatively low values (1050 V and 600 V); this enables the corresponding turns ratios, and therefore the number of turns in the windings, to be reduced as well, leading to lower leakage inductances. Furthermore, the primary and secondary windings of the type 1 and type 2 transformers are partitioned into three sections each, with the primary and secondary sections wound alternately around the cores; such an arrangement serves to further reduce the total leakage inductance. The equation that was used to calculate the leakage inductance of each transformer (derived from [72]), is

$$L_{\text{leak}} = \frac{\mu_0 N_{\text{sec}}^2 \, l_{\text{w}}}{p^2 h_{\text{w}}} \left(\frac{b_{\text{Cu}}}{6} + b_{\text{i}} \right), \tag{4.3.1}$$

where μ_0 is the permeability of free space, N_{sec} the number of secondary turns, l_{w} the average conductor turn length, p the number of interfaces between winding sections, h_{w} the winding width, b_{Cu} the total winding depth, and b_{i} the interwinding insulation thickness. The sum of all the transformers' leakage inductances, as found on their secondary sides, was calculated to be 2665 μH. As was shown in Section 4.2.2 (where the total leakage inductance is reflected to the primary side of a type 1 transformer), this value was found to be acceptable.

The implementation of the step-up transformers are shown in Figure 4.11. Two magnetic core shapes were selected for the transformers: the type 1 and type 2 transformers utilised ETD49 cores, whereas the type 3 and type 4 transformers used E42/21/15 cores. The magnetic core material that was chosen for the transformers, was Ferrite grade 3C90, which is rated to operate up to 200 kHz. The secondary windings of the transformers were wound using 200 μm-diameter copper wire, while 100 μm thick copper plates were used for the primary windings; these dimensions are chosen to satisfy the minimum skin depth requirements [72]. Furthermore, 300 μm layers of Mylar were used as insulation between

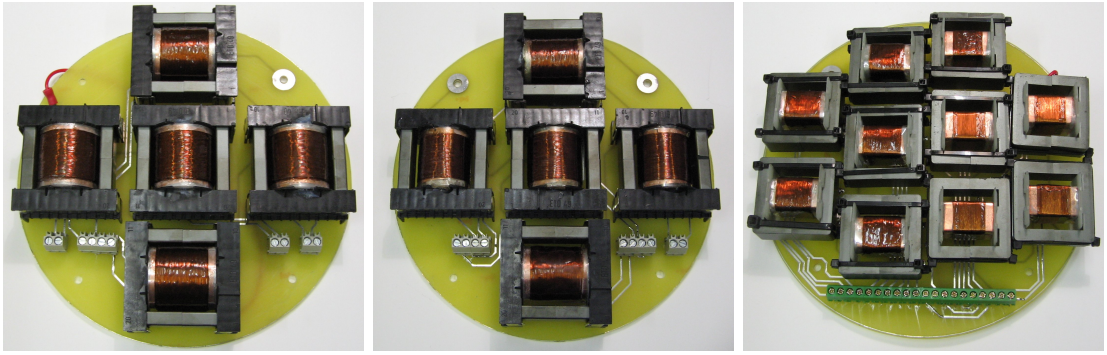

(a) (b) (c)

Figure 4.11: The PCBs mounted with respectively (a) the type 1 transformers, (b) the type 2 transformers, and (c) the type 3 (the five on the left) and type 4 (the five on the right) transformers.

the primary and secondary windings of the transformers, which are capable of blocking up to 15 kV; this takes into account the fact that a single transformer can be exposed to the fully synthesised output voltage on the secondary side. Finally, the transformers were assembled inside an oil tank in order to provide thorough insulation from the high secondary-side voltages. The secondary sides of the transformers were connected in series in such a way that the type 4 transformers were connected to the output ground terminal, while the type 1 transformers were connected to the high-voltage output terminal; Figure 4.12 shows how the transformers are arranged within the oil tank.

4.4 Summary

The realisation of the different components in the cascaded multichannel amplifier, namely the sinusoid generators, the Class-AB amplifiers, and the step-up transformers, are discussed in this chapter. The sinusoid generators were implemented on a digital circuit board, while the Class-AB amplifiers were realised in twenty amplification stages, with each amplification stage consisting of a variable-gain stage and a power stage. Furthermore, the step-up transformers were designed and implemented to accommodate four different frequency channels. The various design goals that guided the implementation of these components, are summarised in Table 4.5.

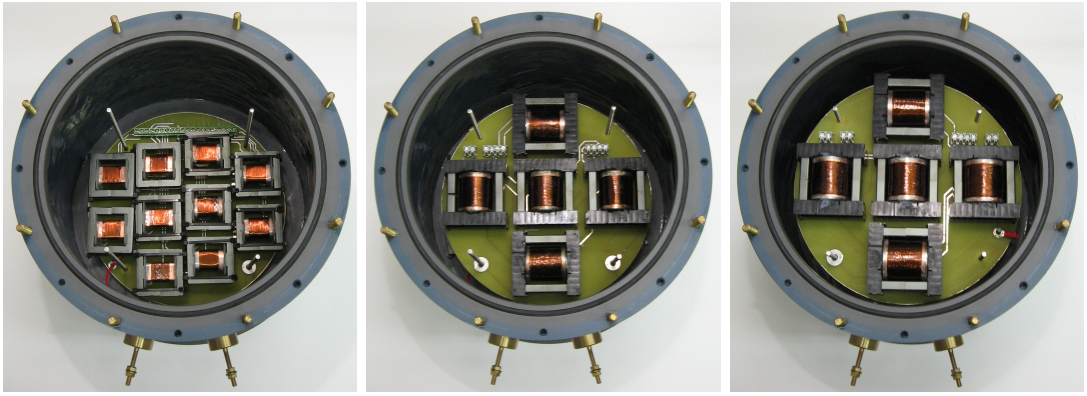

Figure 4.12: The step-up transformers were assembled inside an oil tank to manage the high voltages. The secondary sides of the transformers are connected in series, and are outputted at the high-voltage terminals that can be seen at the bottom of the pictures.

The sinusoid generators	The main design goal for the sinusoid generators is that they must be able to generate the Fourier components of a 200 kHz-bandwidth signal with accuracy.
The Class-AB amplifiers	The Class-AB amplifiers must be able to amplify the Fourier components to the necessary voltage and power levels without introducing distortion.
The step-up transformers	The transformers must be able to transform the Fourier components up to the necessary high voltages and add them on their secondary sides, without introducing distortion into the synthesised waveform.

Table 4.5: A summary of the overall design goals for the various components that comprise the cascaded multichannel amplifier.

Chapter 5

Testing of the cascaded multichannel amplifier

In the previous chapter, the design and implementation of the cascaded multichannel amplifier were discussed. The sinusoid generators are implemented on a digital circuit board, whereas each of the Class-AB amplifiers are realised in a variable-gain and power stage. The step-up transformers, on the other hand, are arranged into four distinct types, with each type encompassing five transformers.

The performance of each of the main components that comprise the cascaded multichannel amplifier, are tested in the present chapter. First off, a set of test waveforms are introduced; these waveforms are used as a measure of the ability of the designed power supply to generate arbitrary waveforms. Next, the output characteristics of the digital circuit board is examined at the hand of the test waveforms; this is followed by measurements of the variable-gain and power stages' transfer functions, as well as their output to the test waveforms. Afterwards, key parameters of the step-up transformers are measured. Finally, the output of the cascaded multichannel amplifier is measured at the high-voltage terminals of the transformers.

5.1 Test waveforms

The ability of the implemented cascaded multichannel amplifier to generate arbitrary waveforms, is tested at the hand of three example waveforms, namely the impulse waveform, the triangular waveform, and the square waveform. These waveforms are chosen to

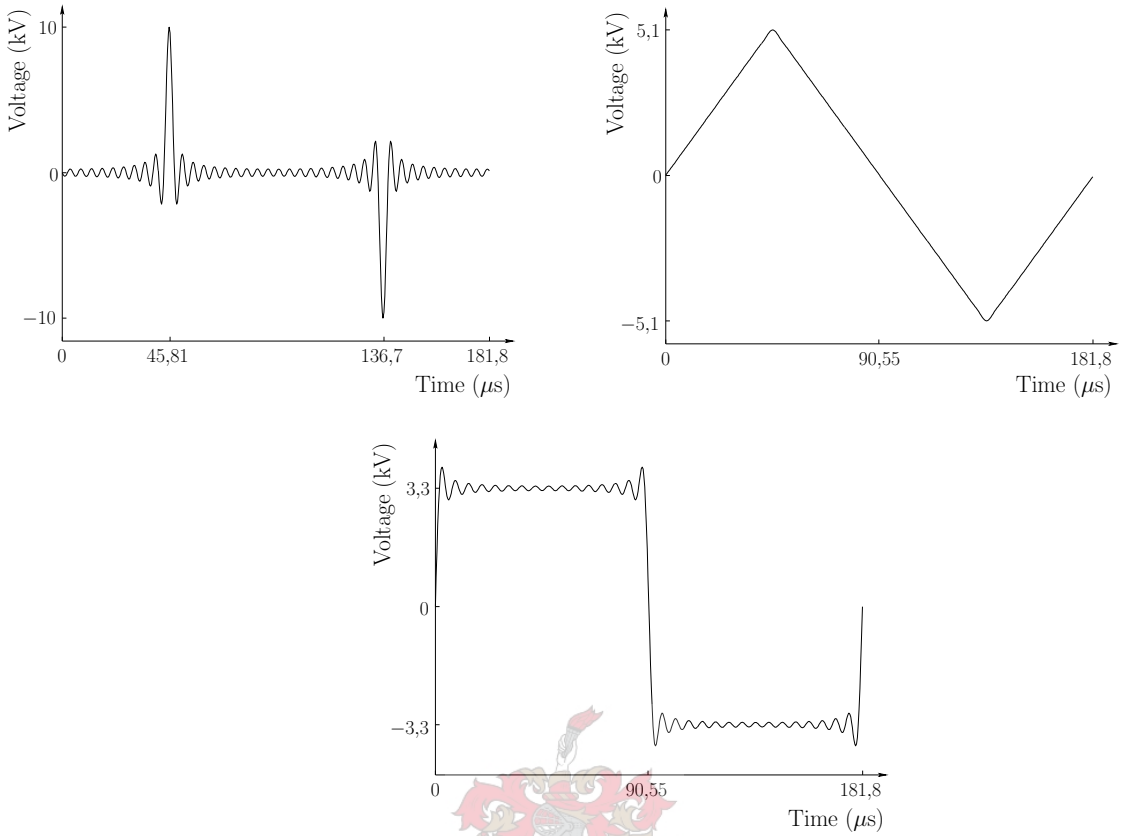

Figure 5.1: The three test waveforms are (a) the impulse waveform, (b) the triangular waveform, and (c) the square waveform.

represent three general scenarios that an arbitrary waveform's magnitude spectrum can be characterised by:

Scenario 1: The magnitude spectrum of the arbitrary waveform consists of many Fourier components that have non-negligible magnitudes, thereby signifying a large signal bandwidth; this scenario is represented by the impulse waveform.

Scenario 2: Most of the Fourier components of the arbitrary waveform have negligible magnitudes, except for a few components near the fundamental frequency; the triangular waveform is used to represent this scenario.

Scenario 3: The arbitrary waveform's bandwidth lie somewhere in between the bandwidths of the two waveforms of the other scenarios; the chosen waveform for this

scenario is the square waveform.

The three test waveforms are illustrated in Figure 5.1[1]. The repetition rates of the three test signals are chosen to be 5500 Hz, i.e. the signals have periods of 181,8 μs. The amplitude of the impulse waveform that is to be generated by the cascaded multichannel amplifier, is set to 12 kV, whereas the amplitudes of the triangular and square waveforms are set to respectively 5,1 kV and 3,3 kV; in order to compare the outputs of the sinusoid generators and Class-AB amplifiers directly to the test waveforms, the waveforms are generated with the assumption that all the amplifier units are capable of delivering 1050 V.

5.2 The sinusoid generators

The sinusoid generators on the digital board are tested by inputting the three test waveforms into the computer program, and then activating the sinusoid generators. In every test case, the voltage signal that is outputted by each sinusoid generator, is saved on a digital oscilloscope (a 300 MHz Tektronix TDS3032)[2]; the measured voltage signals are then added on the digital oscilloscope in order to obtain the equivalent waveform generated by the digital circuit board. The resulting waveforms measured on the output of the digital board, are shown in Figure 5.2.

The maximum voltage amplitude outputted by the digital circuit board, is measured to be 240 mV. The influence that digital generation has on the output voltages of the digital circuit board, can be shown at the hand of Figure 5.3, where the 31st harmonic component of the square waveform is shown. This particular Fourier component is generated with $\sim$16 ($\frac{512}{31}$) samples per period.

5.3 The Class-AB amplifiers

The variable-gain and power stages of the Class-AB amplifiers are first tested separately in order to obtain their transfer functions; these measurements are discussed in Sections 5.3.1

[1]The test waveforms are computed by adding together the twenty sinusoids that are stored in the FPGAs.

[2]In measuring the output of each sinusoid generator, the oscilloscope was triggered against the generated fundamental component, in order to maintain the phases of the different outputs relative to the fundamental component.

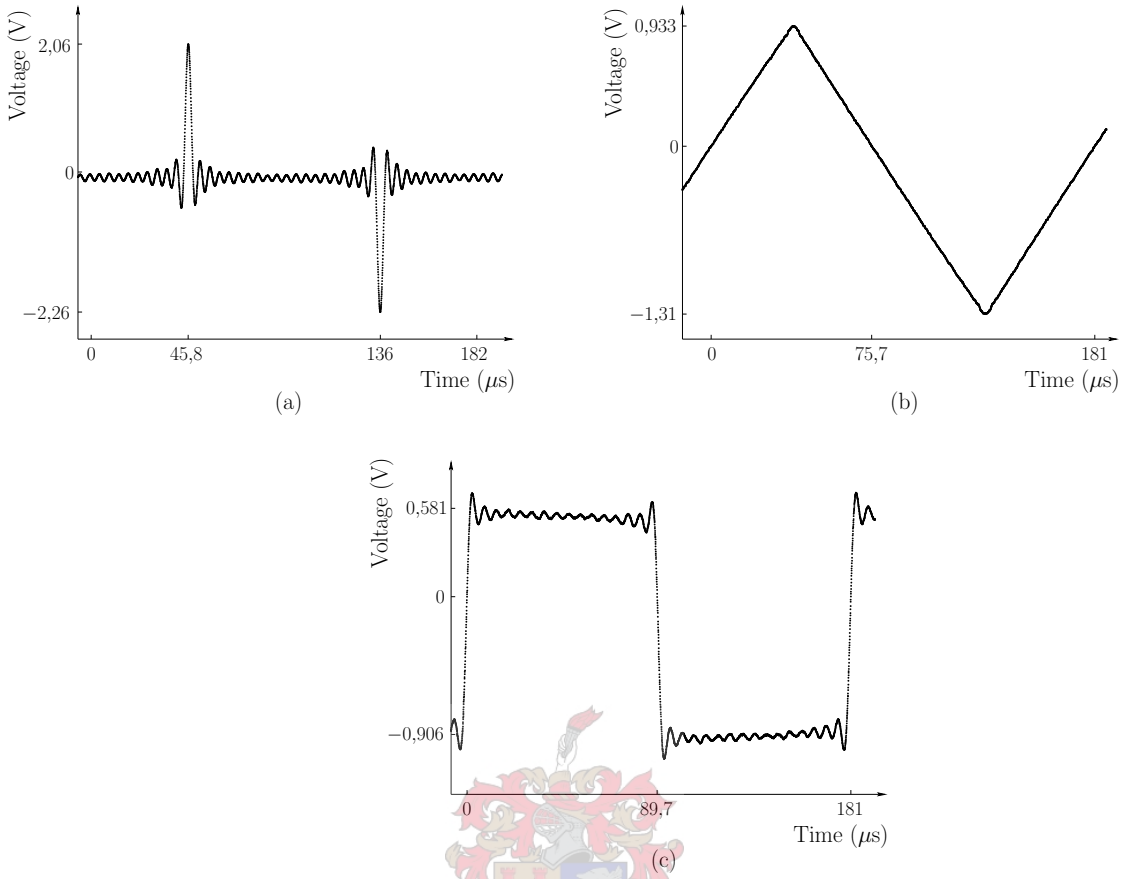

Figure 5.2: The three test waveforms measured at the output of the digital circuit board: (a) the impulse waveform, (b) the triangular waveform, and (c) the square waveform.

and 5.3.2. In Section 5.3.3, the output of the Class-AB amplifiers to the test waveforms are examined by connecting the Class-AB amplifiers to the sinusoid generators.

5.3.1 The variable-gain stage

The transfer function of the variable-gain stage is measured by connecting a function generator (Instek GFG-8210) to the input of one of the variable-gain stages. A sinusoidal voltage is then applied at different frequencies and the output measured with the digital oscilloscope. The gain of the circuit is obtained by calculating the ratio of output to input voltages, while the phase shift is measured as the time delay between the zero-crossings of the rising edges of the input and output voltages. Figure 5.4 shows the transfer function

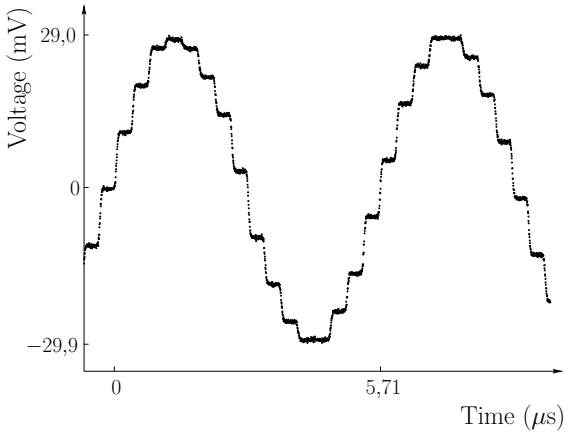

Figure 5.3: The 31st harmonic component of the square waveform that is outputted by the digital circuit board.

measurements of the variable-gain stage; the main characteristics of the measured spectra are summarised in Table 5.1.

5.3.2 The power stage

The measurement of the power stage's transfer function follows the same procedure as is followed with the variable-gain stage. The function generator is connected to the input of one of the power stages[3], and sinusoidal voltages of different frequencies are applied. The gain and phase shift in the output signal is then measured with the digital oscilloscope. The first test is done with an open load, which represents the ideal operating conditions for the power stage; Figure 5.5 presents the results of these measurements.

The transfer function of the power stage is measured next for the case of a capacitive load, making use of the same technique as for the open load. A 2,7 nF capacitor is used as the capacitive load. Figure 5.6 shows the resulting gain and phase shift of the power stage measured at different frequencies.

The power stages are rated to deliver a peak output voltage of 20 V; an input signal with an amplitude of 1,63 V is required to produce such an output voltage. In order to investigate the effects that the power stage has on driving larger output voltages, a test sinusoid is applied to one of the power stages, which is connected to an open load. The

[3]Since the power stages are designed to be identical, testing of a single stage is sufficient.

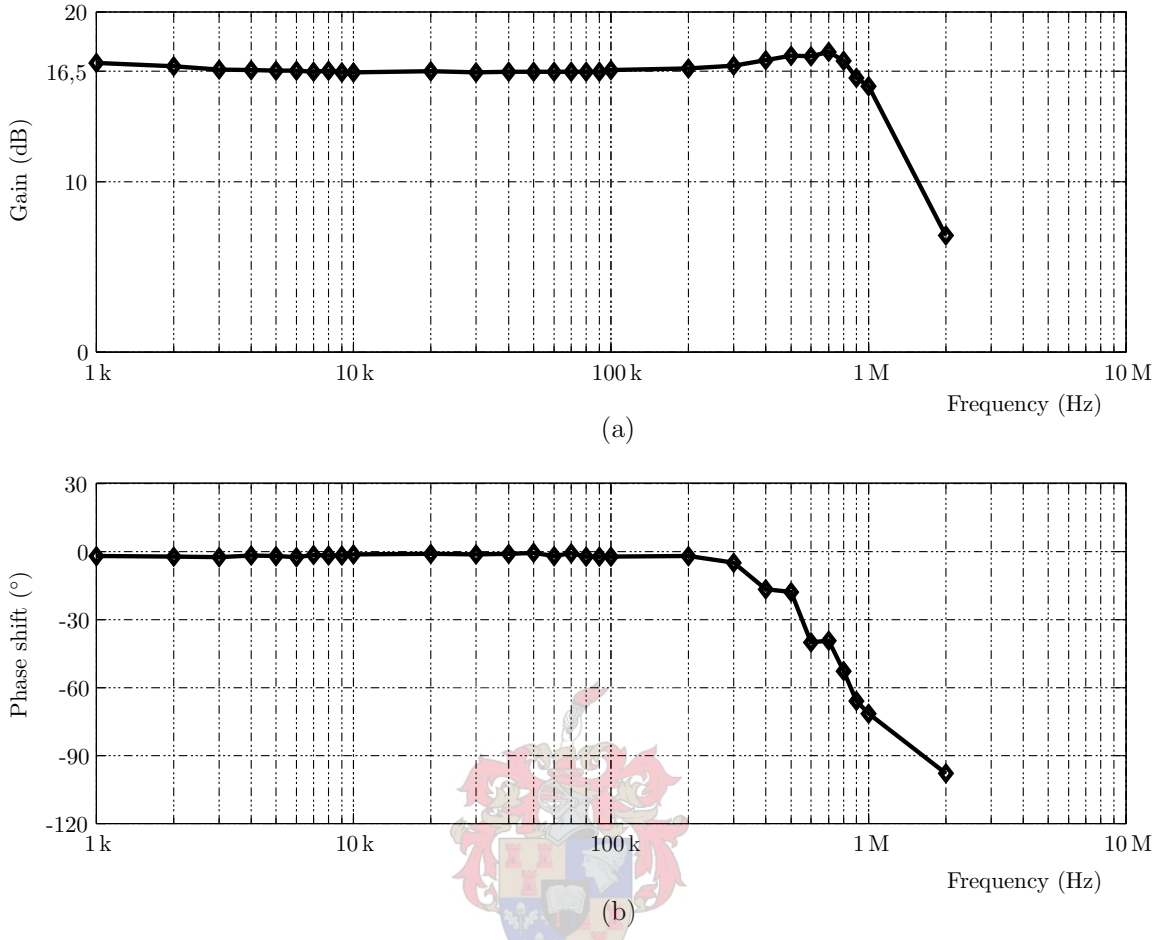

Figure 5.4: The measured transfer function of the variable-gain stage for an open load: (a) shows the gain of the stage, whereas (b) indicates the phase shift.

Bandwidth	MHz	∼1
Value of set gain†	dB	16,5
Maximum gain deviation‡	dB	0,15
Average phase shift‡	°	−1,69
Maximum phase deviation‡	°	1,11

†The gain is set to provide a maximum output voltage of 1,63 V.

‡Measured inside the signal bandwidth (≤200 kHz).

Table 5.1: A summary of the measured characteristics of the variable-gain stage.

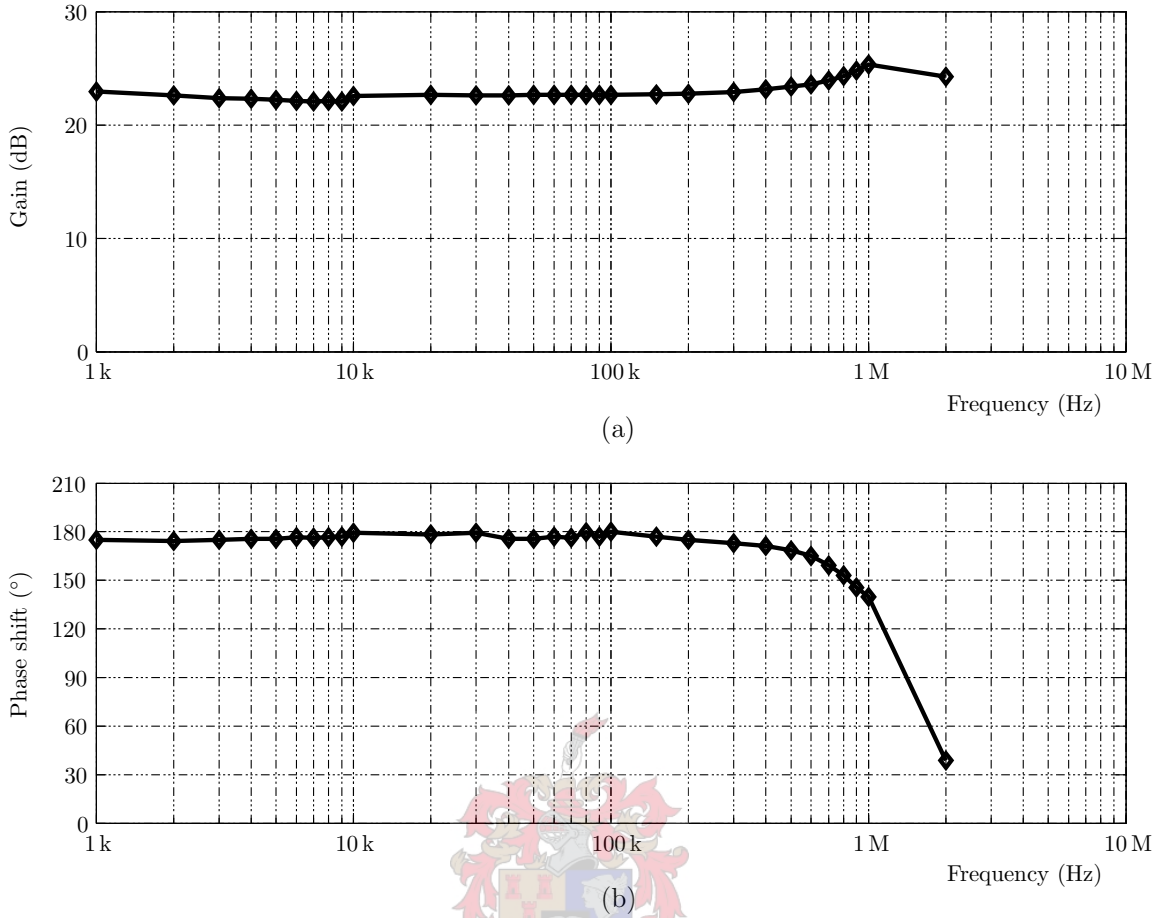

Figure 5.5: The measured transfer function of the power stage for an open load: the power stage's (a) gain and (b) phase shift are shown.

amplitude of the test signal is then increased beyond 1,63 V and the output of the power stage measured with the digital oscilloscope. Figure 5.7(a) shows the output signal v_{O} for an input v_{test} that has an amplitude of 3,2 V and a frequency of 200 kHz.

The power stages are designed to drive a 2,7 nF capacitive load. To investigate the effect that a larger capacitance has on the operation of the power stage, the capacitance connected to the output of the power stage is increased by an order of magnitude to 22 nF. A test sinusoid v_{test}, which has its parameters set for the maximum normal operating conditions (i.e. an amplitude of 1,63 V and a frequency of 200 kHz), is applied to the input of the power stage, while a 22 nF capacitance is connected to the output of the power stage. Figure 5.7(b) shows the resulting output voltage v_{O} that is measured.

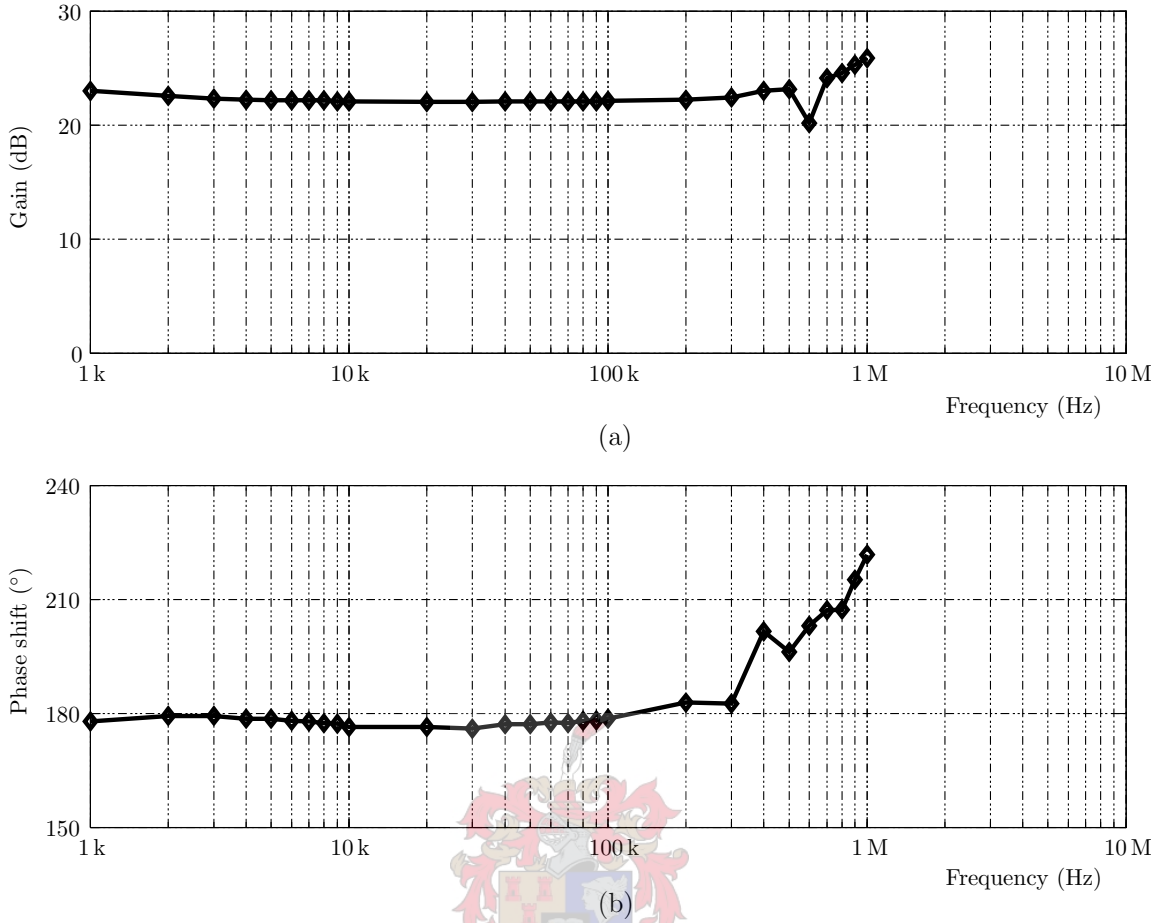

Figure 5.6: The measured transfer function of the power stage for a capacitive load of 2,7 nF: (a) the gain and (b) the phase shift.

The characteristics of the power stage's measured transfer function is summarised in Table 5.2 for both the open and capacitive loads.

5.3.3 The Class-AB amplifiers connected to the sinusoid generators

The ability of Class-AB amplifiers to amplify the Fourier components without introducing distortion, is tested using the three waveforms specified in Section 5.1. The twenty variable-gain stages and twenty power stages of the Class-AB amplifiers are connected to the output of the digital circuit board, with the gains of the variable gain stages calibrated to ensure that each power stage outputs a maximum voltage of 20 V. Each of the three test waveforms are then successively generated on the digital circuit board, and the output of the power stages measured with the digital oscilloscope. The output signals

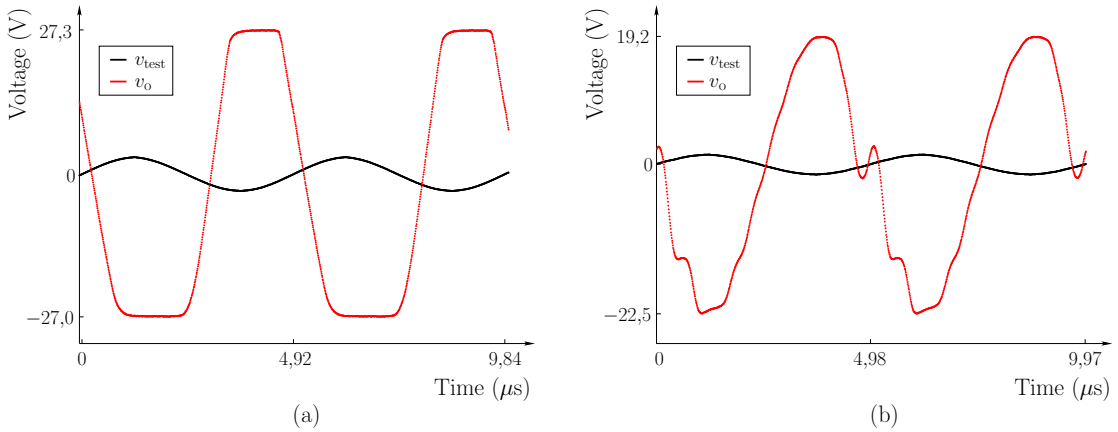

Figure 5.7: (a) The effects on the output voltage v_O of the power stage when the input signal is driven beyond 1,63 V (the voltage necessary for an output of 20 V). (b) The effects on v_O when a larger capacitance than that rated for the power stage, is connected; the capacitance in this case is 22 nF. In both figures, v_{test} is the sinusoidal signal applied to the input of the power stage.

		Open load	2,7 nF load
Bandwidth	MHz	>2	>1
Average gain†	dB	22,5	22,2
Maximum gain deviation†	dB	0,46	0,17
Average phase shift†	°	177	178
Maximum phase deviation†	°	3,20	4,88

†Measured inside the signal bandwidth (≤200 kHz).

Table 5.2: A summary of the measured characteristics of the power stage's transfer function.

of the twenty power stages are added on the digital oscilloscope to form the equivalent output waveform of the Class-AB amplifiers; the resulting equivalent waveforms measured for the three test waveforms, are shown in Figure 5.8.

5.4 Transformer measurements

Three parameters are measured for each of the four types of step-up transformers: the magnetisation inductance, the turns ratio, and the leakage inductance. These measurements are discussed below.

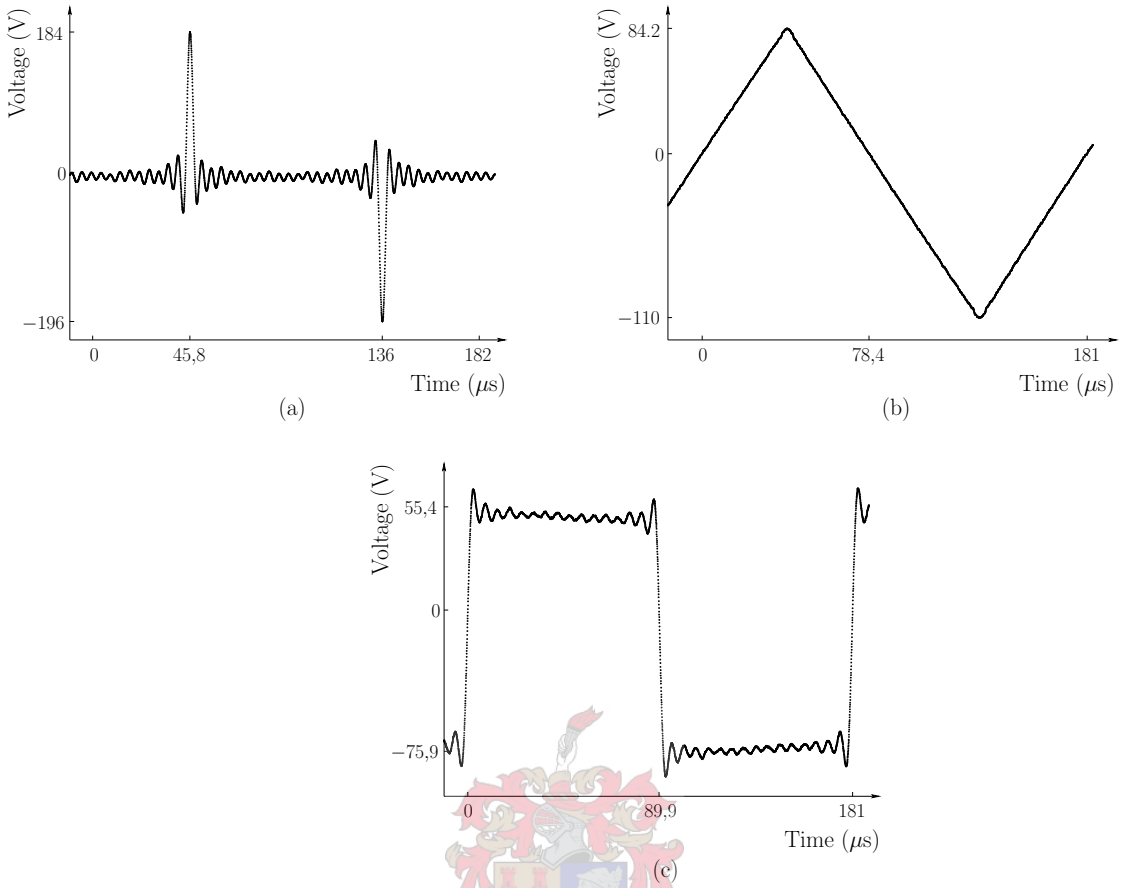

Figure 5.8: The three test waveforms measured at the output of the Class-AB amplifiers: (a) the impulse waveform, (b) the triangular waveform, and (c) the square waveform.

The magnetisation inductance of a transformer is measured by using a function generator along with a capacitance; Figure 5.9 shows the setup. The capacitance C is connected in parallel with the primary side of the transformer (resistance R provides current limiting), while the secondary side is left open circuit. The equivalent inductance in parallel with the capacitance is therefore the magnetisation inductance L_{mag}, since one can assume that the magnetisation inductance is much larger than the leakage inductance. The function generator v_{s} is then connected and set to drive the circuit with sinusoidal signals. The capacitance and magnetisation inductance forms a parallel resonant circuit, which has a resonant frequency $f_{\text{res}} = \frac{1}{2\pi\sqrt{L_{\text{mag}}C}}$; the impedance of the parallel resonant circuit is a maximum at f_{res}, therefore causing the voltage across the primary side, v_1, to peak at this frequency. By measuring v_1 and sweeping the frequency of the function

generator, one is able to find f_{res}, and therefore calculate the value of L_{mag}. Table 5.3 contains the values calculated for the four types of step-up transformers.

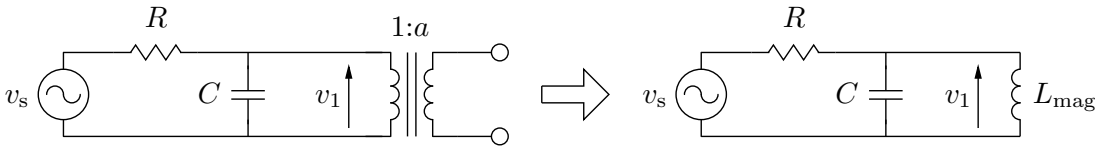

Figure 5.9: The test setup for measuring the magnetisation inductance of one of the step-up transformers.

Transformer	f_{res} (kHz)	L_{mag} (mH)
Type 1†	0,998	2,60
Type 2	5,89	0,730
Type 3	14,9	0,114
Type 4	21,1	0,0569

†$C = 10\,\mu\text{F}$ is used for this measurement.

Table 5.3: The list of magnetisation inductances calculated from the measurements; in the test setup used, $R = 1\,\text{k}\Omega$ and $C = 1\,\mu\text{F}$.

The effective turns ratios of the step-up transformers are obtained by measuring the voltages on respectively the primary sides (v_1) and secondary sides (v_2) of the transformers; Figure 5.10 shows the setup for this measurement. The turns ratio is then calculated from $a = \frac{v_2}{v_1}$; the results are found in Table 5.4.

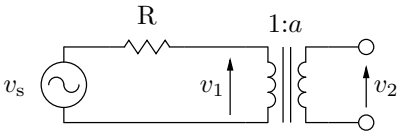

Figure 5.10: The test setup for measuring the effective turns ratio of one of the step-up transformers.

Transformer	v_1 (V)	v_2 (V)	a
Type 1	0,0817	4,00	49
Type 2	1,00	55,0	55
Type 3	3,17	96,7	31
Type 4	3,25	99,6	31

Table 5.4: A summary of the effective turns ratios of the transformers, as calculated from the voltage measurements.

The leakage inductances of the transformers are calculated by again utilising the resonance of the transformers with a capacitance; Figure 5.11 shows the setup for this measurement. The capacitance C is connected in parallel to the primary side of the transformer; however, the secondary side of the transformer is shorted out this time. Since one can assume that the leakage inductance is much smaller than the magnetisation inductance, the equivalent inductance in parallel with the capacitance is the total leakage inductance L_{leak} of the transformer. The leakage inductance forms a parallel resonant circuit with the capacitance, which has a resonant frequency of $f_{\text{res}} = \frac{1}{2\pi\sqrt{L_{\text{leak}}C}}$. As is the case for the magnetisation-inductance measurements, f_{res} is measured at the point where v_1 has its peak value. Table 5.5 shows the subsequently calculated leakage inductances; the leakage inductances of the type 3 and type 4 transformers could not be calculated, since a peak could not be found in their v_1 measurements.

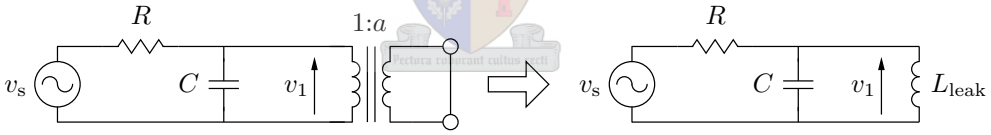

Figure 5.11: The test setup for measuring the leakage inductance of one of the step-up transformers.

5.5 Complete amplifier units

The overall operation of the cascaded multichannel amplifier is first tested by using only five amplifier units: due to the smaller size of this setup, the overall complexity of the system is decreased, while the total current drawn by the amplifiers is also lessened. Sec-

Transformer	f_{res} (kHz)	L_{leak} (nH)
Type 1	161	975
Type 2	204	609
Type 3	-	-
Type 4	-	-

Table 5.5: A summary of the measured leakage inductances of the transformers; in this setup $R = 1\,\text{k}\Omega$ and $C = 1\,\mu\text{F}$.

tion 5.5.1 discusses measurements taken using the aforementioned arrangement, followed by an investigation into the operation of the full twenty amplifier units in Section 5.5.2.

5.5.1 Five amplifier units

The transfer function of a single power stage that has the transformers as load, is measured first. In this arrangement, five power stages are connected to the primary sides of the five type 1 transformers, but only one power stage is driven with an input signal. A function generator is used to drive the input of the selected power stage with sinusoids of different frequencies; the inputs to the other four power stages are left open. The primary sides of the 15 other transformers that are not connected to power stages, are shorted out to minimise their influence on the measurements. The voltage on the output terminals of the transformers is then measured with a high-voltage probe (a Tektronix PS015A) in conjunction with the applied voltage. The voltage gain and phase shift of the power stage combined with the transformers, are calculated from these measurements, and are shown in Figure 5.12.

Five full amplifier units are tested next using the three test waveforms that were selected in Section 5.1. The amplitudes of the three test waveforms are, however, adjusted to accommodate the fact that only five amplifiers are tested; therefore, each of the three test waveforms is set to have 500 V amplitudes. The repetition rates of the test waveforms, however, are kept at 5500 Hz. Figure 5.13(a)-(c) shows the three waveforms that the five amplifier units are tested with.

The arrangement that was used to test the five amplifier units, are shown in Figure 5.14. Each of the test waveforms are generated by five sinusoid generators and then amplified by the five connected Class-AB amplifiers; finally, the output voltage of the step-up transformers, which is the output of the cascaded multichannel amplifier, is measured

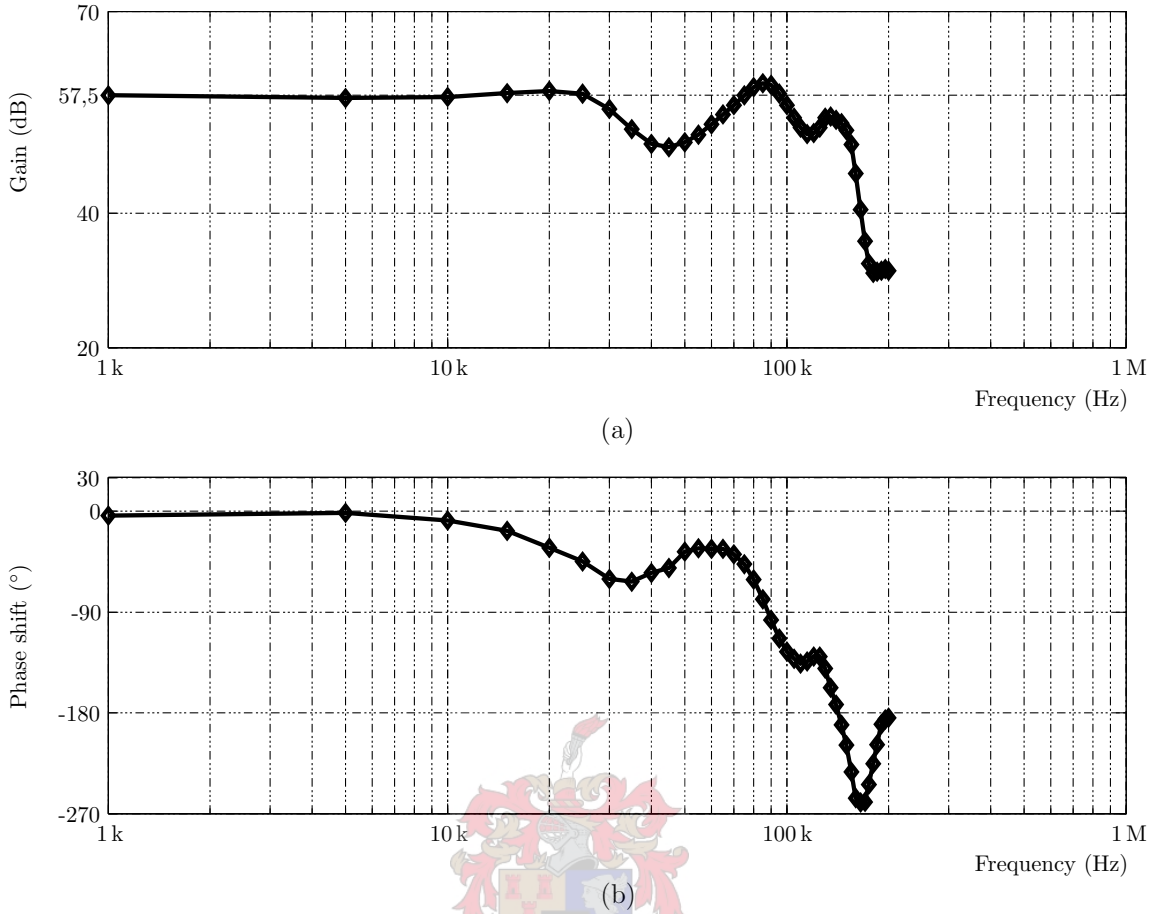

Figure 5.12: (a) The gain and (b) the phase shift of a power stage that has the five type 1 step-up transformers as load.

with the high-voltage probe. The transformers that were used to test the performance of the five amplifier units, are the five type 1 transformers. The primary sides of the transformers that are not connected to power stages, are shorted out in order to reduce their influence on the measurements. The resulting waveforms that were measured at the output of the five amplifier units, are shown in Figure 5.13(d)-(f) alongside the inputted test waveforms.

5.5.2 Twenty amplifier units

All twenty of the sinusoid generators and Class-AB amplifiers were connected to their respective step-up transformers for this arrangement; however, significant problems arose during the testing of this setup. Low-frequency noise (notably at 150 Hz) entered the

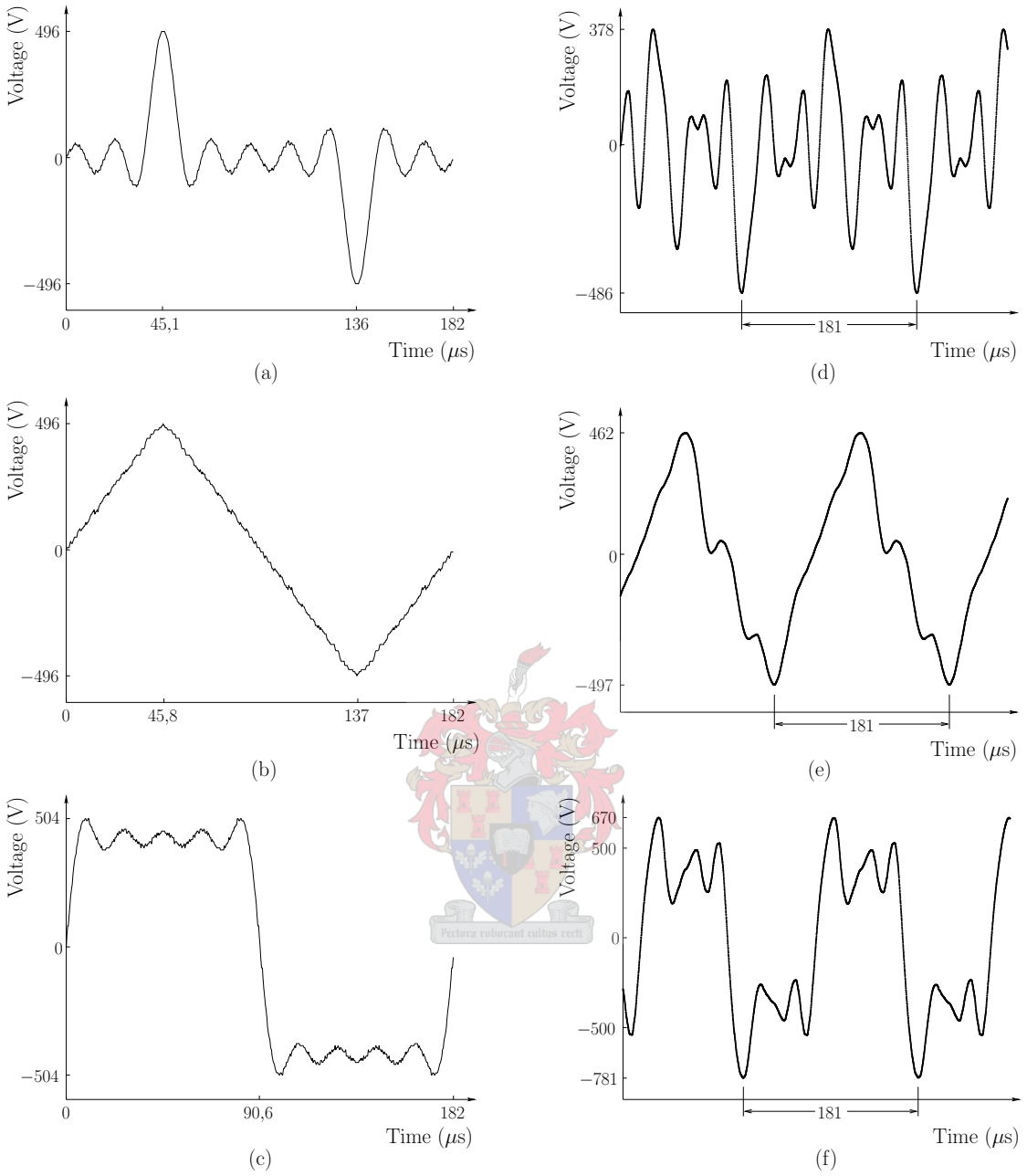

Figure 5.13: The three test waveforms inputted to the five amplifier units, are (a) the impulse waveform, (b) the triangular waveform, and (c) the square waveform. The voltages measured at the output terminals of the step-up transformers for the three test waveforms, are shown in respectively (d)-(f); two periods are shown for the measured voltages, as opposed to the single period of the input waveforms.

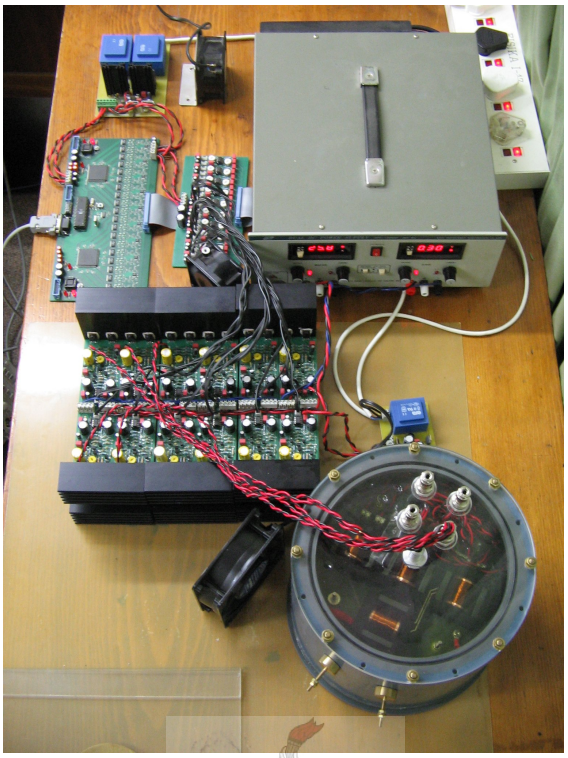

Figure 5.14: The test setup for the five amplifier units. The first five Class-AB amplifiers are connected to their step-up transformers, while the primary sides of the other transformers are shorted out.

signals applied to the step-up transformers; this led to a saturation of the higher-frequency transformer cores, subsequently producing exorbitant currents on the primary sides of the transformers. As a result, some of the amplifier units' components were damaged in the process, and further testing could not be undertaken. The output waveforms that were observed for the twenty amplifier units, however, had similar features to those measured in Section 5.5.1; the measurements of Section 5.5.1 can therefore be considered representative of all the amplifier units' operation.

Chapter 6

Evaluation of the cascaded multichannel amplifier

In Chapter 4, the design goals were stated for each of the components that make up the cascaded multichannel amplifier. Furthermore, tests were conducted in Chapter 5 to measure the performance of these components. The present chapter subsequently evaluates the performance of the cascaded multichannel amplifier in light of the design goals.

The ability of the sinusoid generators to produce the Fourier components of an arbitrary waveform accurately, is examined in Section 6.1. In Section 6.2, the Class-AB amplifiers' amplification of the Fourier components by respectively the variable-gain and power stages, are examined. The step-up transformers are evaluated next in Section 6.3, with the focus on the effects that their characteristics have on the operation of the waveform generator. Finally, some system-wide effects are commented on in Section 6.4.

6.1 The sinusoid generators

A periodic signal can be fully characterised in the frequency domain by its waveform and repetition rate, as is indicated in Section 3.1. The ability of the sinusoid generators to produce the Fourier components necessary for an arbitrary waveform, can therefore be evaluated by comparing the combined spectra of the signals that are outputted by the digital circuit board, with the spectra of the inputted test waveform.

The impulse test waveform, which is shown in Figure 5.1(a), is selected to evaluate the accuracy of the sinusoid generators; this waveform is unique, as it can be generated

in such a way that all of its Fourier components have the same magnitudes and phases[1], which makes analysis of the spectra easy. Figures 6.1(a) and (b) show respectively the magnitude and phase spectra of the impulse waveform $S_{\text{test}}(f)$ that is inputted to the sinusoid generators. Each sinusoid generator must produce a Fourier component that has an amplitude[2] of 110 mV and a phase of 0°; the repetition rate is 5500 Hz.

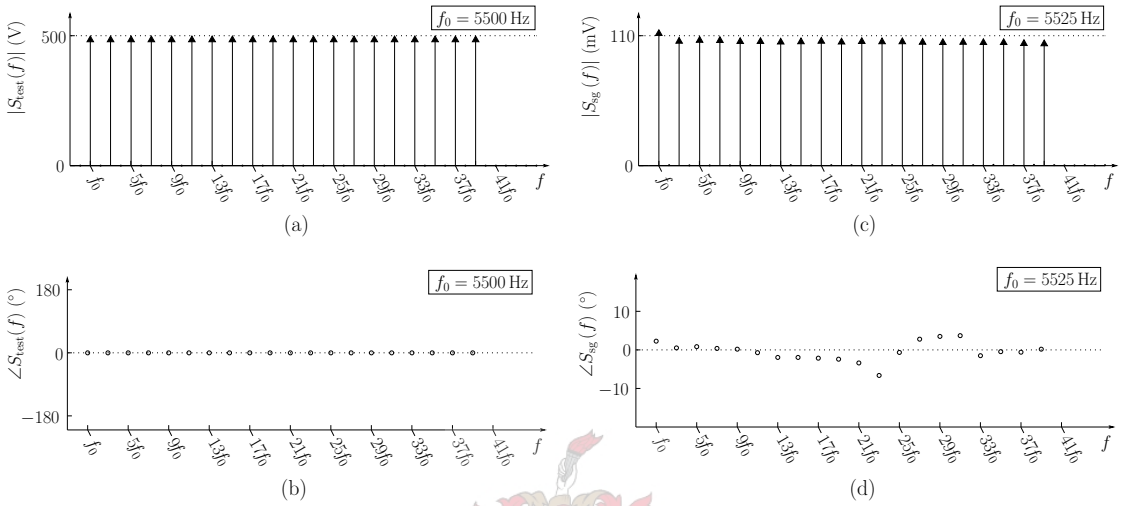

Figure 6.1: (a) The magnitude spectrum and (b) the phase spectrum of the impulse test waveform $S_{\text{test}}(f)$; correspondingly, the magnitude spectrum (c) and the phase spectrum (d) of the sinusoid generators' equivalent output waveform $S_{\text{sg}}(f)$.

The spectra of the equivalent waveform $S_{\text{sg}}(f)$ that is outputted by the sinusoid generators, are determined by using the discrete Fourier transform (DFT) [81]; the Matlab® software package was used to calculated the DFT from the number of measured points in Figure 5.2(a) that constitute a single period of the waveform. Figures 6.1(c) and (d) show

[1]To obtain the same phase for all of the Fourier components, the waveform shown in Figure 5.1(a) has to be shifted with 90° to the left.

[2]The voltage amplitude that is to be outputted by a sinusoid generator, $|v_{\text{d}}|$, is designed to be

$$|v_{\text{d}}| = \left(\frac{V_{\text{c}}}{V_{\text{max}}}\right) v_{\text{d}}\big|_{\text{max}},$$

where V_{c} is the magnitude of the Fourier component, V_{max} is the maximum possible output voltage of the particular amplifier unit, and $v_{\text{d}}\big|_{\text{max}}$ is the designed maximum output voltage of the sinusoid generator.

respectively the magnitude[3] and phase[4] spectra of the DFT, $S_{\text{sg}}(f)$; the characteristics of $S_{\text{sg}}(f)$ compared with those of $S_{\text{test}}(f)$, are summarised in Table 6.1. As can be seen, all the parameters of the Fourier components are produced remarkably accurately by the sinusoid generators; the fractional error in repetition rate (0,45 %) and deviation in phase (6,7°) are very small, while the fractional errors in the magnitudes (4,6 %) can be compensated for in the variable-gain stages. Similar results are obtainable for the triangular and square test waveforms, as well as for other repetition rates of interest (4,5 kHz to 10 kHz). It can therefore be concluded that the sinusoid generators are capable of generating the selected Fourier components of an arbitrary waveform with great accuracy.

Repetition rate	Hz	5525
Repetition-rate error	Hz	25
Average magnitude	mV	108
Maximum magnitude error	mV	4,99
Average phase	°	−0,402
Maximum phase error	°	6,66

Table 6.1: A summary of the sinusoid generator's output spectra for the impulse test waveform, as calculated from the DFT.

The sinusoid generators can accurately generate the selected Fourier components necessary for an arbitrary waveform; yet, distortion can still be introduced in the form of unwanted harmonics, due to digital generation and nonlinear effects in the electronic components. The total harmonic distortion (THD) of a system states the power ratio between the unwanted and signal harmonics in the output; in the case of the impulse waveform produced by the sinusoid generators, the following equation is used:

$$THD = \frac{\sum\limits_{\substack{k>0 \\ k\neq n}}^{\frac{N}{2}} V_k^2}{\sum\limits_{\substack{n>0 \\ n \text{ odd}}}^{39} V_n^2}, \tag{6.1.1}$$

[3]In Figure 6.1(c), the dc component that is present in the equivalent waveform of Figure 5.2(a), is ignored, since the measurement was taken with an open load.

[4]The phases of the harmonic components that have even ordinals or are beyond the bandwidth of the signal, are omitted to elucidate the phase spectra, since the power of these components are negligible.

where V_k are the RMS voltages of all the unwanted harmonics in the magnitude spectrum of $S_{\text{sg}}(f)$, V_n are the RMS voltages of the test waveform's Fourier components, and N is the number of samples measured for a single period of the sinusoid generators' equivalent output waveform. The THD of the sinusoid generators are calculated to be 0,013 %, i.e. for every 1 W in the signal harmonics, 0,13 mW is generated in unwanted harmonics. The sinusoid generators therefore introduce very little harmonic distortion.

A scenario in which the sinusoid generators do introduce distortion, is when the Fourier components that are assigned to the amplifier units, have very small magnitudes compared to the maximum magnitudes for which the amplifier units are designed. This distortion is called quantisation noise, and can be seen in Figures 5.13(a)-(c) as the small jags in the voltages. Quantisation noise is caused by the limitation of using 8-bit resolution in the RAM blocks of the FPGAs to store the Fourier components. Since these Fourier components have low magnitudes compared to the typical amplitude of an intended arbitrary waveform, the effects of quantisation noise on the overall waveform are limited in scope.

6.2 The Class-AB amplifiers

In Section 3.3.2, it is shown that the criterion for distortionless amplification is a transfer function that has constant gain and a linear phase shift with frequency. The variable-gain and power stages of the Class-AB amplifiers were designed to reflect these requirements, as was shown in Chapter 4. The extent to which the implemented Class-AB amplifiers achieve these goals, is evaluated in this section by means of the measurements taken in Chapter 5.

The performance of the variable-gain stage is examined first. The transfer function of the implemented variable-gain stage, of which the characteristics are summarised in Table 5.1, shows that the variable-gain stage satisfies the design conditions. Firstly, the gain is constant over the signal bandwidth ($\leq$200 kHz), with only minor deviations (0,15 dB) present; furthermore, harmonic components that are introduced via the digital generation of the Fourier components (harmonic frequencies greater than 2 MHz), are attenuated with at least 20 dB. Secondly, the phase shift of the variable-gain stage is effectively constant over the signal bandwidth, with the maximum deviation in phase shift being only 1,11°. The combination of these factors ensures that the variable-gain

stages amplify their inputs without introducing distortion.

The transfer function of the power stage, which was measured under both open-load and capacitive-load conditions, is summarised in Table 5.2. The following conclusions can be made (with results stated for both of the test conditions): (a) the power stage's gain (respectively 22,5 dB and 22,2 dB) is close to the value it was designed for, i.e. 23,4 dB; (b) the gain is effectively constant over the signal bandwidth, with deviations small (respectively 0,46 dB and 0,17 dB); and (c), the phase shift is close to the optimal value of 180°, and can be considered constant over the signal bandwidth (the maximum deviations are respectively 3,20° and 4,88°). The characteristics of the transfer function of the power stage therefore fulfil the requirements set out for distortionless amplification.

The impulse test waveform is once again used to verify the performance of the Class-AB amplifiers. Following the same procedure as in Section 6.1, $S_{\text{sg+amp}}(f)$, the DFT of a single period in Figure 5.8(a) (which represents the equivalent waveform that is outputted by the Class-AB amplifiers) is calculated. The resulting spectra are shown in Figure 6.2, and summarised in Table 6.2. According to the design, the voltage amplitude[5] of each Class-AB amplifier's output must be 9,52 V, while the phase must be kept at 0°. In comparing the output spectra with the above-mentioned expected values, it is clear that the amplification of the Fourier components takes place with minimal distortion: the maximum fractional magnitude error is 1,26 %, while the maximum phase error is 7,85°. The variable-gain stage therefore succeeds in calibrating the gains of the amplifier units, as the magnitude errors introduced by the sinusoid generators are reduced; on the other hand, the slight increase in phase error is still within acceptable limits. Additionally, the *THD* calculation for the Class-AB amplifiers shows an improvement to 0,0046 %, showing that unwanted harmonics are attenuated further.

The limitations of the Class-AB amplifiers are investigated by means of two tests. First off, the maximum output voltage that is attainable by the Class-AB amplifier, is determined by driving it with an input that is larger than the rated value; Figure 5.7(a) shows the resulting output voltage. The maximum output voltage of the Class-AB am-

[5]The voltage amplitude that is to be outputted by a Class-AB amplifier, $|v_{\text{O}}|$, is designed to be

$$|v_{\text{O}}| = \left(\frac{V_{\text{c}}}{V_{\text{max}}}\right) v_{\text{O}}\big|_{\text{max}},$$

where V_{c} is the magnitude of the Fourier component, V_{max} is the maximum possible output voltage of the particular amplifier unit, and $v_{\text{O}}\big|_{\text{max}}$ is the designed maximum output voltage of the Class-AB amplifier.

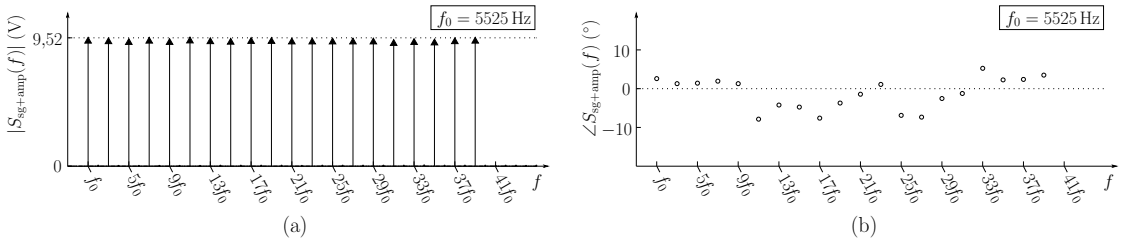

Figure 6.2: (a) The magnitude spectrum and (b) the phase spectrum of the DFT, $S_{\text{sg+amp}}(f)$, calculated for the Class-AB amplifiers' equivalent output waveform; the output is the result of generating the impulse test waveform with the sinusoid generators.

Average magnitude	V	9,52
Maximum magnitude error	V	0,120
Average phase	°	−1,22
Maximum phase error	°	7,85

Table 6.2: A summary of the spectra of the amplifier units, as calculated from the DFT of the output of the Class-AB amplifiers for the impulse test waveform.

plifiers is limited to ±27 V, due to the 30 V power supply used for the power stages; however, this maximum value falls to ±20 V when the rated capacitive load is connected. Furthermore, the slew rate[6] of the Class-AB amplifier, which manifests itself in the slope of the output in Figure 5.7(a), is determined to be 58,6 V·μs^{-1}. Finally, the ability of the Class-AB amplifiers to drive larger capacitances is also investigated; Figure 5.7(b) shows the resulting output for an order-of-magnitude increase in the load capacitance. The large load capacitance introduces significant distortion in the output voltage, which is a result of parasitic capacitances in the components of the power stage interacting with the load. Loading the Class-AB amplifiers with capacitances that are larger than the rated value (2,7 nF), must therefore be avoided.

6.3 The step-up transformers

The function of the step-up transformers is to transform the Fourier components that are outputted by the Class-AB amplifiers, to the necessary high voltages; furthermore, the transformers also perform the summation of the Fourier components through the series connection of their secondary sides. The ability of the step-up transformers to fulfil these

[6]Slew rate is an indication of the maximum $\frac{\mathrm{d}v}{\mathrm{d}t}$ possible at the output of a circuit.

tasks, is evaluated in this section.

The measured parameters of the step-up transformers are discussed first. The effective turns ratios of the transformers, of which the measurements are shown in Table 5.4, are close to their designed values (see Table 4.4); the small discrepancies are due to non-ideal effects within the step-up transformers, and can be compensated for in the computer program. The measured leakage inductances, on the other hand, are much larger than what they were designed for: in comparing the leakage inductances in Table 5.5 with those in Table 4.4, one can see that the total leakage inductance is an order of magnitude larger than expected. This is due to the insulation layers of the transformers being larger than anticipated. Although a large leakage inductance is undesirable, it will be shown later that the leakage inductances do not play the dominant role in the performance of the step-up transformers. Finally, the measured magnetisation inductances (see Table 5.3) are shown to be large in comparison to the leakage inductances, and can therefore be ignored when modelling the leakage inductances.

The performance of the step-up transformers is illustrated via the three test waveforms that are shown in Figures 5.13(a)-(c); Figures 5.13(d)-(f) show the output of the five amplifier units that contain the type 1 transformers, to the above-mentioned test waveforms. It is clear from the figures that the step-up transformers succeed in synthesising the test waveforms' Fourier components; however, significant distortion is introduced in the process.

The distortion in the output of the step-up transformers is investigated by means of the transfer function that includes the five power stages and transformers used. This transfer function must be characterised by a constant gain and linear phase shift, in order for the Fourier components to be transmitted without the introduction of distortion. Figure 5.12 shows the transfer function for one of the power stages connected to the five transformers; it indicates that multiple poles and zeros that lie within the bandwidth of the input, are responsible for the distortion. A complex, dynamic interaction therefore exists between the step-up transformers and the power stages of the Class-AB amplifiers.

Interpretation of the behaviour in Figure 5.12 requires a more complete transformer model than the one used in the design (where only the inductances were taken into account). Figure 6.3(a) shows the complete circuit model of a lossless transformer[7] [83];

[7]The winding and core losses are assumed to be negligible, and are therefore omitted in the figure.

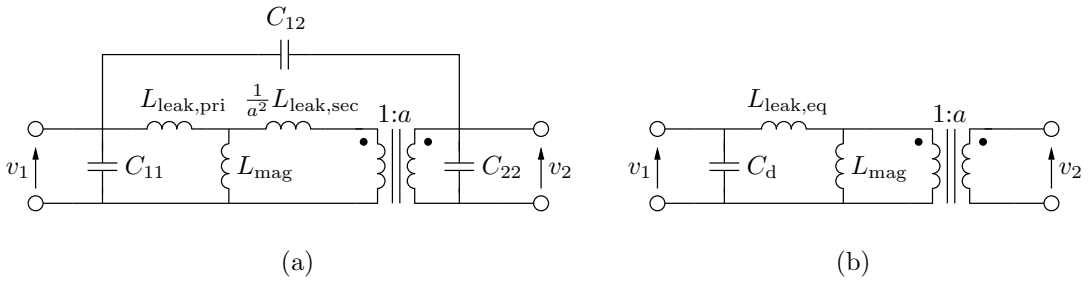

Figure 6.3: (a) The complete circuit model of a lossless transformer, with the primary self capacitance (C_{11}), secondary self capacitance (C_{22}), and interwinding capacitance (C_{12}) indicated. (b) The transformer circuit model that uses the distributed capacitance C_{d} to approximate the effects of the various stray capacitances.

C_{11} and C_{22} are the winding self capacitances of respectively the primary and secondary windings, whereas C_{12} is the interwinding capacitance. The effects of the three capacitances can be represented by the total distributed capacitance C_{d} [84], which is shown in Figure 6.3(b). The type 1 transformers' distributed capacitances were subsequently determined by measuring the self-resonance frequencies of the transformers [84]; it was found that C_{d} ranges from 0,688 μF to 2,76 μF. The distributed capacitances are three orders of magnitude larger than the rated load capacitance of the Class-AB amplifiers, and are therefore the cause of the dynamic interaction between the transformers and the amplifiers. The high transformer capacitances can be ascribed to the large number of turns in the secondary windings (contributing to the secondary-winding self capacitances), as well as the interleaved manner in which the primary and secondary windings are wound (contributing to the interwinding capacitances). In order to verify the influence of the distributed capacitances, a PSpice simulation was run using Figure 6.3(b) to model the five type 1 transformers as the load to a single power stage; the circuit model used in the simulation, can be found in Appendix C. The resulting behaviour of the simulated transfer function, which is shown in Figure 6.4, shows good agreement with that of the transfer function that was measured in Figure 5.12. The difference in maximum gain is due to the simulated circuit not taking the voltage gain of the signal-driven transformer into account, while the difference in phase shift can be ascribed to the fact that the phase shift in Figure 5.12 is influenced by all twenty transformers, as opposed to the five modelled transformers included in Figure 6.4. The influence of the transformers' distributed capacitances on the operation of the Class-AB amplifiers are therefore confirmed. The zeros in the transfer function are due to the interaction of the interwinding capacitances with the inductances of the transformers [83]; one can therefore infer that

the interwinding capacitances play the dominant role in the distributed capacitances of the transformers.

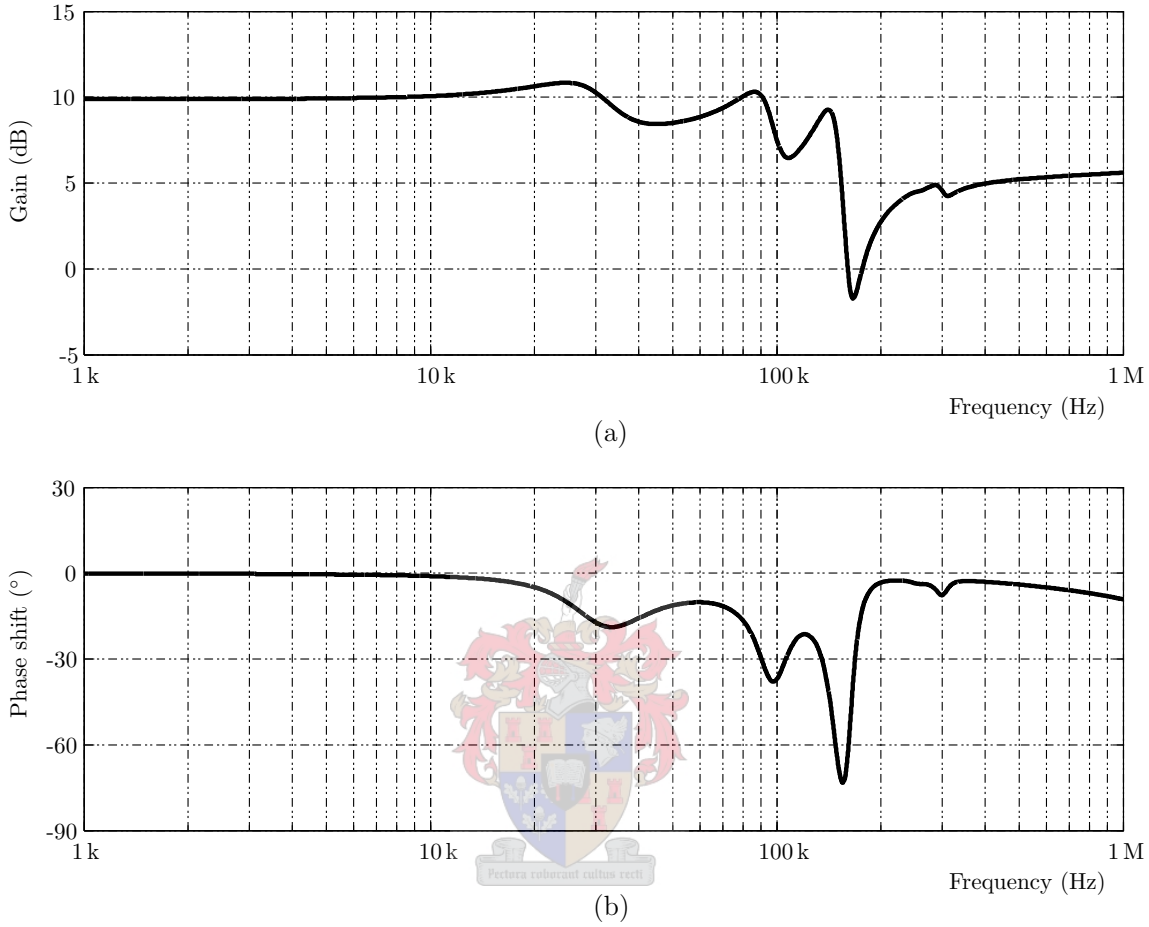

Figure 6.4: (a) The gain and (b) the phase shift of the PSpice model that simulates the influence of the transformers' distributed capacitances on the output of the Class-AB amplifiers.

6.4 System-wide effects

During the testing of the cascaded multichannel amplifier, a number of effects that are linked to the layout of the system, were observed to have an influence on the operation

of the waveform generator. These effects are briefly discussed here.

Firstly, the distributed capacitances of the step-up transformers, apart from introducing distortion into the output, also cause the current on the secondary sides of the transformers to be excessive. These large currents are subsequently reflected to the primary sides of all the transformers, causing significant, extraneous power to be dissipated in the power transistors of the output stages. In order to curb the dissipation in the transistors, the maximum voltage amplitude that is attainable at the output of the transformers, had to be limited to below 1 kV.

The ground plane of the cascaded multichannel amplifier is extensive; this is due to the fact that the individual ground planes of respectively the digital board (and through the RS232 port the computer as well), the variable-gain stages, and the power stages (along with the amplification stages' various power supplies), are all interconnected. The size of the setup therefore makes the system susceptible to EMI, especially low-frequency harmonics from the mains. As a consequence, care had to be taken in the connection of the different components (e.g. by minimising the length of any cables used), in order to minimise the introduction of noise into the system.

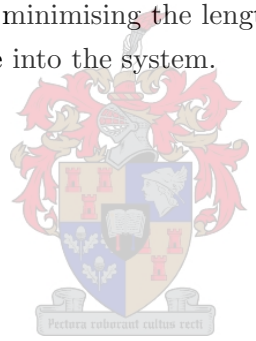

Chapter 7

Conclusions

This project set out to develop a high-voltage arbitrary-waveform generator that can be used to excite DBDs. The novel cascaded multichannel amplifier, which is based on the principle of Fourier synthesis, was chosen as the topology for this project, as the alternative topologies that were considered, are all technically difficult to implement.

Three main components comprise the cascaded multichannel amplifier, namely the sinusoid generators, the Class-AB amplifiers and the step-up transformers. Fourier theory was successfully used to determine the design requirements of these components. Upon implementation and testing of the cascaded multichannel amplifier, the following conclusions can be made regarding the performance of the three main components (the impulse waveform was used as a benchmark of the main components' performance):

- The sinusoid generators are capable of producing the Fourier components of an arbitrary waveform with great accuracy, given the limitation that a maximum of only twenty Fourier components can be generated. In the case of the generation of the impulse waveform, the fractional errors in the repetition rate and the magnitude of the Fourier components are less than respectively 1 % and 5 %, whereas the phases of the Fourier components are shifted by less than 7° from the required values. The implementation of the sinusoid generators is therefore a success.

- The Class-AB amplifiers are capable of amplifying the Fourier components under both open-load and capacitive-load conditions without introducing distortion; errors in the generated Fourier components' magnitudes can be minimised through the proper calibration of the variable-gain stages, while the amplification stages' overall contributions to errors in phase are kept small. The connection of loads

larger than the rated 2,7 nF, however, leads to the introduction of significant distortion in the generated waveform. The Class-AB amplifiers' implementation can therefore also be considered to be successful.

- The step-up transformers are able to add the Fourier components together on their secondary sides; however, due to the presence of large distributed capacitances within the transformers, significant distortion is introduced into the generated arbitrary waveform. Furthermore, the distributed capacitances also adversely affect the operation of the Class-AB amplifiers. Therefore, the implementation of the step-up transformers is only partially successful.

The cascaded multichannel amplifier's principle of operation has been proven, i.e. it is possible to generate arbitrary voltage waveforms by synthesising their separately-generated Fourier components. Furthermore, the digital generation of the Fourier components makes the system very flexible, as the parameters of the Fourier components can be set from a computer; it is therefore easy to generate different waveforms.

The biggest impediment to the proper operation of the cascaded multichannel amplifier is the large distributed capacitances of the step-up transformers; these distributed capacitances represent a combination of the interwinding capacitances, as well as the winding self capacitances. Due to the dominant role of the interwinding capacitances, high-frequency currents are coupled between the primary and secondary sides of the transformers, leading to a dynamic interaction between the transformers and the power stages of the Class-AB amplifiers. As a result, distortion is introduced into the generated arbitrary waveform. Furthermore, the maximum output amplitude is limited to less than 1 kV, due to excessive currents caused by the interaction between the transformers and power stages. Another factor that influences the operation of the cascaded multichannel amplifier, is the large effective ground plane of the implemented system; the size of the ground plane makes the arbitrary-waveform generator susceptible to EMI, and must be taken into account. As a consequence of the above-mentioned problems, the cascaded multichannel amplifier was not tested on a DBD load.

7.1 Recommendations

Several measures can be taken in order to improve the operation of the cascaded multichannel amplifier:

- The large distributed capacitances of the step-up transformers are a side effect from the design of the transformers (namely the number of turns in the windings, and the maximum output voltage amplitude), and measures must therefore be taken to reduce their influence. Although the winding self capacitances cannot be reduced easily, the interwinding capacitances can; this can be achieved by inserting two single-turn, grounded copper sheets, which are called Faraday shields, in between the primary and secondary windings of the transformers. Faraday shields can lead to a reduction of the interwinding capacitance by 50 dB to 70 dB [85].

- The large ground plane of the cascaded multichannel amplifier makes the system susceptible to EMI, which leads to distortion in the output and the possible failure of components. In order to reduce the size of the system's total ground plane, the ground planes between different sections of the system need to be isolated. This can be accomplished by utilising linear optocouplers between the variable-gain and power stages. The optocouplers provide electrical isolation, and also protect the sinusoid generators from possible faults on the secondary side of the transformers.

- The overall complexity of the cascaded multichannel amplifier can be reduced by decreasing the number of amplifier units employed. Such an action lowers the currents that each of the power stages need to manage, but also causes a loss in flexibility when it comes to arbitrary waveforms that can be generated accurately.

7.2 Future work

Various additional approaches to the implementation of the presented cascaded multichannel amplifier can be investigated:

- The dynamic nature of the step-up transformers creates problems for the operation of the cascaded multichannel amplifier, as was illustrated before. One possible solution is to remove the need for using transformers to provide the necessary high voltages; this can be done by utilising high-voltage Class-AB amplifiers that are stacked in series. In such a setup, MOSFETs or IGBTs that are capable of handling up to 800 V each, are used in the place of the low-voltage power transistors that were implemented in this project; the drive circuitry of the high-voltage power transistors would correspondingly also be replaced. Additionally, each of the power stages would require its own isolated high-voltage power supply, while the linear drive signals from the sinusoid generators need to be electrically isolated as well.

Such an arrangement has the further benefit of being able to drive larger capacitive loads.

- The Fourier transform projects a square-integrable, piecewise-continuous, periodic waveform onto a set of orthogonal sinusoids, which are known as Fourier components; on the other hand, the Hadamard transform can be used to project the same waveform onto a set of orthogonal square waves, which are called Walsh functions. The operation of the cascaded multichannel amplifier can therefore also be based on the utilisation of the Hadamard transform; this entails the programming of the digital circuit board to produce square waves, and making use of switch-mode power amplifiers (as opposed to the linear Class-AB amplifiers). Such a configuration can be implemented without the use of step-up transformers; furthermore, the use of switch-mode amplifiers significantly increases the efficiency of the system, and larger currents can therefore be provided to the DBD load.

- In this project, the cascaded multichannel amplifier was designed with arbitrary periodic waveforms in mind; however, the digital circuit board can also be programmed to produce arbitrary pulses. This can be a accomplished by inserting suitable delays between the individual periods that are produced by the sinusoid generators.

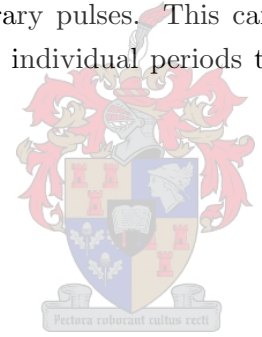

Appendices

Appendix A

Circuit diagrams

A.1 The digital circuit board

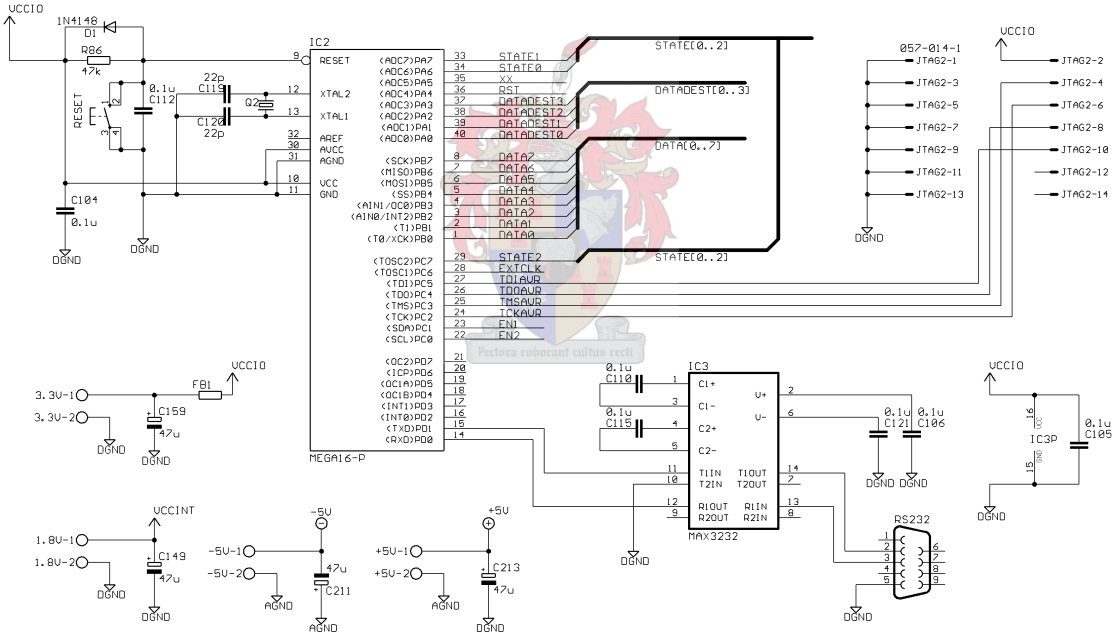

Figure A.1: The circuit diagram of the microcontroller.

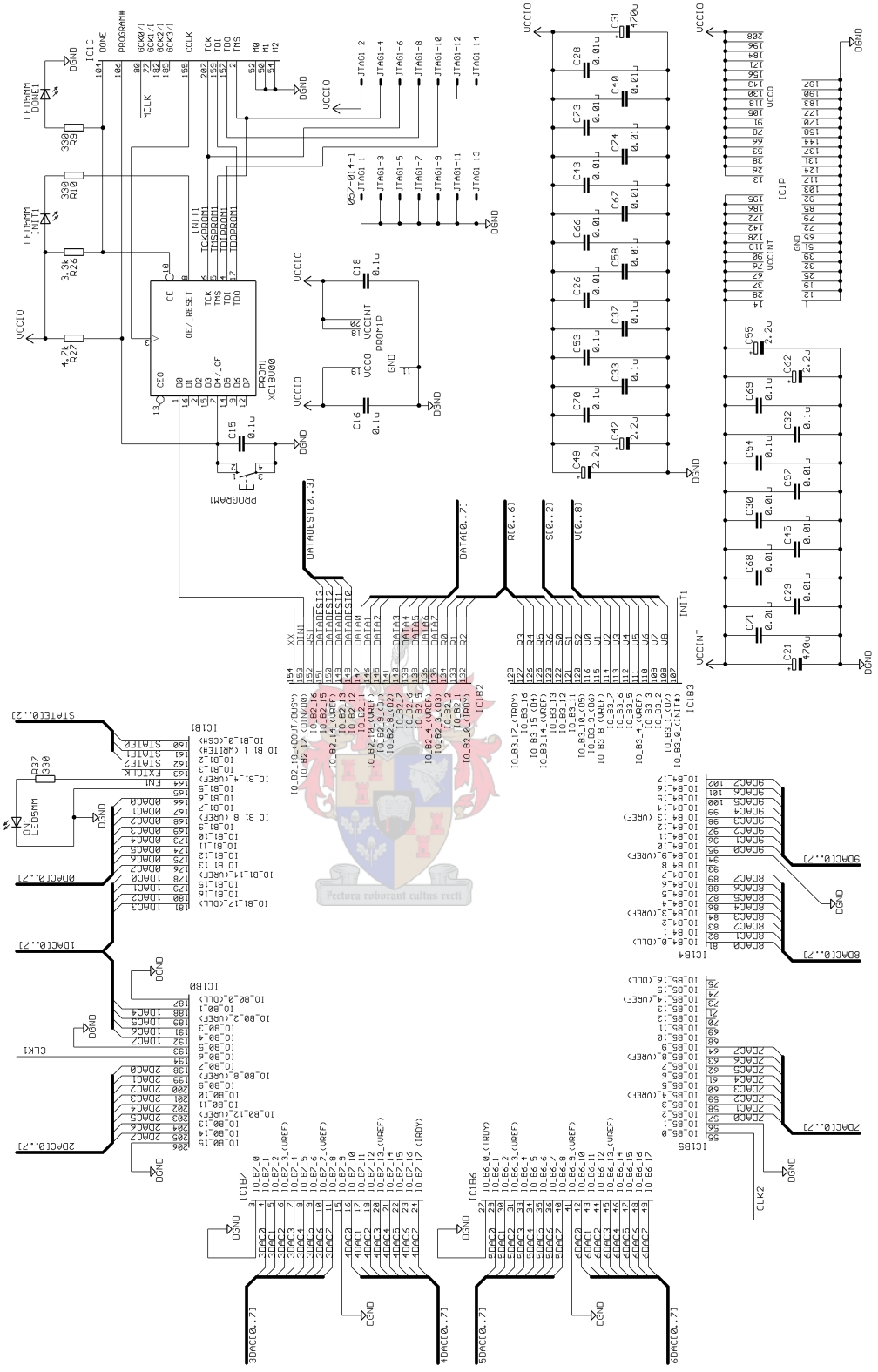

Figure A.2: The circuit diagram of the first FPGA and its accompanying PROM.

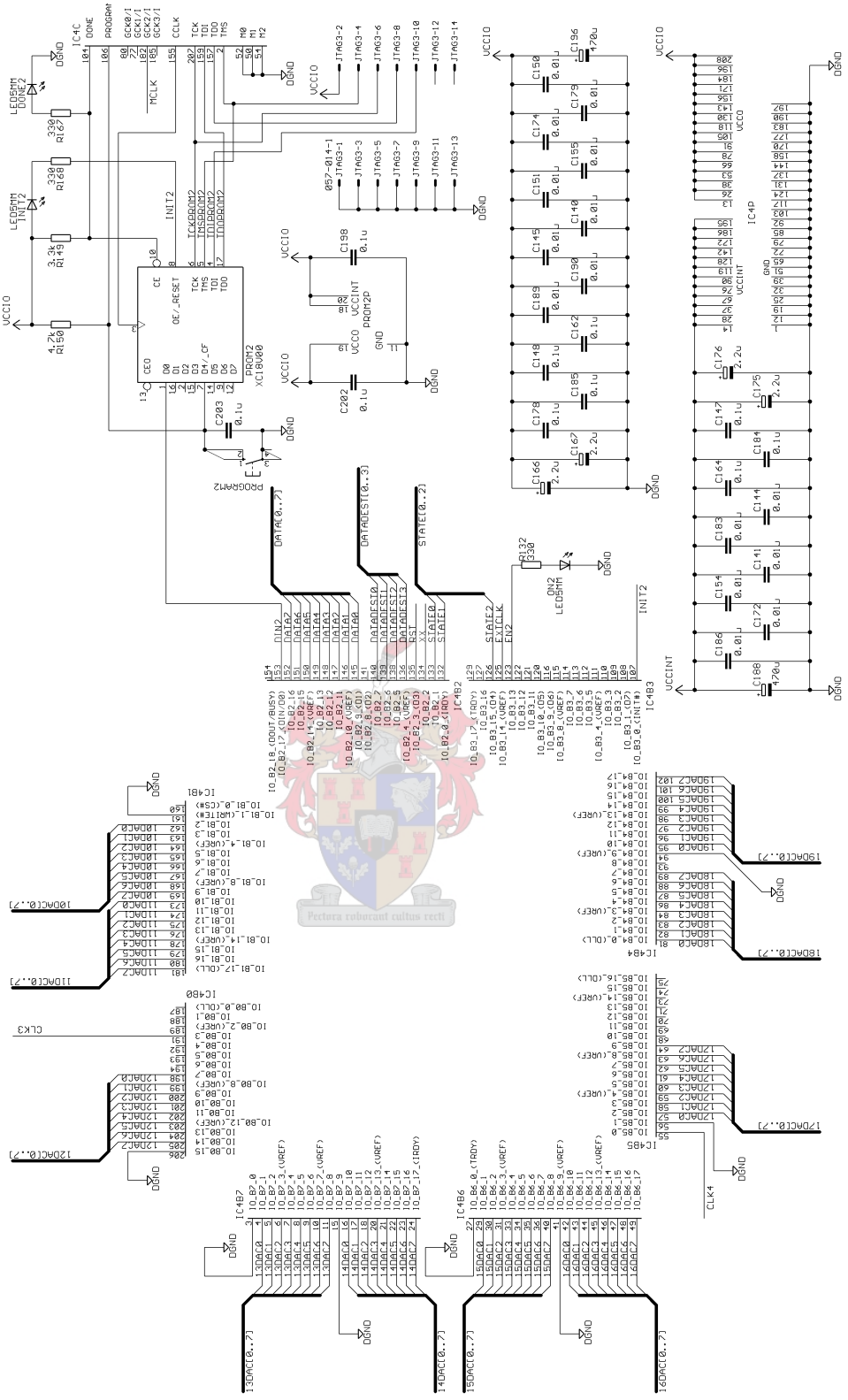

Figure A.3: The circuit diagram of the second FPGA and its accompanying PROM.

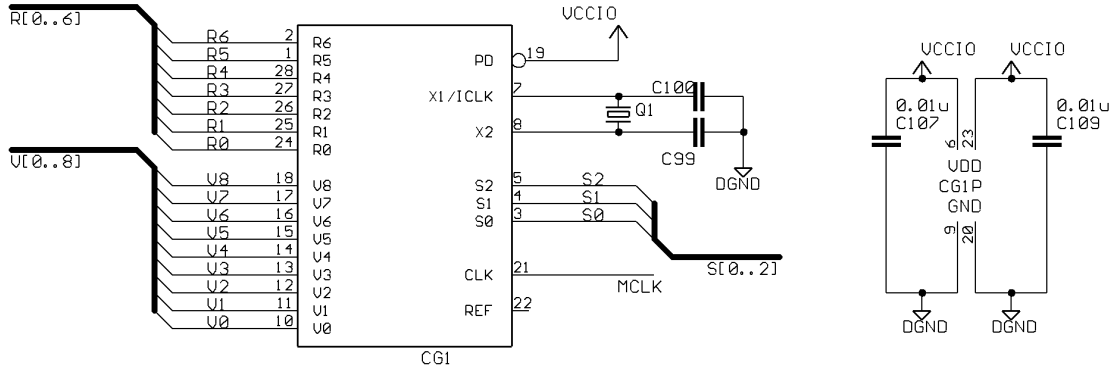

Figure A.4: The circuit diagram of the master clock.

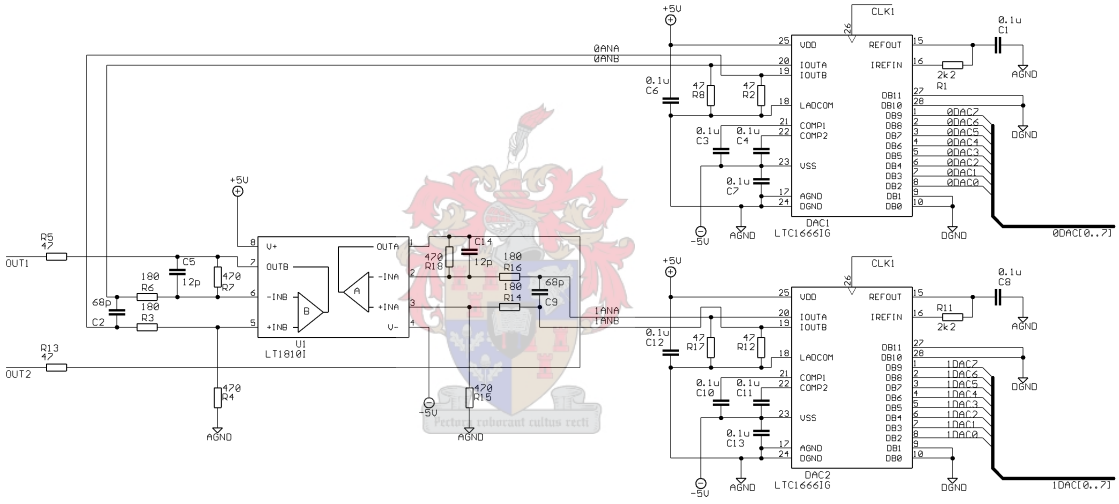

Figure A.5: The circuit diagram of two DACs connected to their differential amplifiers. All the other DAC circuits are identical to this figure.

A.2 The Class-AB amplifiers

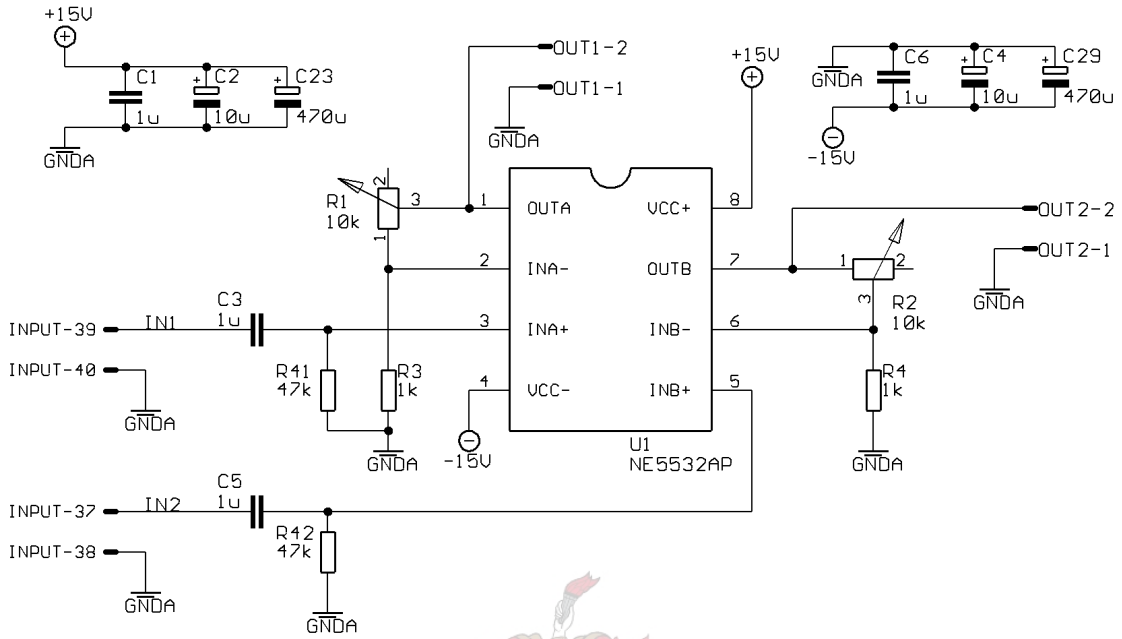

Figure A.6: A circuit diagram representative of two variable gain stages, as implemented on a NE5532AP dual operational amplifier.

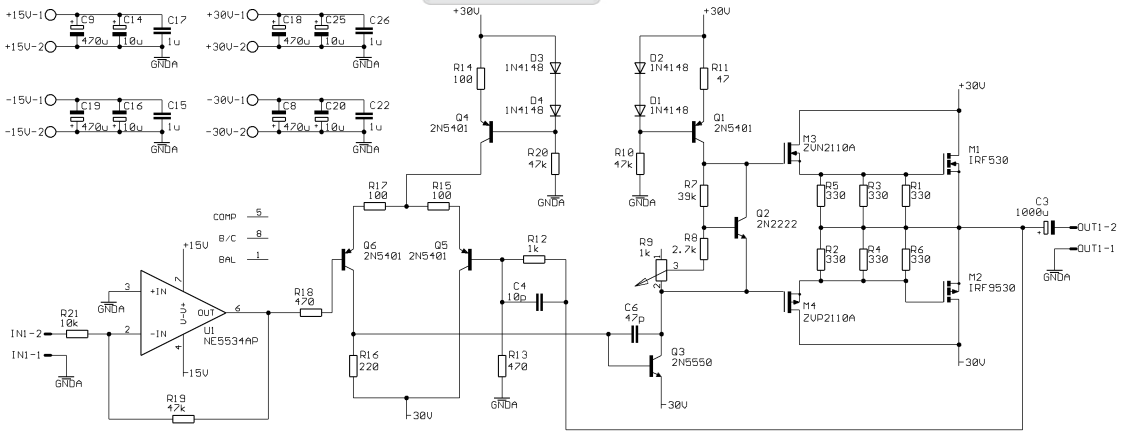

Figure A.7: The circuit diagram of the power stage.

Appendix B

Spreadsheet-aided calculations of the transformer parameters

In the following tables, the shaded cells indicate design decisions, whereas the white cells are calculated parameters.

			Type 1	**Type 2**	**Type 3**	**Type 4**
$V_{\text{peak,sec}}$	Peak secondary voltage	V	1050	1050	600	600
$V_{\text{peak,pri}}$	Peak primary voltage	V	20	20	20	20
f_{min}	Minimum frequency	kHz	4,5	9	30	45
f_{max}	Maximum frequency	kHz	45	90	300	450
P	Power	V·A	10	10	2	2
n	Number of transformers	-	5	5	5	5

Table B.1: The main characteristics of the step-up transformers.

			Type 1	Type 2	Type 3	Type 4
A_e	Effective core cross-section	mm^2	211	211	178	178
l_e	Effective core length	mm	114	114	97	97
B_{sat}	Saturation magnetic flux density	mT	250	250	200	200
μ_r	Relative permeability	-	4000	4000	4000	4000

Table B.2: The parameters of the chosen transformer cores, i.e. the ETD49 core for the type 1 and 2 transformers, and the E42/21/15 core for the type 3 and 4 transformers.

			Type 1	Type 2	Type 3	Type 4
H_{sec}	Minimum secondary hold-off	mV·s	74,3	37,1	6,37	4,24
H_{pri}	Minimum primary hold-off	mV·s	1,41	0,71	0,21	0,14
N_{sec}	Number of secondary turns	-	1260	630	150	150
N_{pri}	Number of primary turns	-	24	12	5	5
a	Turns ratio	-	52,5	52,5	30,0	30,0
$I_{rms,sec}$	Secondary RMS current	A	0,1818	0,1818	0,1818	0,1818
$I_{rms,pri}$	Primary RMS current	A	9,5459	9,5459	5,4548	5,4548
$A_{Cu,sec}$	Secondary conductor cross-section	mm^2	0,0364	0,0364	0,0364	0,0364
$A_{Cu,pri}$	Primary conductor cross-section	mm^2	1,9092	1,9092	1,0910	1,0910
δ_{min}	Minimum skin depth	mm	0,353	0,250	0,137	0,112
$k_{Cu,sec}$	Secondary copper fill factor	-	0,7	0,7	0,6	0,6
$k_{Cu,pri}$	Primary copper fill factor	-	0,7	0,7	0,6	0,6
p	Number of winding interfaces	-	5	5	1	1
$A_{w,sec}$	Secondary winding window	mm^2	65	33	9	9
$A_{w,pri}$	Primary winding window	mm^2	65	33	9	9

Table B.3: The transformer winding parameters.

			Type 1	**Type 2**	**Type 3**	**Type 4**
h_{w}	Winding width	mm	25	25	28	20
l_{w}	Average turn length	mm	90	90	50	40
b_{i}	Interwinding insulation thickness	mm	0,60	0,60	0,20	0,20
$b_{\mathrm{Cu,sec}}$	Secondary winding depth	mm	2,62	1,31	0,32	0,45
$b_{\mathrm{Cu,pri}}$	Primary winding depth	mm	2,62	1,31	0,32	0,45
$L_{\mathrm{leak,sec}}$	Leakage inductance†	μH	423,1	74,43	15,56	19,88
$L_{\mathrm{leak,total}}$	Total leakage inductance †	μH	2665			
$L_{\mathrm{leak,total}}$	Total leakage inductance ‡	nH	967	967	2960	2960

†On the secondary side of the transformer.

‡On the primary sides of the transformers.

Table B.4: Calculation of the transformer leakage inductances.

Appendix C

PSpice simulation model

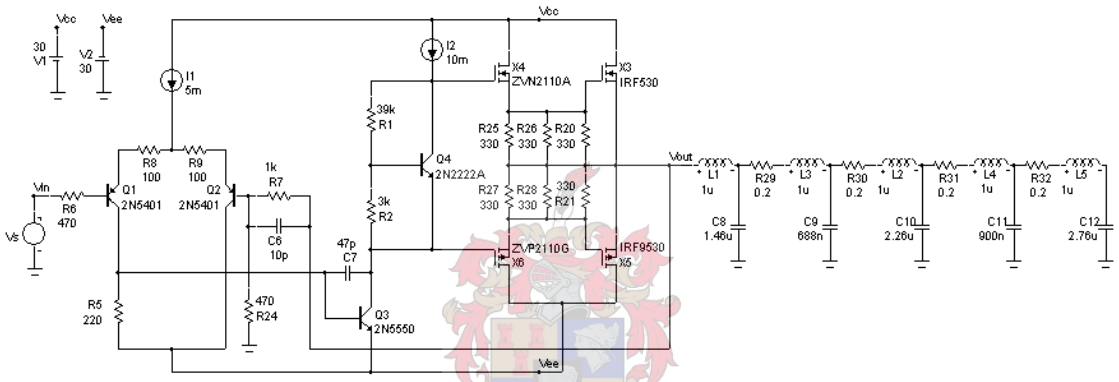

Figure C.1: The circuit diagram modelled in PSpice in order to simulate the interaction between a power stage and five step-up transformers connected to it. Each transformer is represented by its equivalent leakage inductance and distributed capacitance.

List of References

[1] U. Kogelschatz, B. Eliasson, and W. Egli, "Dielectric-barrier discharges: their history, discharge physics, and industrial applications," *Plasma Chem. Plasma Proc.*, Vol. 23, No. 1, pp. 1–46, 2003.

[2] H. Conrads and M. Schmidt, "Plasma generation and plasma sources," *Plasma Sources Sci. Technol.*, Vol. 9, No. 4, pp. 441–454, 2000.

[3] A. Napartovich, "Overview of Atmospheric Pressure Discharges Producing Nonthermal Plasma," *Plasmas and Polymers*, Vol. 6, No. 1/2, pp. 1–14, 2001.

[4] A. Fridman, A. Chirokov, and A. Gutsol, "Non-thermal atmospheric pressure discharges," *J. Phys. D: Appl. Phys.*, Vol. 38, No. 2, pp. R1–R24, 2005.

[5] V. Gibalov and G. Pietsch, "The development of dielectric barrier discharges in gas gaps and on surfaces," *J. Phys. D: Appl. Phys.*, Vol. 33, No. 20, pp. 2618–2636, 2000.

[6] W. Siemens, "Über die elektrostatische Induction und die Verzögerung des Stroms in Flaschendräten," *Poggendorffs Ann. Phys. Chem.*, Vol. 102, p. 66, 1857.

[7] T. Manley, "The electrical characteristics of the ozonator discharge," *Trans. Electrochem. Soc.*, Vol. 84, pp. 83–94, 1943.

[8] U. Kogelschatz, "Advanced Ozone Generation," in *Process Technologies for Water Treatment* (S. Stucki, ed.), pp. 87–120, New York: Plenum Press, 1988.

[9] G. Pietsch and V. Gibalov, "Dielectric barrier discharges and ozone synthesis," *Pure Appl. Chem.*, Vol. 70, No. 6, pp. 1169–1174, 1998.

[10] R. Thyen, K. Höpfner, N. Kläke, and C.-P. Klages, "Cleaning of Silicon and Steel Surfaces Using Dielectric Barrier Discharges," *Plasmas and Polymers*, Vol. 5, No. 2, pp. 91–102, 2000.

[11] F. Massines, G. Gouda, N. Gherardi, M. Duran, and E. Croquesel, "The Role of Dielectric Barrier Discharge Atmosphere and Physics on Polypropylene Surface Treatment," *Plasmas and Polymers*, Vol. 6, No. 1/2, pp. 35–49, 2001.

[12] J. Roth, Z. Chen, D. Sherman, F. Karakaya, P.-Y. Tsai, K. Kelly-Wintenberg, and T. Montie, "Increasing the Surface Energy and Sterilization of Nonwoven Fabrics by Exposure to a One Atmosphere Uniform Glow Discharge Plasma (OAUGDP)," *Int. Nonwoven Journal*, Vol. 10, pp. 34–47, 2001.

[13] R. Seeböck, H. Esrom, M. Charbonnier, M. Romand, and U. Kogelschatz, "Surface modification of polyimide using dielectric barrier discharge treatment," *Surf. Coat. Technol.*, Vol. 142, pp. 455–459, 2001.

[14] P. Rehn and W. Viöl, "Dielectric barrier discharge treatments at atmospheric pressure for wood surface modification," *Holz Roh-Werkstoff*, Vol. 61, pp. 145–150, 2003.

[15] S. Kanazawa, M. Kogoma, T. Moriwaki, and S. Okazaki, "Stable glow plasma at atmospheric pressure," *J. Phys. D: Appl. Phys.*, Vol. 21, No. 5, pp. 838–840, 1988.

[16] T. Yokoyama, M. Kogoma, S. Kanazawa, T. Moriwaki, and S. Okazaki, "The improvement of the atmospheric-pressure glow plasma method and the deposition of organic films," *J. Phys. D: Appl. Phys.*, Vol. 23, No. 3, pp. 374–377, 1990.

[17] Y. Sawada, S. Ogawa, and M. Kogoma, "Synthesis of plasma-polymerized tetraethoxysilane and hexamethyldisiloxane films prepared by atmospheric pressure glow discharge," *J. Phys. D: Appl. Phys.*, Vol. 28, No. 8, pp. 1661–1669, 1995.

[18] C.-P. Klages, K. Höpfner, N. Kläke, and R. Thyen, "Surface Functionalization at Atmospheric Pressure by DBD-Based Pulsed Plasma Polymerization," *Plasmas and Polymers*, Vol. 5, No. 2, pp. 79–89, 2000.

[19] F. Massines, N. Gherardi, and F. Sommer, "Silane-Based Coatings on Polypropylene, Deposited by Atmospheric Pressure Glow Discharge Plasmas," *Plasmas and Polymers*, Vol. 5, No. 3/4, pp. 151–172, 2000.

[20] M. Chang and T. Tseng, "Gas-Phase Removal of H_2S and NH_3 with Dielectric Barrier Discharges," *J. Environ. Eng.*, Vol. 122, No. 1, pp. 41–46, 1996.

[21] K. Takaki, M. Jani, and T. Fujiwara, "Removal of Nitric Oxide in Flue Gases by Multipoint to Plane Dielectric Barrier Discharge," *IEEE Trans. Plasma Sci.*, Vol. 27, No. 4, pp. 1137–1145, 1999.

[22] S. Müller, J. Conrads, and W. Best, "Reactor for decomposing soot and other harmful substances contained in flue gas," in *Proc. 7th Int. Symp. on High Pressure Low Temperature Plasma Chemistry (HAKONE VII)*, Vol. 2, (Greifswald, Germany), pp. 340–344, 2000.

[23] H. Ma, P. Chen, M. Zhang, X. Lin, and R. Ruan, "Study of SO_2 Removal Using Nonthermal Plasma Induced by Dielectric Barrier Discharge (DBD)," *Plasma Chem. Plasma Proc.*, Vol. 22, No. 2, pp. 239–254, 2002.

[24] S. Yagi and N. Tabata, "Silent discharge cw CO_2 laser," *IEEE J. Quantum Electron.*, Vol. 17, No. 12, p. 2376, 1981.

[25] K. Yasui, M. Kuzumoto, S. Ogawa, M. Tanaka, and S. Yagi, "Silent-Discharge Excited TEM_{00} 2.5kW CO_2 Laser," *IEEE J. Quantum Electron.*, Vol. 25, No. 4, pp. 836–840, 1989.

[26] B. Eliasson and U. Kogelschatz, "UV excimer radiation from dielectric barrier discharges," *Appl. Phys. B*, Vol. 46, No. 4, pp. 299–303, 1988.

[27] U. Kogelschatz, "Silent-discharge driven excimer UV sources and their applications," *Appl. Surf. Sci.*, Vol. 54, pp. 410–423, 1992.

[28] S. Mikoshiba, "Gas-discharge displays," in *Wiley Encyclopedia of Electrical and Electronic Engineering* (J. Webster, ed.), Vol. 8, pp. 233–238, New York: Wiley-Interscience, 1999.

[29] J. Boeuf, "Plasma display panels: physics, recent developments and key issues," *J. Phys. D: Appl. Phys.*, Vol. 36, No. 6, pp. R53–R79, 2003.

[30] M. Laroussi, "Sterilization of Contaminated Matter with an Atmospheric Pressure Plasma," *IEEE Trans. Plasma Sci.*, Vol. 24, No. 3, pp. 1188–1191, 1996.

[31] J. Birmingham and D. Hammerstrom, "Bacterial Decontamination Using Ambient Pressure Nonthermal Discharges," *IEEE Trans. Plasma Sci.*, Vol. 28, No. 1, pp. 51–55, 2000.

[32] T. Montie, K. Kelly-Wintenberg, and J. Roth, "An Overview of Research Using the One Atmosphere Uniform Glow Discharge Plasma (OAUGDP) for Sterilization of Surfaces and Materials," *IEEE Trans. Plasma Sci.*, Vol. 28, No. 1, pp. 41–50, 2000.

[33] H. Ohkawa, T. Akitsu, M. Tsuji, H. Kimura, M. Kogoma, and K. Fukushima, "Pulse-modulated, high-frequency plasma sterilization at atmospheric-pressure," *Surf. Coat. Technol.*, Vol. 200, pp. 5829–5835, 2006.

[34] J. Roth, D. Sherman, and S. Wilkinson, "Electrohydrodynamic Flow Control with a Glow-Discharge Surface Plasma," *AIAA J.*, Vol. 38, No. 7, pp. 1166–1172, 2000.

[35] C. Enloe, T. McLaughlin, R. VanDyken, K. Kachner, E. Jumper, and T. Corke, "Mechanisms and Responses of a Single Dielectric Barrier Plasma Actuator: Plasma Morphology," *AIAA J.*, Vol. 42, No. 3, pp. 589–594, 2004.

[36] P. Bletzinger, B. Ganguly, and A. Garscadden, "Influence of dielectric barrier discharges on low mach number shock waves at low to medium pressures," *J. Appl. Phys.*, Vol. 97, No. 11, pp. 113303–1–113303–6, 2005.

[37] J. Boeuf and L. Pitchford, "Electrohydronamic force and aerodynamic flow acceleration in surface dielectric barrier discharge," *J. Appl. Phys.*, Vol. 97, No. 10, pp. 103307–1–103307–10, 2005.

[38] S. Starikovskaia, "Plasma assisted ignition and combustion," *J. Phys. D: Appl. Phys.*, Vol. 39, No. 16, pp. R265–R299, 2006.

[39] V. Tudor, M. Ohadi, M. Salehi, and J. Lawler, "Advances in control of frost on evaporator coils with an applied electric field," *Int. J. Heat Mass Transfer*, Vol. 48, pp. 4428–4434, 2005.

[40] K. Donohue, B. Bures, M. Bourham, and R. Roe, "Mode of Action of a Novel Nonchemical Method of Insect Control: Atmospheric Pressure Plasma Discharge," *J. Econ. Entomol.*, Vol. 99, No. 1, pp. 38–47, 2006.

[41] B. Eliasson and U. Kogelschatz, "Modeling and Applications of Silent Discharge Plasmas," *IEEE Trans. Plasma Sci.*, Vol. 19, No. 2, pp. 309–323, 1991.

[42] S. Okazaki, M. Kogoma, M. Uehara, and Y. Kimura, "Appearance of stable glow discharge in air, argon, oxygen and nitrogen at atmospheric pressure using a 50Hz source," *J. Phys. D: Appl. Phys.*, Vol. 26, No. 5, pp. 889–892, 1993.

[43] F. Massines, A. Rabehi, P. Decomps, R. Gadri, P. Ségur, and C. Mayoux, "Experimental and theoretical study of a glow discharge at atmospheric pressure controlled by dielectric barrier," *J. Appl. Phys.*, Vol. 83, No. 6, pp. 2950–2957, 1998.

[44] M. Kogoma and S. Okazaki, "Raising of ozone formation efficiency in a homogeneous glow discharge plasma at atmospheric pressure," *J. Phys. D: Appl. Phys.*, Vol. 27, No. 9, pp. 1985–1987, 1994.

[45] F. Massines, R. Messaoudi, and C. Mayoux, "Comparison Between Air Filamentary and Helium Glow Dielectric Barrier Discharges for the Polypropylene Surface Treatment," *Plasmas and Polymers*, Vol. 3, No. 1, pp. 43–59, 1998.

[46] F. Massines and G. Gouda, "A comparison of polypropylene-surface treatment by filamentary, homogeneous and glow discharges in helium at atmospheric pressure," *J. Phys. D: Appl. Phys.*, Vol. 31, No. 24, pp. 3411–3420, 1998.

[47] S. Guimond, I. Radu, G. Czeremuszkin, D. Carlsson, and M. Wertheimer, "Biaxially Oriented Polypropylene (BOPP) Surface Modification by Nitrogen Atmospheric Pressure Glow Discharge (APGD) and by Air Corona," *Plasmas and Polymers*, Vol. 7, No. 1, pp. 71–88, 2002.

[48] J. Roth, J. Rahel, X. Dai, and D. Sherman, "The physics and phenomenology of One Atmosphere Uniform Glow Discharge Plasma (OAUGDP™) reactors for surface treatment applications," *J. Phys. D: Appl. Phys.*, Vol. 38, No. 4, pp. 555–567, 2005.

[49] Y. Golubovskii, V. Maiorov, J. Behnke, and J. Behnke, "Influence of interaction between charged particles and dielectric surface over a homogeneous barrier discharge in nitrogen," *J. Phys. D: Appl. Phys.*, Vol. 35, No. 8, pp. 751–761, 2002.

[50] E. Aldea, P. Peeters, H. De Vries, and M. Van De Sanden, "Atmospheric glow stabilization. Do we need pre-ionization?," *Surf. Coat. Technol.*, Vol. 200, pp. 46–50, 2005.

[51] T. Yokoyama, M. Kogoma, T. Moriwaki, and S. Okazaki, "The mechanism of the stabilisation of glow plasma at atmospheric pressure," *J. Phys. D: Appl. Phys.*, Vol. 23, No. 8, pp. 1125–1128, 1990.

[52] S. Okazaki, M. Kogoma, and H. Uchiyama in *Proc. 3rd Int. Symp. on High Pressure Low Temperature Plasma Chemistry (HAKONE III)*, (Strasbourg, France), pp. 101–107, 1991.

[53] R. Brandenburg, K. Kozlov, N. Gherardi, P. Michel, C. Khampan, H.-E. Wagner, and F. Massines, "Spatio-temporally resolved spectroscopic diagnostics of the atmospheric pressure glow discharge in nitrogen," in *Proc. 8th Int. Symp. on High Pressure Low Temperature Plasma Chemistry (HAKONE VIII)*, Vol. 1, (Tartu, Estonia), pp. 28–32, 2002.

[54] J. Tepper and M. Lindmayer, "Investigations on two Different Kinds of Homogeneous Barrier Discharges at Atmospheric Pressure," in *Proc. 7th Int. Symp. on High Pressure Low Temperature Plasma Chemistry (HAKONE VII)*, Vol. 1, (Greifswald, Germany), pp. 38–43, 2000.

[55] D. Trunec, A. Brablec, and J. Buchta, "Atmospheric pressure glow discharge in neon," *J. Phys. D: Appl. Phys.*, Vol. 34, No. 11, pp. 1697–1699, 2001.

[56] S. Liu and M. Neiger, "Excitation of dielectric barrier discharges by unipolar submicrosecond square pulses," *J. Phys. D: Appl. Phys.*, Vol. 34, No. 11, pp. 1632–1638, 2001.

[57] K. Okazaki and T. Nozaki, "Ultrashort pulsed barrier discharges and applications," *Pure Appl. Chem.*, Vol. 74, No. 3, pp. 447–452, 2002.

[58] T. Somekawa, T. Shirafuji, O. Sakai, K. Tachibana, and K. Matsunaga, "Effects of self-erasing discharges on the uniformity of the dielectric barrier discharge," *J. Phys. D: Appl. Phys.*, Vol. 38, No. 12, pp. 1910–1917, 2005.

[59] X. Deng and M. Kong, "Electrically Efficient Production of a Diffuse Nonthermal Atmospheric Plasma," *IEEE Trans. Plasma Sci.*, Vol. 31, No. 1, pp. 7–18, 2003.

[60] J. Shin and L. Raja, "Dynamics of pulse phenomena in helium dielectric-barrier atmospheric-pressure glow discharges," *J. Appl. Phys.*, Vol. 94, No. 12, pp. 7408–7415, 2003.

[61] S. Liu and M. Neiger, "Electrical modelling of homogeneous dielectric barrier discharges under an arbitrary excitation voltage," *J. Phys. D: Appl. Phys.*, Vol. 36, pp. 3144–3150, 2003.

[62] D. Neamen, *Electronic Circuit Analysis and Design.* Chicago: Irwin, first ed., 1996.

[63] W. Leach, *Introduction to Electroacoustics and Audio Amplifier Design.* Kendall/Hunt, second, revised ed., 2001.

[64] J. Rodríguez, J. Lai, and F. Peng, "Multilevel Inverters: A Survey of Topologies, Controls, and Applications," *IEEE Trans. Ind. Electron.*, Vol. 49, No. 4, pp. 724–738, 2002.

[65] L. Tolbert, F. Peng, and T. Habetler, "Multilevel Converters for Large Electric Drives," *IEEE Trans. Ind. Applicat.*, Vol. 35, No. 1, pp. 36–44, 1999.

[66] F. Peng, J. McKeever, and D. Adams, "A Power Line Conditioner Using Cascade Multilevel Inverters for Distribution Systems," *IEEE Trans. Ind. Applicat.*, Vol. 34, No. 6, pp. 1293–1298, 1998.

[67] A. Nabae, I. Takahashi, and H. Akagi, "A new neutral-point clamped pwm inverter," *IEEE Trans. Ind. Applicat.*, Vol. 17, No. 5, pp. 518–523, 1981.

[68] T. Meynard and H. Foch, "Multi-level choppers for high voltage applications," *EPE J.*, Vol. 2, No. 1, pp. 45–50, 1992.

[69] P. Hammond, "A new approach to enhance power quality for medium voltage AC drives," *IEEE Trans. Ind. Applicat.*, Vol. 33, No. 1, pp. 202–208, 1997.

[70] M. Manjrekar, P. Steimer, and T. Lipo, "Hybrid Multilevel Power Conversion System: A Competitive Solution for High-Power Applications," *IEEE Trans. Ind. Applicat.*, Vol. 36, No. 3, pp. 834–841, 2000.

[71] C. Rech, H. Pinheiro, H. Gründling, H. Hey, and J. Pinheiro, "Analysis and Comparison of Hybrid Multilevel Voltage Source Inverters," in *Proc. IEEE PESC'02*, Vol. 2, (Cairns, Australia), pp. 491–496, 2002.

[72] N. Mohan, T. Undeland, and W. Robbins, *Power Electronics: Converters, Applications, and Design*. New York: John Wiley & Sons, second ed., 1995.

[73] L. Tolbert and T. Habetler, "Novel Multilevel Inverter Carrier-Based PWM Method," *IEEE Trans. Ind. Applicat.*, Vol. 35, No. 5, pp. 1098–1107, 1999.

[74] O. Godoy-Cabrera, J. Benítez-Read, R. López-Callejas, and J. Pacheco-Sotelo, "A high voltage resonant inverter for dielectric discharge barrier cell plasma applications," *Int. J. Electron.*, Vol. 87, No. 3, pp. 361–376, 2000.

[75] J. Alonso, J. Cardesín, E. Lopez Corominas, M. Rico-Secades, and J. García, "Low-Power High-Voltage High-Frequency Power Supply for Ozone Generation," *IEEE Trans. Ind. Applicat.*, Vol. 40, No. 2, pp. 414–421, 2004.

[76] J. Pacheco-Sotelo, R. Valdivia Barrientos, M. Pacheco-Pacheco, J. Ramos Flores, M. Durán García, J. Benítez-Read, R. Peña Eguilez, and R. López-Callejas, "A Universal Resonant Converter for Equilibrium and Nonequilibrium Plasma Discharges," *IEEE Trans. Plasma Sci.*, Vol. 32, No. 5, pp. 2105–2112, 2004.

[77] J. Alonso, J. García, A. Calleja, J. Ribas, and J. Cardesín, "Analysis, Design, and Experimentation of a High-Voltage Power Supply for Ozone Generation Based on Current-Fed Parallel-Resonant Push-Pull Inverter," *IEEE Trans. Ind. Applicat.*, Vol. 41, No. 5, pp. 1364–1372, 2005.

[78] J. Nilsson and S. Riedel, *Electric Circuits*. New Jersey: Prentice Hall, sixth ed., 2000.

[79] R. Steigerwald, "A comparison of half-bridge resonant converter topologies," *IEEE Trans. Power Electron.*, Vol. 3, No. 2, pp. 174–182, 1988.

[80] R. Ziemer and W. Tranter, *Principles of Communications: Systems, Modulation, and Noise*. New York: John Wiley & Sons, fourth ed., 1995.

[81] R. Bracewell, *The Fourier Transform and Its Applications*. Singapore: McGraw Hill, third ed., 2000.

[82] G. Franklin, J. Powell, and A. Emami-Naeini, *Feedback Control of Dynamic Systems*. New York: Addison-Wesley, third ed., 1994.

[83] C. Trask, "Designing Wide-band Transformers for HF and VHF Power Amplifiers." Available at: `http://www.arrl.org/qex/2005/qx3Trask.pdf`, [2007, January 23].

[84] K. Creel, "Measuring Transformer Distributed Capacitance." Available at: `http://www.datatronics.com/pdf/distributed_capacitance_paper.pdf`, [2007, January 23].

[85] "Shielding & Noise Attenuation." Available at: `http://www.marelco.com/application7.html`, [2007, January 23].